Modeling Diffusion in the Gasification Reaction with Carbon Dioxide: Comparison of Diffusion Models

by

Amirreza Karimi Nemch

A Thesis
in the Department of
Mechanical, Industrial and Aerospace Engineering
Presented in Partial Fulfilment of the Requirements
For the Degree of
Master of Applied Science (Mechanical Engineering)
at Concordia University
Montreal, Quebec, Canada

December, 2020

CONCORDIA UNIVERSITY
School of Graduate Studies

This is to certify that the thesis prepared

By: Amirreza Karimi Nemch

Entitled: Modeling Diffusion in the Gasification Reaction with Carbon Dioxide: Comparison of Diffusion Models

and submitted in partial fulfillment of the requirements for the degree of

Master of Applied Science (Mechanical Engineering)

complies with the regulations of the University and meets the accepted standards with respect to originality and quality.

Signed by the final examining committee:

_____

Supervisor and chair, Dr. Alex De Visscher,
Department of Chemical and Materials Engineering

_____

Examiner, Dr. Melanie Hazlett,
Department of Chemical and Materials Engineering

_____

Examiner, Dr. Rolf Wuthrich,
Department of Mechanical, Industrial and Aerospace Engineering

_____

External Examiner, Dr. Fariborz Haghighat.
Department of Building, Civil, and Environmental Engineering

Approved by _____

Chair of Department, Dr. Martin Pugh

December 11, 2020 _____

Dean, Dr. Mourad Debbabi

Abstract

Modeling Diffusion in the Gasification Reaction with Carbon Dioxide:
Comparison of Diffusion Models
Amirreza Karimi Nemch

As one of the most effective ways to produce energy from a solid carbon, gasification becomes more popular among the industries. The feedstock of gasification passes through multiple steps and reactions to produce syngas, which is a mixture of CO and H_2. However, diffusion limitations play an important role in the kinetics of gasification reaction and should be determined. A thermogravimetric analyzer (TGA) is used to investigate the gasification kinetics by studying the mass loss of the sample over time. The influence of mass transfer limitations is typically evaluated using an effectiveness factor, which is a function of the Thiele modulus.

In this work, a mathematical model is developed in MATLAB to investigate the mass transfer limitations in the CO_2 gasification of petroleum coke and activated carbon using different diffusion theories and various scenarios. Unlike previous studies, various multicomponent and binary diffusion flux theories are compared in this work. Starting with Fick's law of diffusion, which is the simplest diffusion theory for binary mixtures to the most recent ones such as the dusty-gas model (DGM), and the cylindrical pore interpolation model (CPIM).

Simulation results show that using Fick's law (binary case) may underestimate the diffusion limitations in the bed and the gas part. Equally important are the assumptions made about the fate of minor elements in the carbonaceous material, such as oxygen or hydrogen. Therefore, a multicomponent flux theory is required to model the diffusion. The dusty-gas model provides a better estimation of the experimental rates compared to the other theories (CPIM and Fick's law). Moreover, the diffusion limitations are more significant for the more reactive component, activated carbon, and cannot be eliminated. For petcoke, external diffusion is the mass transfer limiting step in a closed-bottom crucible. For activated carbon, the effects of external and inter-particle diffusion on the overall rate are almost the same order of magnitude. Eventually, the model is verified with the experimental results of Malekshahian et al. (2014). The proposed model shows a good consistency with the experimental results in all initial masses. However, the intrinsic rate constant should be modified with a kinetic model accounting for CO inhibition to enhance the match with the experimental results.

Acknowledgements

I would like to express my deep and sincere gratitude to my supervisor, Dr. Alex De Vissscher, for his valuable advice and constant support through my studies. His thoughts and ideas have always inspired me during different stages of my work. In addition, I am extremely grateful to my dear colleague, Paolla Chrystine Pinheiro Patricio, for her precious advices and support.

I am thankful to my parents and siblings, who have been there for me all the time and their unconditional love and guidance kept me motivated. Moreover, I am thankful to my dear friends, Amirreza, Shayan and Mohammadreza, for being a great source of encouragement and motivation in my daily life.

I also thank my official referees, Dr. Fariborz Haghighat, Dr. Melanie Hazlett and Dr. Rolf Wuthrich for their participation in the assessment of my thesis.

Dedication

To my beloved parents

Who supported me throughout this journey

and gave me their love.

Table of Contents

List of Tables

List of Figures

List of Symbols

Symbol	Definition
A	Cross sectional area of the crucible
A_m	External surface area of the particle per mass of carbon
A_A	Coefficient in pressure gradient equation
A_K	Pressure gradient coefficient in the Knudsen regime
A_C	Pressure gradient coefficient in the continuum regime
B_0	Dusty-gas model fitting parameter
c_i	Molar concentration of species *i*
c_0	CO_2 concentration at the bulk flow
c_{sb}	CO_2 concentration on bed surface
c_b	Local CO_2 concentration in bed
c_{sp}	CO_2 concentration on particle outer surface
c_g	Reaction gas concentration
c	Total molar concentration
d	Average particle diameter
D_{ij}	Binary diffusion coefficient
D_{ij}^{eff}	Effective binary diffusion coefficient
$D_{i,K}$	Knudsen diffusion coefficient of species *i*
$D_{i,K}^{eff}$	Effective Knudsen diffusion coefficient
D^{eff}	General effective diffusion coefficient
$D_{i,m}$	Pseudo binary diffusion coefficient of species *i*
D_A	Diffusion coefficient at arbitrary *Kn* (CPIM)
D	Pore diameter
$f(x)$	Function which describes the structural change of sample during reaction
ΔH	Heat of the reaction
J_i	Molar flux of species *i* (defined relative to the average movement of molecules)
k	Intrinsic n^{th} order rate constant

Kn	Knudsen number
k_{eff}	Effective rate constant
k'	permeability
L_C	Height of the crucible
L_g	Height of the gas part
m	Instantaneous mass
m_0	Initial mass
M_i	Molar mass of species *i*
N_i	Molar flux of species *i* (defined in a fixed frame of reference)
n	Intrinsic reaction order
p	Total pressure
p_i	Partial pressure of component *i*
R_m	Intrinsic reaction rate on mass basis
R'_m	Overall reaction rate on mass basis
R_S	Intrinsic surface reaction rate
R_V	Intrinsic reaction rate on volume basis
R'_V	Overall reaction rate on volume basis
R_g	Gas constant
r_i	Reaction rate of species *i*
R_{pore}	Pore radius
r	Radius of the crucible (cylindrical part and spherical cap)
r_c	Radius of the cylindrical part of the crucible
r_s	Radius of spherical cap
r'	r coordinate of the center of the spherical cap
T	Temperature
t	Time
V_b	Volume of the bed in the control volume
V_g	Volume of the gas in the control volume
V_{bv}	Volume of the bed void space in the control volume
V_{CV}	Volume of the control volume

V_{cap}	Volume of spherical cap
x	Conversion
y_i	Mole fraction of species *i*
z	Distance
z'	z coordinate of the center of the spherical cap

Greek letters

β	Mass transfer coefficient
θ	Thiele modulus
ρ	Density
ε	Porosity
τ	Tortuosity
δ	Height of the sample bed
μ_i	Viscosity of species i
μ	Viscosity of the mixture
η_p	Particle effectiveness factor
$\overline{\eta_p}$	Mean particle effectiveness factor
η_b	Bed effectiveness factor
η_e	External effectiveness factor
υ_i	Stoichiometric coefficient of species i
λ	Mean free path of the molecule
$\emptyset_{ij}$	Viscosity factor

CHAPTER ONE: INTRODUCTION

Due to the growth of fuel price in recent years and environmental concerns, gasification is getting more attention as a potential source of energy. Gasification is described as a series of processes that produce energy and valuable gases from a carbonaceous substance, such as petcoke and biomass. The product of gasification has a variety of applications in generating electricity or useful chemicals, fuels, syngas, hydrogen, and chemical fertilizers. Using gasification on a large scale dates back to more than 75 years ago. There are currently more than hundreds of gasification operating plants across the globe. In addition, gasification can be an appropriate replacement for the direct use of natural gas, as they can use waste materials like biomass or municipal solid waste and turn them into valuable sources of energy due to their high capacity and cost-efficient capture and sequestration of CO_2 (Higman & van der Burgt, 2008); (Malekshahian, 2011).

However, there are some challenges in implementing the gasification, such as high capital cost, low reliability of some feedstocks, and lack of a highly efficient reactor design that industries are facing (Sansaniwal et al., 2017). Moreover, several studies have shown the impact of mass transfer effects on the gasification kinetics that should be evaluated.

Thermogravimetric Analysis (TGA) is a widely used tool to study gasification by monitoring the mass loss of the sample over time. In a typical TGA experiment, the reactant gas (CO_2 in this case) indirectly passes through the sample holder, which contains a few milligrams of the sample at a particular concentration and temperature. Because of the mentioned configuration, the mass and heat transfer limitations are important and may affect the results significantly in such that the obtained rate may not be sufficiently accurate for scaling up the process (Malekshahian & Hill, 2011a); (Higman & van der Burgt, 2008).

In this study, the effect of mass transfer was investigated using effectiveness factors. This factor is a function of the Thiele modulus and is the ratio of the reaction considering diffusion limitations to the rate at bulk conditions. The concentration profile of the reactant gas within the crucible is required. Therefore, an adequate diffusion flux theory is needed in order to model the diffusion and reaction.

Over time, the study of transport phenomena to develop new models to accurately simulate the diffusion of the reactants into the porous media has been a crucial and important aspect of chemical

engineering. Researchers have been using different approaches, ranging from Fick's law, which is the most straightforward diffusion theory, to the more complex multicomponent flux models such as, Stefan-Maxwell model (SMM), dusty-gas model (DGM), and the recently established cylindrical pore interpolation model (CPIM). However, these more complex models are rarely used.

Fick's law is the simplest way to model the transport mechanism into the porous medium. Keeping in mind that it is only valid for binary mixtures. For multicomponent diffusion and concentrated mixtures, the Stefan-Maxwell model (SMM) is recommended due to Fick's law limitations. The SMM has been used successfully in a variety of fields, including diffusion in distillation, diffusion in an electrostatic force field and diffusion in a centrifugal force field. However, it does not consider the collision of the gas molecules with the pore walls and cannot accurately describe gas diffusion in porous media. Many of these shortcomings are being addressed with the dusty-gas model (DGM). The predictive capability of the DGM is well documented, and the DGM is the method of choice for gas transport in porous media (Kong et al., 2012); (Evans et al., 1961).

The DGM has been a recommended choice of multicomponent flux model because of its apparent ability to account for both Knudsen and bulk diffusion. However, there is a gap between the slip-flow regime and the Knudsen regime, where there is no clear way to parameterize the DGM. Furthermore, it has been criticized because of its algebraic complexity and the physical principles used in its derivation (Kerkhof, 1996). Young and Todd presented a new multicomponent flux model called the cylindrical pore interpolation model (CPIM). Their model had explicit assumptions, resulting in a conveniently compact set of equations (Young & Todd, 2005); (Lim & Dennis, 2012). Nevertheless, there is only minimal experience with the CPIM, which means it is poorly validated.

The **objectives** of the present study:

- Comparing different diffusion theories by developing a model to account for the mass transfer limitations in the CO_2 gasification of petcoke and activated carbon in a TGA apparatus using MATLAB.
- A numerical method is implemented to evaluate the mass transfer limitations by discussing the intraparticle, inter-particle and external effectiveness factors in various cases.
- Eventually, investigating the effect of initial mass on different models.

CHAPTER TWO: LITERATURE REVIEW

This chapter begins by introducing the gasification process. In the following section, the effect of mass transfer on the gasification kinetics and evaluating them using a thermogravimetric analyzer (TGA) is discussed. Eventually, after providing a brief introduction to the different diffusion theories in porous media, some of the previous research in modelling diffusion and reaction using these theories is reviewed.

2.1 Introduction to the gasification:

2.1.1 Gasification definition

Gasification is technically defined as the thermochemical transformation of a solid carbon in the form of coke or char into a combustible gaseous product such as carbon monoxide (CO) and hydrogen (H_2) by utilizing carbon dioxide (CO_2) or steam as the gasifying agent (Ma et al., 2011); (Bremaud et al., 2005). The composition of products varies with the type of feedstock, process and final application of the product gas. Producing heat and electricity or processing into liquid hydrocarbons can be named as some of these applications (Coda et al., 2007).

2.1.2 Gasification steps

Industrial gasification, regardless of the type of feedstock, includes three main steps (Fermoso et al., 2008); (Qian et al., 2013); (Zhao et al., 2009):

- **Pyrolysis reactions (devolatilization):** First of all, to produce char and release volatiles, the solid fuel is heated up to 700 °C to cause a set of pyrolysis reactions. There is a possibility of tars production when volatiles liquefy at low temperatures. The **slowest step** during the gasification is the char gasification step, which controls the overall rate of the process. Hence, the char gasification rate plays a significant role in designing the gasifiers.
- **Oxidation reactions**: In the following step, the essential gasifying agents (CO_2 and steam) and CO are produced as a result of the combustion of char and volatiles with oxygen. The heat released in this exothermic reaction will be used for the next step.

- **Reduction reactions:** Finally, in this step, char and hydrocarbons in a set of endothermic reactions gasify with CO_2 and steam, which leads to the production of synthesis gas (syngas), mainly CO, H_2, and CH_4. Steam helps the steam reforming of char and tar, as well as water-gas shift reactions (Hernández et al., 2013); (Hernandez et al., 2012a).

2.1.3 Gasifying reactions

The most important reactions involved in the gasification are presented in equations (2-1) to (2-6), with thermodynamic data at standard conditions (Higman & van der Burgt, 2008):

Combustion reactions:

$$C + \frac{1}{2}O_2 \rightarrow CO \qquad \Delta H = -111 \text{ MJ/kmol} \qquad (2\text{-}1)$$

$$CO + \frac{1}{2}O_2 \rightarrow CO_2 \qquad \Delta H = -283 \text{ MJ/kmol} \qquad (2\text{-}2)$$

$$H_2 + \frac{1}{2}O_2 \rightarrow H_2O \qquad \Delta H = -242 \text{ MJ/kmol} \qquad (2\text{-}3)$$

The Boudouard reaction (governing reaction):

$$C + CO_2 \rightleftharpoons 2CO \qquad \Delta H = +172 \text{ MJ/kmol} \qquad (2\text{-}4)$$

The water-gas reaction:

$$C + H_2O \rightleftharpoons CO + H_2 \qquad \Delta H = +131 \text{ MJ/kmol} \qquad (2\text{-}5)$$

And the methanation reaction:

$$C + 2H_2 \rightleftharpoons CH_4 \qquad \Delta H = -75 \text{ MJ/kmol} \qquad (2\text{-}6)$$

During the CO_2 gasification at low temperatures (lower than 1000 °C), the overall rate is controlled by the Boudouard reaction (Ahmed & Gupta, 2011); (Tremel & Spliethoff, 2013); (Mahinpey & Gomez, 2016). At higher temperatures, by combining steam and CO_2 gasification, which are endothermic reactions, the H_2 yield can be improved. The H_2/CO ratio will be increased in the final product by water-gas shift reaction, but it does not have a considerable effect on the heating value of the syngas due to the similar molar combustion heats of H_2 and CO.

2.1.4 Gasification reactors:

Moving bed, fluidized bed, and entrained-flow gasifiers are the three main groups of reactors for the gasification process. These gasifiers vary in different parameters such as size, feed and product flow rates, residence time, and reaction temperature. Therefore, the composition of the product gas differs for each gasifier. The properties of the feedstock like reactivity or particle size and the desired product gas heating value determine which process should be used.

In **moving bed reactors** (MBR), the gasifying agents enter the bottom of the gasifier, and the gaseous product leaves from the top. Due to the constant height of the solid bed, this process is considered as a fixed bed reactor. Then, the dry ash is removed from the bottom of the bed depending on the temperature of the bed. This process can bear particles with sizes up to 50 mm (Kabe et al., 2004). Lurgi, B.G. Slagging Lurgi and Wellman-Galusha are categorized as moving bed reactors. The temperature of the released gas in a moving bed gasifier changes between 698 K to 923 K (Higman & van der Burgt, 2008).

In the next type of gasifiers, **entrained flow reactors** (EFR), mostly both feed and the gasifying agents are fed into the top of the reactor. All the feed particles are entrained due to the fast motion of the gas through the reactor. The challenging part of using an entrained flow gasifier can be grinding and achieving the desired feed size since this type of reactor requires a very small particle size. EFRs are the most popular type of gasifiers in the industry due to their high conversion and flexibility (Collot, 2006). The operating condition of this reactor usually ranges between 1200°C to 1600°C and 2 MPa to 8 MPa (McKendry, 2002); (Minchener, 2005); (Mahinpey & Gomez, 2016).

Finally, **fluidized bed reactors** (FBR) have been used in coal gasification for quite a while (McKendry, 2002). In this type of gasifiers, there is an upward motion of gasifying agent through the bed of finely powdered particles, and the gas fluidizes the particles. In fluidized bed gasifiers, a homogeneous contact of gas and solids is provided. The particle size of interest is between 6 to 10 mm, and caking coals cannot be used in this type of reactor (Higman & van der Burgt, 2008). The temperature of the emitted gas ranges between 1173-1773 K, which is moderate compared to other processes (Higman & van der Burgt, 2008). U- Gas, Hy-Gas and Winkler processes are some examples of the usage of fluidized bed gasifiers (Mahinpey & Gomez, 2016).

2.1.5 Gasification kinetic studies

Although coal gasification kinetics has always been an important matter of research, there is limited progress in the area to enable a satisfactory design for commercial gasification reactors. Temperature, surface area and reaction gas concentration are some of the parameters that influence the overall gasification rate. The overall kinetic expression of gasification can be written as equation (2-7) due to the variation of surface area as a function of conversion while the reaction is happening (Malekshahian and Hill, 2011).

$$\frac{dX}{dt} = R_s(c_g, T)f(X) \tag{2-7}$$

In equation (2-7), X is the conversion, t is time, R_s is the intrinsic surface reaction rate, which is a function of the temperature and reaction gas concentration, T and c_g respectively. Lastly, $f(X)$ is a function used to describe the structural change of the sample during the reaction.

There are two main groups of models which describe pore structure changing throughout the reaction (Bhatia & Perlmutter, 1980):

1. models that assume reaction occurs on the surface of nonporous grains
2. other models that assume the reaction takes place on the pore surface.

The grain model, which is of the first category, considers that the solid reactant includes an assembly of uniformly sized nonporous grains in which the reaction takes place on the outside of a shrinking core within the particle (Szekely & Evans, 1970). In the shrinking core model, the reaction zone moves back to the center of the particle during the reaction (Levenspiel, 1999). Hence, the reactive core radius reduces while the surface area and particle diameter are constant.

On the other hand, Bhatia and Perlmutter developed the popular random-pore model, representing the second group (Bhatia & Perlmutter, 1980). This model considers that the pore surface is the start point of the reaction. Over time, the pore volume and surface area increase until the adjacent pores overlap. Hence, in this model, the structure will change during the reaction.

Although multiple studies have used these two models (grain and random-pore model) to model char gasification, their ultimate application does not work due to the structural change during gasification and consequently its effect on the reactivity (Kajitani et al., 2006); (Fermoso et al., 2008); (Fermoso et al., 2009). However, the random-pore model, because of its capability to

anticipate the maximum rate and being simple, is the most used model to estimate the gasification rate (Su & Perlmutter, 1985); (Chi & Perlmutter, 1989).

2.1.6 Effect of process conditions and char properties on char gasification

Temperature, pressure and heating rate of the pyrolysis process can have an impact on the active surface area of the created char, and therefore on its reactivity. As a result, among the variables that affect the rate of gasification are gasification operating conditions such as temperature and pressure. By increasing temperature, the gasification rate increases. By increasing reactant pressure, reactivity increases as well.

Another parameter that affects the gasification rate is the existence of mass transfer limitations. By increasing the particle size or the initial mass of the sample, mass transfer limitations become more significant. Consequently, increasing the particle size and initial mass have a negative effects on the gasification rate. Change in the char properties besides the mass transfer limitations can explain the variation of the rate with particle size.

2.1.7 Petroleum coke and activated carbon gasification

Petroleum coke (petcoke) is a carbon-based material derived from the thermal cracking of heavy oil fractions at a high temperature and pressure in the coking process. The nature of the feedstock and the coking process determines the physical and chemical properties of petcoke, as well as its commercial application (Totten et al., 2003). Petcoke gasification is mainly known as one of the most promising and economical implementations of petcoke. Due to its high heating value which is 20% higher than coal (30.25–34.91 MJ/kg versus 24.45– 30.25 MJ/kg) and lower ash content, utilization of petcoke is a reliable source of energy (‘Perry's handbook’, 2008).

On the other hand, low reactivity and high sulphur (5.5-7.5 wt %) and vanadium content of petcoke make it a challenging feedstock for gasification (Zhan et al., 2010). The sulphur in petcoke leads to the production of undesired gas products such as H_2S and SO_2.

Table 2-1 provides the proximate and ultimate composition of the delayed coke (10 years old, Suncor Energy Inc.) as well as the prepared char from delayed coke that was used in the model presented here (Hill et al., 2014). As can be seen, by adding more heat to the delayed coke, the volatile matter is removed and there is an increase in the fixed carbon percentage.

The availability of raw material (petcoke) for gasification right in the refinery site makes the case of petcoke as a gasification feedstock more compelling and economical.

Table 2-1. Ultimate and proximate analysis of petcoke and char at 1248 K on a dry basis (Hill et al., 2014)

	Petcoke (delayed coke)	**Char (delayed coke char)**
Ultimate Analysis (wt%)		
Carbon (C)	84	89
Hydrogen (H)	3.8	0.3
Nitrogen (N)	1.8	1.7
Sulphur (S)	6.5	5.1
Oxygen (O)	3.8	3.4
Proximate Analysis (wt%)		
Moisture	0.3	
Ash	3.7	4.2
Volatile	15	0
Fixed Carbon	82	96

Activated Carbon (AC) or activated charcoal is a carbon derived material with small pores to increase the surface area. Activated carbon is called activated coal when it is derived from coal, and it is referred as activated coke when it is derived from coke. Activated carbon is considered a highly reactive component because of its high microporosity, which can be more than 3000 m^2/g. Activated Carbon consists of 70-80% carbon as well as hydrogen, nitrogen, sulphur and oxygen. Due to the high porosity and low ash content, over 50 % of the activated carbons are produced from biomass as a precursor (fruit shells, fruit stones, agricultural residues, wood, etc.) (Marsh & Rodríguez-Reinoso, 2006). Table (2-2) shows the composition of commercial activated carbon (Tuas & Masduqi, 2019).

Table 2-2. Chemical composition of commercial activated carbon (Tuas & Masduqi, 2019)

Element	Wt%
Carbon (C)	62.20
Oxygen (O)	29.36
Sodium (Na)	4.24
Chlorine (Cl)	1.97
Copper (Cu)	1
Potassium (K)	0.58
Magnesium (Mg)	0.34
Iron (Fe)	0.11
Silicon (Si)	0.18

2.1.8 Gasification applications

The introduction of gasification to produce energy as an alternative to the conventional processes and fossil fuels has brought various advantages to the industry. Unusable wastes i.e. forestry residues and any type of biomass, can be converted to useful forms of energy by applying gasification. This process can be beneficial in many environmental and economical aspects. For instance, gasification preserves lands and reduces storage costs due to the usage of agricultural waste and other useless material to produce energy.

One of the other applications of gasification is using IGCC[1] power plants with a combination of gasification and power generation to generate energy efficiently. IGCC power plants can be seen in many large companies across the world, such as Siemens, GE, ConocoPhillips, and Shell (Hoffmann & Szklo, 2011). Figure (2-1) shows a variety of products derived from synthesis gas which is a product of gasification reaction (Higman & van der Burgt, 2008).

[1] Integrated Gasification Combined Cycle

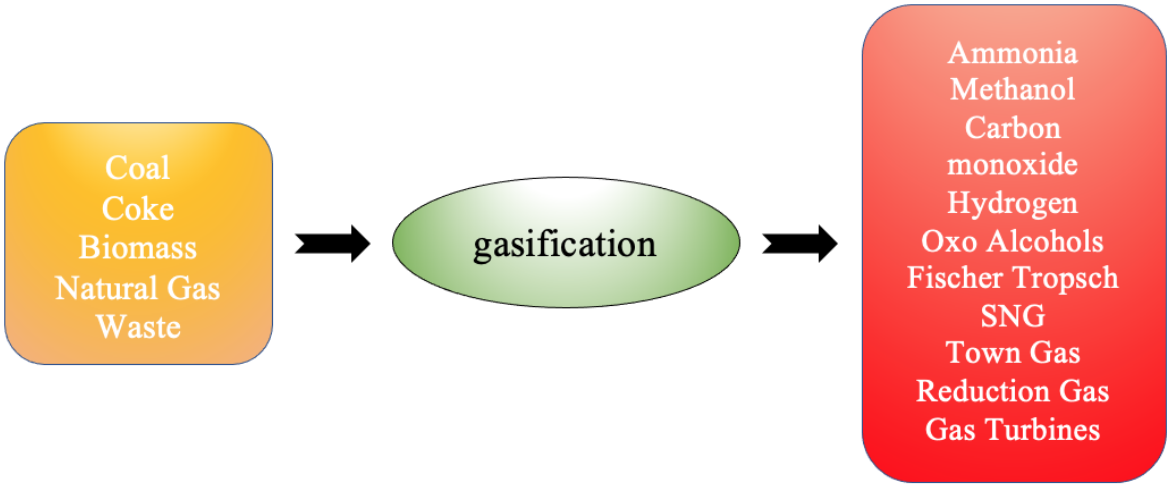

Figure 2-1. Gasification applications (Higman & van der Burgt, 2008)

2.2 Mass transfer effects on the gasification kinetics using TGA

Increasing the gasification rate at lower temperatures, which is crucial to its implementation, has attracted researchers across the globe to the gasification kinetics. Thermogravimetric analysis (TGA) has become a well-established method for studying the kinetics of gasification reactions. In a TGA experiment, the mass loss of the sample is being monitored during isothermal or non-isothermal exposure to various conditions. Due to the mentioned configuration of TGA, heat and mass transfer limitations play an important role in the gasification kinetics (Jess & Andresen, 2010); (Gómez-Barea et al., 2005). However, the diverse information provided in the literature with conflicting results and conditions makes it hard to compare or relate different studies.

2.2.1 CO_2 gasification studies using thermogravimetric analysis (TGA)

Thermogravimetric analysis (TGA) uses an uncomplicated reactor design to investigate gasification kinetics by studying the mass loss of the sample over time while the temperature varies. It is widely used in various studies regarding CO_2 gasification (Gómez-Barea et al., 2005); (Ollero et al., 2002); (Jess & Andresen, 2010); (J. Song et al., 2010).

In a typical thermogravimetric analyzer, pure gas, furnace gas and reaction gas flow in the system. The pure gas (helium), which flows through the balance, is used to reduce the furnace heat moving upward and reduce the contamination of the balance as a result of the reaction. Furnace gas (Nitrogen) by flowing through the furnace controls the furnace temperature. Finally, the reaction gas (nitrogen and carbon dioxide for gasification) flows through the reactor while mass controllers

are used to control and measure the flow rates for these gases. TGA results can be used to measure phase transitions, absorption and adsorption as well as transport phenomena and solid-gas reaction studies (Coats & Redfern, 1963). Figure (2-2) illustrates the flow diagram for a typical thermogravimetric analyzer.

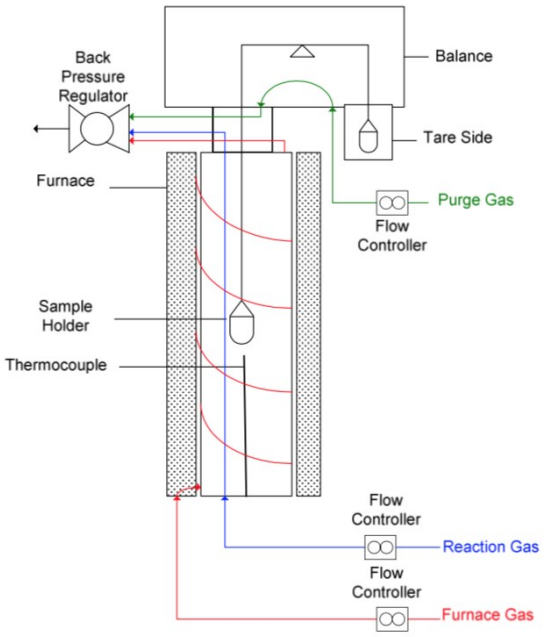

Figure 2-2. Flow diagram of a thermogravimetric analyzer (Malekshahian, 2011)

In a controlled environment like TGA, the char gasification studies can help gain information regarding the diffusion effects in a char particle inside a gasifier (Mani et al., 2011). TGA is a favourable tool for studying gasification due to the ability of reading the information continuously and accurately throughout the reaction progress (Wall et al., 2002). Nevertheless, one drawback of using TGA is that, except for the determination of global kinetics, the selectivity of competing reactions cannot be estimated. For instance, it is possible to predict the global kinetics of gasification, but analyzing the competing reactions in char gasification is not a straightforward task (Mahinpey & Gomez, 2016).

Ollero et al. assessed the importance of diffusion limitations during char conversion by using TGA. In order to prove diffusional effects on the conversion, they used various configurations of char within the crucible in their experiments. Moreover, a 2D model was developed by the same group for reaction diffusion phenomena within a crucible in TGA (Ollero et al., 2002)(Gómez-Barea et al., 2005).

As previously mentioned, in a typical TGA experiment, the reactant gas flows upward in the reactor tube through the sample holder, which contains a small amount of the sample at a certain temperature and concentration. However, a sample holder itself may have an impact on the transportation of species to the sample. Basically, the flow of the gasifying agent (CO_2) experiences three steps to reach the active surface of the particles. Firstly, due to the exposure of reactant gas (CO_2) to the open top of the char filled crucible, a stagnant gas layer between the bulk of the gas and the surface of the char bed is formed (**external diffusion**). The gasifying agent (CO_2) then diffuses through the macropores in the bed to reach the external surfaces of the porous char particles (**inter-particle diffusion**). Finally, CO_2 and heat diffuse into the internal surface of the char particles (**intraparticle diffusion**). Subsequently, on the external and internal surface of the particles, adsorption of CO_2, the surface reaction and desorption of CO take place. Finally, we have the counter-diffusion (intraparticle, inter-particle and external) of the reaction product. A way to reduce intraparticle diffusion limitations is to crush the particles to a smaller size. It is not adequate to increase the fluid flow in order to avoid external mass transfer limitations because of the development of a stagnant gas layer within the crucible (Ollero et al., 2002) (Gómez-Barea et al., 2005).

In TGA, the mass change versus time or temperature result gives information about the sample conversion during the processes and consequently, by this method, kinetic variables can be obtained. In order to estimate the gasification rate from the TGA result, carbon conversion (X) should be calculated.

$$X = \frac{m_0 - m}{m_0} \tag{2-8}$$

m is the instantaneous char mass on a dry basis and m_0 is the initial mass of the sample. Therefore, the gasification rate can be determined by both equations (2-9), and (2-10) (Molina & Mondragón, 1998); (Jess & Andresen, 2010):

$$R_m = -\frac{dm}{mdt} = \frac{dX}{(1-X)dt} \tag{2-9}$$

$$R_m = -\frac{dm}{m_0 dt} = \frac{dX}{dt} \tag{2-10}$$

2.2.2 Assumptions and simplifications within the literature

Despite progress in diffusion modelling of the gasification process during the past few years, there are many assumptions in the kinetic modelling which have not been clearly stated and understanding each model considerations needs a significant amount of time and effort. To improve the kinetics, some implicit assumptions related to mass transfer limitations must be reviewed.

Ahmed et al. and Khalil et al. assumed that, at temperatures below 1000°C, where the chemical reaction is the controlling step, the effect of mass transfer is negligible (Ahmed & Gupta, 2011); (Khalil et al., 2009). However, this assumption should be reconsidered, because it may have an effect on the results. Mandapati et al. developed a one-dimensional reaction diffusion model for CO_2 gasification of four Indian coals using a TGA. They found that when the char is finely powdered, the pore diffusion (intraparticle) resistance may be neglected because of the short intraparticle diffusion path. They used different configurations of char and crucible with different diameters and depths to demonstrate that. They also mentioned a strong impact of the bed diffusion (inter-particle) limitations on the overall rate of the reaction (Mandapati et al., 2012).

Stanmore et al. assumed the particle layer as a porous flat plate and studied the effects of oxygen transfer in particle beds on carbon burning rates. They found that the bed Thiele modulus value, which is the ratio of the surface reaction rate to the rate of diffusion, calculated regardless if combustion occurred throughout the bed or in a surface layer. Moreover, oxygen provided to the surface layer was generally diminished when the value of bed Thiele modulus was high (Stanmore et al., 1994).

Gomez-Barea et al. assumed a pseudo-steady state hypothesis (PSH) for both mass and heat transfer. They believed this assumption is valid since the molar ratio of the reactant gas to the solid reactant is very small. Consequently, the gas phase reaches steady state orders of magnitude faster than the solid phase, as suggested by Froment and Bischoff[2] (Gómez-Barea et al., 2005).

Song et al. assumed the temperature of the particle layer instead of the surrounding gas temperature in the TGA crucible to calculate intrinsic reactivity and subsequent kinetic studies due to the absence of temperature gradient in the particle layer and considerable difference with the surrounding gas (J. Song et al., 2010).

[2] Froment GF, Bischoff KB. Chemical reactor analysis and design. 2nd ed. New York: Wiley; 1990.

2.2.3 Investigating the mass transfer effects by using effectiveness factors

Numerous studies have shown the impact of mass transfer limitations on the gasification kinetics in TGA and evaluated it by using an effectiveness factor (Jess & Andresen, 2010) (Bandyopadhyay et al., 1991); (Ollero et al., 2002); (Q. Song et al., 2006); (Song et al., 2010). The effectiveness factor is defined as:

$$\eta = \frac{reaction\ rate\ considering\ diffusion}{reaction\ rate\ at\ the\ bulk(Diffusion\ unaffected\ rate)} \tag{2-11}$$

This factor depends on the Thiele modulus, which is the ratio of the surface reaction rate to diffusion rate. Information about the intrinsic rate constant is required in order to apply the Thiele modulus directly. Thus, it cannot be determined by the rate constants measured directly when we have mass transfer limitations in the system. One way to estimate heat and mass transfer limitations in the TGA experiment is to measure the intrinsic rate in a different apparatus and applying it to the results gained from a TGA apparatus (Malekshahian et al., 2014).

Satterfield et al. described a spherical and a flat plate model regarding diffusion and reaction in porous materials. In their studies, the impact of mass transfer was evaluated by an effectiveness factor which was derived from the Thiele modulus. They also developed a formula to calculate the Thiele modulus[3]. Bandyopadhyay et al. studied a heat and mass transfer model for CO_2–CO gasification of graphite and coconut char in a TGA experiment. They predicted the intrinsic chemical reactivity free from heat and mass transfer limitations using the theoretically calculated effectiveness factors (Bandyopadhyay et al., 1991). Ollero et al. described an overall effectiveness factor which was the ratio of the reaction rate with diffusion over the reaction rate for the bulk. In their particular case, this factor showed to be as low as 0.2. Furthermore, Song and his co-workers studied the impact of intraparticle, interparticle and external diffusion in TGA. They evaluated the effect of mass transfer limitations for each diffusion step separately by using effectiveness factors to compare their influence on controlling the overall rate of the process.

Jess and Andresen determined the overall rate (the rate affected by diffusion limitations) by the following equation (Jess & Andresen, 2010):

[3] Satterfield, C. N. *Mass transfer in heterogeneous catalysis*; MIT Press: Cambridge, MA, 1970.

$$R'_m = k_{eff} c_g \tag{2-12}$$

where c_g is the concentration of bulk flowing over the crucible (mol/m^3). k_{eff} is the effective rate constant (m^3/kg.s), which takes pore diffusion (effectiveness factor η_{pore}) and external diffusion (mass transfer coefficient β) into account.

$$k_{eff} = \left(\frac{1}{\eta_{pore} k} + \frac{1}{\beta A_m} \right)^{-1} \tag{2-13}$$

In equation (2-13), A_m represents the external surface area of the particle per mass of carbon (m^2/ kg), k is the reaction rate constant (m^3/kg.s), and η_{pore} is the effectiveness factor, which is a function of the Thiele modulus (θ) and it is given by:

$$\eta_{pore} = \frac{\tanh \theta}{\theta} \tag{2-14}$$

where for a spherical pellet (θ) can be written as:

$$\theta = L \sqrt{\frac{k \rho_s}{D_{ij}^{eff}}} \tag{2-15}$$

where L is the characteristic length (initial height of the sample (m)), ρ_s is density of the solid (kg/m^3), and D_{ij}^{eff} is the effective diffusion coefficient.

2.3 Diffusion in porous media

Pore volumes, pore surfaces and the solid matrix are the three different diffusion methods in porous media. Although the importance of each path is dependent on several parameters, the majority of the diffusion process at normal and high temperatures takes place in the pore volumes. Accurate modelling of diffusion and reaction is crucial in gasification studies, especially when considering how the reacting pellets interact with the fluid dynamic environment within a porous medium in a gasifier. Several studies have used numerical modelling to study diffusion and reaction in porous

media (Malekshahian et al., 2014). However, a reliable diffusion theory is required in order to model the process correctly. Modelling diffusion by Fick's law is limited accuracy in most cases since industrial reactions mostly include more than two species. Therefore, a multicomponent flux model such as the Stefan-Maxwell model (SMM) or dusty-gas model or CPIM is required (Lim & Dennis, 2012).

2.3.1 Fick's law of diffusion

Adolf Fick described Fick's law in 1855, which is the most straightforward theory to model diffusion:

$$J_i = -D_{ij}\left(\frac{dc_i}{dz}\right) \tag{2-16}$$

where J_i is the molar flux of component *i* (mol/m^2.s), D_{ij} is the binary diffusion coefficient (m^2/s), c_i is the molar concentration of *i* (mol/m^3) and *z* is the distance (m).

Although Fick's law is reliable for studying diffusion in binary mixtures, it is only an estimation in the case of multicomponent mixtures. Thus, a more complex theory like Stefan-Maxwell model or dusty-gas model is required to investigate the diffusion in more complex mixtures.

2.3.2 Stefan-Maxwell model (SMM)

There is an important difference between binary diffusion and multicomponent diffusion. In binary diffusion the movement of species *i* is always proportional to the negative of the concentration gradient of species *i*. However, other interesting scenarios such as reverse diffusion, osmotic diffusion, diffusion barrier may take place in multicomponent diffusion.

James Clerk Maxwell[4] and Josef Stefan[5] developed equations representing Stefan-Maxwell model for dilute gases and fluids respectively. This multicomponent diffusion theory is mainly used for gases at low density, where the ideal-gas law applies, and it is an extended version of Fick's law. Equation (2-17) determines the concentration gradient of component *i* in the mixture:

[4] J. C. Maxwell: On the dynamical theory of gases, The Scientific Papers of J. C. Maxwell, 1965, **2**, 26–78

[5] J. Stefan: Über das Gleichgewicht und Bewegung, insbesondere die Diffusion von Gemischen, Sitzungsberichte der Kaiserlichen Akademie der Wissenschaften Wien, 2te Abteilung a, 1871, **63**, 63-124.

$$\frac{\partial c_i}{\partial z} = \sum_{\substack{i=1 \\ j\neq 1}}^{N} \frac{N_j y_i - N_i y_j}{D_{ij}} \tag{2-17}$$

In this equation, N_i and y_i are the flux (mol/m^2.s) and mole fraction of component *i*. The difference between J_i and N_i is that J_i is the flux defined relative to the average movement of all molecules, whereas N_i is the flux defined relative to a fixed frame of reference.

The idea behind the SMM is to consider each compound in the mixture as a distinct fluid. The movement of these fluids in the same volume with different velocities causes drag forces and pressure (De Visscher, 2019).

2.3.3 Dusty-gas model (DGM)

The dusty-gas model (DGM) is one of the main theories in practical use for diffusion in a porous medium. Evans et al. described the DGM, which is an extension of the Stefan-Maxwell equations (Evans et al., 1961); (Evans et al., 1962). They believed that their model provides a rigorous treatment for the transitional Knudsen regimes. The idea of DGM comes from the assumption of the similarity of a gas mixture flow through a porous solid to the flow through an irregular array of solid spheres. In this model, the solid part of the porous medium is assumed as an extra compound, which is called dust. This assumption leads to the following equation:

$$\frac{\partial c_i}{\partial z} = \sum_{\substack{i=1 \\ j\neq 1}}^{N} \frac{N_j c_i - N_i c_j}{c D_{ij}^{eff}} - \frac{N_i}{D_{i,k}^{eff}} \tag{2-18}$$

D_{ij}^{eff} and $D_{i,k}^{eff}$ are the effective binary diffusivity and effective Knudsen diffusivity which are determined by $\frac{\varepsilon}{\tau} D_{ij}$ and $\frac{\varepsilon}{\tau} D_{i,k}$ respectively, where ε expresses the porosity and τ represents the tortuosity of the porous media. However, the second term on the righthand side is neglected if the Knudsen diffusion is insignificant and equation (2-18) is reduced to the SMM equations (De Visscher, 2019). Additional assumptions are needed in the case of a pressure drop.

Despite all the accomplishments of the DGM as a multicomponent flux model due to its apparent ability to account for both Knudsen and bulk diffusion, there are some issues with the physical principles and the mathematical development used in the derivation of its equations (Kerkhof,

1996)(Young & Todd, 2005). Kerkhof criticized DGM in his research regarding permeation through inert membrane. He found that in the case of pure liquids permeation and diffusion with a stagnant component, the DGM equations led to unreasonable results (Kerkhof, 1996).

Young and Todd mentioned the incapability of the DGM in the transitional flow where both molecular and Knudsen diffusion are important. They also found out that the DGM could not be written consistently in the mass formulation because of its neglect of diffusion slip. In the same paper, they introduced a new multicomponent flux model, which was called the Cylindrical Pore Interpolation Model (CPIM). This new model had clear assumptions, resulting in a conveniently compact set of equations (Young & Todd, 2005).

2.3.4 Cylindrical pore interpolation model (CPIM)

Young and Todd developed a multicomponent flux model which was based on the Stefan-Maxwell equations adjusted by a momentum balance. They called it Cylindrical Pore Interpolation Model (CPIM) and it was distinguished from its competitors by a relatively more precise treatment of continuum flow, a more clear interpolation procedure for transitional flow, and a compact form of equations which helps to clear up the roles of the governing parameters. Moreover, unlike DGM it can be written in both the molar and mass formulation (Young & Todd, 2005); (Lim & Dennis, 2012).

The CPIM works based on an interpolation method, which depends on the symmetry of the equations at the highest pore sizes according to the flow of a single radius in long tubes to describe the flow in intermediate pore sizes. Finally, the research of Young and Todd resulted in the set of equations below.

$$\frac{dy_j}{dz} = \frac{\tau^2 R_g T}{\varepsilon p} \sum_{i=1}^{N} \left[\frac{y_j J_i}{D_{A,ij}} - \frac{y_i J_j}{D_{A,ji}}\right] \tag{2-19}$$

$$\frac{dp}{dz} = -\frac{\tau^2 A_A}{\varepsilon} \sum_{i=1}^{N} M_i^{\frac{1}{2}} J_i \tag{2-20}$$

y_i and J_i represents the mole fraction and molar flux of component i (mol/m^2.s), M_i is the molar mass of i (kg/mol), R_g is the gas constant (m^3.Pa/K.mol), T is the temperature (K), p is the total

pressure (Pa), z shows the distance (m) and N is the total number of species. A_A and D_A are CPIM parameters which are determined by interpolating between the extremes of continuum and Knudsen flow using:

$$\frac{1}{D_{A,ij}} = \frac{1}{D_{i,k}} + \frac{1}{D_{ij}} \tag{2-21}$$

$$\frac{1}{A_A} = \frac{1}{A_K} + \frac{1}{A_C} \tag{2-22}$$

where $D_{i,k}$ and D_{ij} are the Knudsen diffusivity and binary diffusivity, respectively. The CPIM parameters A_K and A_C, are the coefficients in the pressure gradient equation in the continuum and Knudsen regime, respectively. They are given by:

$$A_K = \frac{3}{4R_{pore}}\left(\frac{\pi R_g T}{2}\right)^{\frac{1}{2}} \tag{2-23}$$

$$A_C = \frac{8\mu}{cR_{Pore}^2 \sum_{i=1}^{N} X_i M_i^{\frac{1}{2}}} \tag{2-24}$$

R_{pore} indicates the pore radius (m), μ is the viscosity of the mixture (Pa.s) and N is the total number of species.

2.3.5 Comparison of different diffusion theories in the literature

As previously stated, finding an appropriate multicomponent diffusion flux theory to model diffusion and reaction within the porous media is crucial since most of the industrial operations and reactions involve more than two species. Several studies have compared different diffusion theories in various circumstances (Kaza & Jackson, 1980); (Lim & Dennis, 2012); (Abashar & Elnashaie, 1993). For instance, Kaza and Jackson studied a general approach for an isothermal pellet. They applied the dusty-gas model (DGM) to a pellet of catalyst where multiple independent reactions were happening (Kaza & Jackson, 1980). Kaza et al. generalized the approach to a non-isothermal case (Kaza et al., 1980). Abashar et al. described the steam-reforming of natural gas

and used a simpler version of the DGM. By assuming viscous flow was insignificant, they excluded the pressure gradient term in this simplified version of DGM (Abashar & Elnashaie, 1993). Graaf et al. applied the DGM to an isothermal pellet to acquire an equation accounting for the pressure gradient within the pellet, the pressure change was disregarded in the actual simulation based on the subsidiary calculations showing that the pressure difference was small (Graaf et al., 1990). Solsvik and Jakobsen have tried several multicomponent flux models to study intraparticle diffusion in catalysts of the steam methane reforming reaction as well as low pressure methanol synthesis. Even though they established different versions of the SMM and the DGM in both the mass and molar formulations, the obtained equations were complex, due to their expression in an explicit Fickian form (Solsvik & Jakobsen, 2011).

Haberman and Young implemented Cylindrical Pore Interpolation Model (CPIM) to describe a multicomponent diffusion model in the porous structures of solid oxide fuel cells by considering the effects of the catalyzed methane reforming and water-gas shift reactions. They observed that the water-gas shift reaction has positive effects on fuel cell performance (Haberman & Young, 2006).

Lim and Dennis compared the CPIM and the dusty-gas model (DGM) for intraparticle diffusion of a non-isothermal, spherical pellet of catalyst in methanation reaction. Although in most scenarios they found minor differences between the prediction of the two theories, considerable deviations were observed when the catalyst pellet reacted at low pressure (Lim & Dennis, 2012).

Malekshahian et al. (2014) used Fick's law as their main theory of diffusion and advection with an iterative method to evaluate the diffusion limitations in the CO_2 gasification of petroleum coke and activated carbon in TGA. Using Fick's law provided a relatively good agreement with the experimental results. However, it is limited to the binary mixtures which can result in neglecting the effect of other components on the simulation.

2.3 Conclusion

In conclusion, this chapter provided background information for the gasification process as well as recent research works in this area. The influences of mass transfer on the gasification kinetics using TGA were also reviewed in this chapter. Finally, different diffusion theories for transport in the porous media were discussed and compared in the literature.

CHAPTER THREE: MODEL DEVELOPEMENT

A mathematical model is developed for the CO_2 gasification of petroleum coke and activated carbon in a thermogravimetric analyzer (TGA) using different diffusion theories. This chapter includes all the assumptions as well as the derivation of the material balances and diffusion flux equations. The effectiveness factor equations are also discussed in order to evaluate the mass transfer limitations. A numerical solution is adopted to solve the set of equations simultaneously by using MATLAB. Finally, the physical properties that were used in the calculations are summarized at the end of this chapter.

3.1 Model description and assumptions

The developed model describes the CO_2 gasification of petcoke and activated carbon, occurring in a bottom closed crucible in a thermogravimetric analyzer. The two types of feedstock were chosen because of the difference in their reactivity to demonstrate the mass transfer limitations in the system. In this model, three different zones are considered: **the gas part**, which is the stagnant gas layer at the top of the crucible; **the bed part**, which consists of fine particles at the bottom of the crucible, and **the bed surface**, which is the interface layer between the gas and the bed part. As previously mentioned in the literature review chapter, the external diffusion of the reactant gas to the surface of the solid bed takes place in the stagnant gas layer, the inter-particle and intraparticle diffusion of the gas through the bed and pores occurs in the porous solid bed. The chemical reaction is only happening in the bed part, where adsorption of reactant, surface reaction, and desorption of the products take place. The overall reaction for the CO_2 gasification of petcoke and activated carbon is considered to be:

$$C(s) + CO_2(g) \rightarrow 2CO(g) \tag{3-1}$$

which is the basic reaction of carbon and carbon dioxide. However, according to the ultimate analysis of the **petcoke**, the molar percentage of hydrogen is significant and neglecting that, may affect the results (refer to Table (2-1)). Hence, two different cases are considered here as well:

Case (1) Hydrogen gas released from the cracking reaction (equation (3-2)) does not react with the reactant gas (CO_2). Therefore, in this case, reactions (3-1) and (3-2) take place in the crucible:

$$C_nH_m(g) \rightarrow nC(g) + \frac{m}{2}H_2(g) \quad (3\text{-}2)$$

Case (2) In this case, the released hydrogen gas completely reacts with CO_2 and produces water and carbon monoxide. Water-gas shift reaction describes the reaction between the reactant gas (CO_2) and hydrogen (H_2):

$$CO_2(g) + H_2(g) \rightleftarrows H_2O(g) + CO(g) \quad (3\text{-}3)$$

On the other hand, the molar percentage of hydrogen in the **activated carbon** is negligible. In fact, carbon (C) and oxygen (O) are the main elements in the structure of activated carbon. Therefore, in **case (1)**, oxygen remains in the ash and the basic reaction of carbon and carbon dioxide (equation (3-1)) would be the only reaction happening.

In **case (2)**, for activated carbon, released oxygen (O) is assumed to react with carbon (C) or carbon monoxide (CO) and produces carbon dioxide (CO_2):

$$C(s) + 2O(s) \rightarrow CO_2(g) \quad (3\text{-}4)$$

Therefore, in both cases for activated carbon, CO_2 and CO would be the main components, and for the sake of simplicity, stoichiometric coefficients of the species in each case were implemented into the reaction term of the material balance to account for different scenarios.

Based on the literature and the configuration of the system, several assumptions have been adopted:

- Due to the configuration of the TGA reactor the reactant gas diffuses only in the z direction.
- Since the impact of turbulence on mass transfer is insignificant compared to molecular diffusion, it can be neglected inside the crucible (Malekshahian et al., 2014).
- The system is considered to be one-dimensional. Therefore, the radial dispersion of the species is neglected. (this assumption makes sense, considering the height of the bed and the diameter)
- The ideal gas law is assumed all over the system.

- n^{th} order kinetics is used to describe the gasification of carbon with carbon dioxide and the orders of the reaction for petcoke and activated carbon with CO_2 are assumed to be 0.6 and 0.8, respectively (Tyler & Smith, 1975); (Zou et al., 2007); (Wigmans et al., 1983).
- The temperature is assumed to be uniform within the bed as well as across the particle and both equal to the bed average temperature (T=1223 K). This temperature was determined from an energy balance at the bottom of the crucible based on the work of Malekshahian et al. (2014).
- Product (CO) inhibition for petcoke and activated carbon gasification is negligible.
- Particles are assumed to be porous spheres.
- In the CO_2 gasification of petcoke and activated carbon we have a small amount of other components like N_2, CH_4, etc. To simplify the calculation, the effects of other components are neglected in the code.
- Initially, there is just reactant gas (CO_2) in the crucible at the $t = 0$.

3.1.1 Geometry of the problem

The gasification reaction is performed in a closed-bottom crucible with a cylindrical body and a bottom shaped as a spherical cap. Figure (3-1) illustrates the geometry of the problem and the main features.

It is assumed that the gas part is entirely in the cylindrical part of the crucible which its radius is equal to the radius of the spherical cap ($r_s = r_C = 9\ mm$). Height of crucible (L_C) is 20 mm and maximum height of the bed is also considered for the calculations.

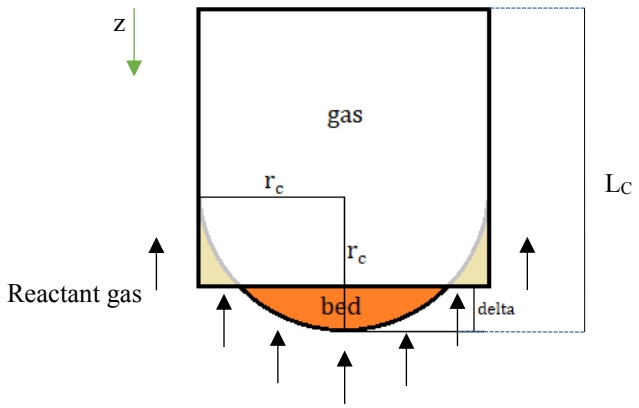

Figure 3-1. Schematic of the crucible (the gas is in the cylindrical

part of the crucible and the sample bed is in the spherical cap)

The bed height (δ) is calculated as a function of the initial mass added to the crucible. Because the bed does not have the same height as the radius of the cap, there is one part of the gas phase that is contained in the spherical cap. However, the gas part is assumed to be entirely cylindrical with the height of:

$$Height\ of\ gas\ part\ (L_g) = Height\ of\ the\ crucible\ (L_C) - Height\ of\ the\ bed\ (\delta) \quad (3\text{-}5)$$

Even though this assumption is not realistic, the effect on the results is negligible, and this approach simplifies the calculation. The radius of the crucible (r) is then calculated as a function of the depth of the crucible (z).

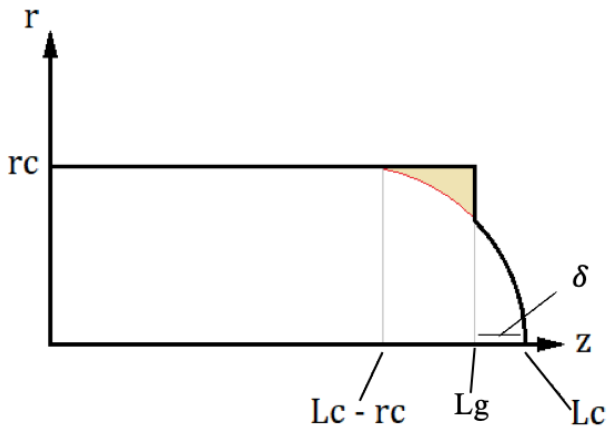

Figure 3-2. The radius of the crucible (r) as a function of its depth (z)

Thus, for all z between 0 and L_g , the radius of crucible (r) is equal to the radius of the cylindrical part of the crucible (r_c). When z (depth) is higher than L_g, r is a function of z. To determine this function, we used the equation of a sphere with the center of $((L_C - r_c), 0)$.

$$(z - z')^2 + (r - r')^2 = r_c^2$$

In the previous equation, z' and r' are the coordinates of the center of the spherical cap of the crucible, $(L_C - r_c)$ and 0, respectively. This leads to:

$$[z - (L_C - r_c)]^2 + r^2 = r_c^2$$

$$z^2 - 2z\,(L_C - r_c) + (L_C - r_c)^2 + r^2 = r_c^2$$

$$r^2 = r_c^2 - z^2 + 2\,z\,L_C - 2\,z\,r_c - L_C^2 + 2\,L_C\,r_c - r_c^2$$

$$r^2 = -(L_C - z)^2 + 2\,r_c(L_C - z)$$

Solving the equation for r :

$$r = \sqrt{2\,r_c(L_C - z) - (L_C - z)^2} \tag{3-6}$$

Equation (3-6) and Figure (3-2) show the changes of the radius (r) as a function of the depth (z), where L_C is the crucible height and r_c is the constant radius of the crucible in the cylindrical part.

3.2 Material balance

As it is mentioned, three main different zones are considered for the model. In this section, material balance equations are derived for each component in different zones. Therefore, since we are using stoichiometric coefficients to account for the production of hydrogen or water, different scenarios are summarized as below:

- Material balance in the gas part.
- Material balance in the bed part.
- Material balance in the bed surface.

3.2.1 Material balance in the gas part

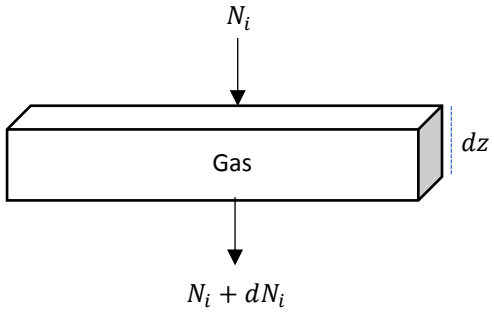

Figure 3-3. Material balance on a planar element in the gas part

The material balance in the gas part is defined on a planar element. The cross-sectional area of the crucible (A) is the same for flux going in and out of the control volume (cylindrical). Since there is no reaction in the gas part, the material balance equations for CO_2 and CO can be written as:

$$accum = in - out + gen$$

The generation term is omitted, since there is no reaction happening in the gas part:

$$V_{CV}\frac{\partial c_i}{\partial t} = N_{i_{in}}A_{in} - N_{i_{out}}A_{out}$$

$$V_{CV}\frac{\partial c_i}{\partial t} = N_i A - (N_i + dN_i)A$$

$$A\,dz\frac{\partial c_i}{\partial t} = N_i A - N_i A - A dN_i$$

Cancelling out the terms and rewriting the equation leads to:

$$\frac{\partial c_i}{\partial t} = -\frac{dN_i}{dz} \tag{3-7}$$

where V_{CV} is the volume of the element, A is the crucible cross sectional area, N_i is the flux of component i, c_i is the molar concentration of component i and z is the distance. According to the equation (3-7), the material balance in the gas part is quite simple.

3.2.2 Material balance in the bed part

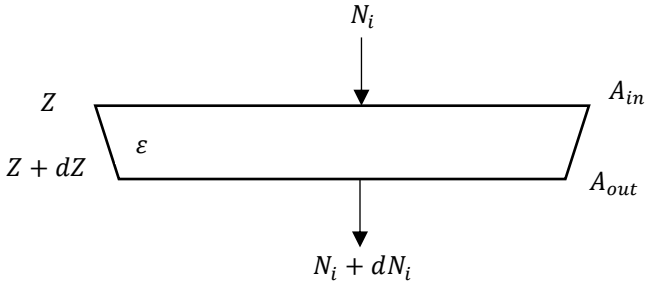

Figure 3-4. Material balance on a planar element in the porous bed

For the material balance in the bed part, the cross sectional areas of the flux going in and the flux going out of the control volume (spherical cap) are not the same anymore. Therefore, in and out areas should be determined according to their corresponding diameters from equation (3-6).
While analyzing the bed part, it is important to observe that the control volume is just the void in the bed. Thus, the accumulation can occur only in the gas phase contained in the void, with the volume of εV_{CV}. Although the reaction only happens in the solid, the reaction rate was given based on the volume of the bed (not just the solid). The material balance equations in the bed is given by:

$$accum = in - out + gen$$

Substituting each term, considering the void volume in the bed as the control volume:

$$\varepsilon\, V_{CV} \frac{\partial c_i}{\partial t} = N_i A - (N_i + dN_i)(A + dA) + (r_i)V_{CV}$$

Since the area is changing throughout the control volume, an average area is defined as:

$$A_{avg} = \frac{A_{in} + A_{out}}{2}$$

This leads to:

$$\varepsilon\, A_{avg} dz \frac{\partial c_i}{\partial t} = N_i A - N_i A - N_i dA - A dN_i - dN_i dA + (r_i)A_{avg} dz$$

The above equation simplifies to:

$$\frac{\partial c_i}{\partial t} = -\frac{d(N_i A)}{\varepsilon A_{avg} dz} + \frac{(r_i)}{\varepsilon}$$

Substituting r_i by $\upsilon_i . \overline{\eta_p} . k . c_i^n$, where υ_i is the stoichiometric coefficient of species *i* and $\overline{\eta_p}$ is the mean particle effectiveness factor:

$$\frac{\partial c_i}{\partial t} = -\frac{1}{\varepsilon A_{avg}} \frac{d(N_i A)}{dz} + \frac{\upsilon_i . \overline{\eta_p} . k . c_i^n}{\varepsilon}$$

Replacing A_{avg} and A by πr_{avg}^2 and πr^2 respectively:

$$\frac{\partial c_i}{\partial t} = -\frac{1}{\varepsilon\, \pi r_{avg}^2} \frac{d(N_i \pi r^2)}{dz} + \frac{\upsilon_i . \overline{\eta_p} . k . c_i^n}{\varepsilon}$$

$$\frac{\partial c_i}{\partial t} = -\frac{1}{\varepsilon r_{avg}^2}\left(N_i \frac{dr^2}{dz} + r^2 \frac{dN_i}{dz}\right) + \frac{v_i . \overline{\eta_p} . k . c_i^n}{\varepsilon}$$

Considering that $r = \sqrt{2\, r_c (L_C - z) - (L_C - z)^2}$ leads to:

$$r^2 = -z^2 + 2\, z\, L_C - 2\, z\, r_c - L_C^2 + 2\, L_C r_c$$

The derivative of r^2 with respect to z :

$$\frac{dr^2}{dz} = 2(-z + L_C - r_c)$$

Substituting and simplifying the equation leads to:

$$\frac{\partial c_i}{\partial t} = -\frac{1}{\varepsilon r_{avg}^2}\left(2N_{CO_2}(-z + L_C - r_c) + r^2 \frac{dN_i}{dz}\right) + \frac{v_i . \overline{\eta_p} . k . c_{CO_2}^n}{\varepsilon} \qquad (3\text{-}8)$$

As can be seen, the material balance equation in the bed is more complex than the gas part due to the variation of the crucible radius (r) and the reaction happening in the bed. It should be noted that the concentration in the last term of equation (3-8) is the CO_2 concentration regardless of the material balance.

3.2.3 Material balance in the bed surface

Modelling the bed surface layer is a challenging task since it is the interface between the gas and the bed part. In this model, the bed surface (interface layer) was treated separately from the gas and the bed part, since the concentration gradient and the flux show a break at this point. Figure (3-5) demonstrates the interface layer and the numerical method adopted to derive the material balance equations for this layer.

The overall methodology for solving the partial differential equations will be discussed in section 3.5. The overall solution method is based on finite differences and defines a number of layers separated by grid points.

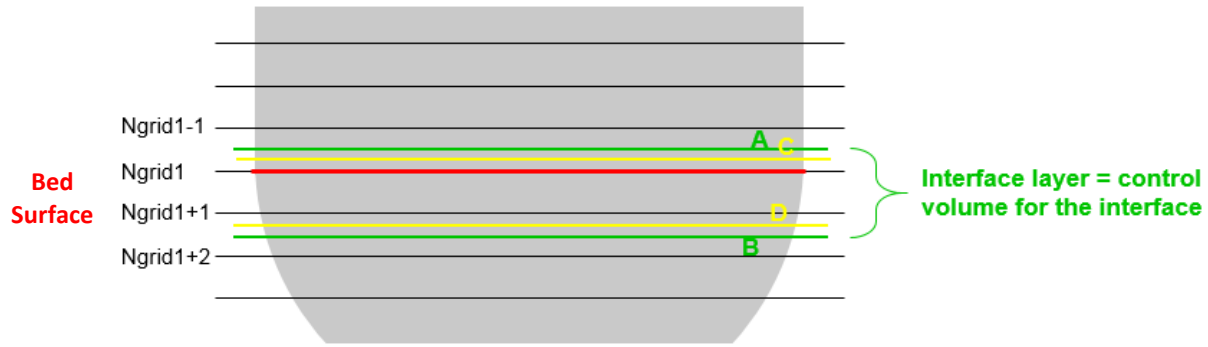

Figure 3-5. Schematic of the bed surface layer (numerical method adopted to model the interface layer)

Figure (3-5) shows the interface layer control volume and the bed surface (red line). A numerical method has been adopted to separate the interface layer. In order to numerically simulate the process. The gas and the bed part are divided into *Ngrid1* and *Ngrid2* layers (parts) respectively. Therefore, the grid point (*Ngrid1*) would be the bed surface. The grid points (*Ngrid1-1*), (*Ngrid1+1*) and (*Ngrid1+2*) are also showed in Figure (3-5). The beginning of the interface layer control volume is the average point between the grid points (*Ngrid1-1*) and (*Ngrid1*), and its end is the average point between the grid points (*Ngrid1+1*) and (*Ngrid1+2*). Green lines A and B in figure (3-5) represent the control volume for the bed surface layer. The length of each increment in the gas part is *dz1* while this length is *dz2* for the grid points inside the porous bed. However, the distance between *Ngrid1* and *Ngrid1+1* is set equal to zero, so the concentrations are the same at these grid points. However, because *Ngrid1* and *Ngrid1+1* have different cross sectional areas, they will have different fluxes.

After the geometry of the interface is completely detailed, the material balance can be developed. As it is illustrated in Figure (3-5), the material balance for the bed surface layer is applied to the specified control volume and can be written as:

$$accum = in - out + gen$$

$$V_{CV}\frac{\partial c_i}{\partial t} = N_{i_{in}}A_{in} - N_{i_{out}}A_{out} + (-r_i)V_{bed}$$

$$\left(V_g + V_{bv}\right)\frac{\partial c_i}{\partial t} = N_{i_{in}}A_{in} - N_{i_{out}}A_{out} + \left(v_i.\overline{\eta_p}.k.c_{sb}^n\right)V_b$$

$$\frac{\partial c_i}{\partial t} = \frac{N_{i_{in}}A_{in} - N_{i_{out}}A_{out} + \left(v_i.\overline{\eta_p}.k.c_{sb}^n\right)V_b}{V_g + V_{bv}} \qquad (3\text{-}9)$$

where c_{sb} is the CO_2 concentration at the bed surface. V_g, V_b and V_{bv} are volumes of the gas, bed and the void space of the bed, in the specified control volume. A_{in} and A_{out} are in and out areas that flux enters and leaves the control volume at the average points A and B and they are calculated by the following equation[6]:

$$A_{in} = \frac{\left(r^2(Ngrid1-1) + r^2(Ngrid1)\right)}{2} \tag{3-10}$$

For calculating A_{out}:

$$A_{out} = \frac{\left(r^2(Ngrid1+1) + r^2(Ngrid1+2)\right)}{2} \tag{3-11}$$

Keeping in mind that $r(Ngrid1)$ is the radius of the crucible at grid point $Ngrid1$. Now, in order to calculate the volume of the gas in the control volume (V_g), A_g is needed:

$$A_g = \frac{\frac{\left(r^2(Ngrid1-1) + r^2(Ngrid1)\right)}{2} + r^2(Ngrid1)}{2}$$

$$A_g = \frac{r^2(Ngrid1-1) + 3\,r^2(Ngrid1)}{4}$$

Since the length of each increment in the gas part is $dz1$, volume of the gas part in the interface layer can be determined as:

$$V_g = \frac{r^2(Ngrid1-1) + 3\,r^2(Ngrid1)}{4} \times \frac{dz1}{2} \tag{3-12}$$

For calculating the V_b and V_{bv} , area of the bed in the interface control volume is required:

$$A_b = \frac{\frac{\left(r^2(Ngrid1+1) + r^2(Ngrid1+2)\right)}{2} + r^2(Ngrid1+1)}{2}$$

$$A_b = \frac{3\,r^2(Ngrid1+1) + r^2(Ngrid1+2)}{4}$$

The height of the bed in the specified control volume is $\frac{dz2}{2}$. Therefore, bed and bed void volumes are calculated as follows:

[6] π cancels out in the material balance equation

$$V_b = \frac{3\,r^2(Ngrid1+1) + r^2(Ngrid1+2)}{4} \times \frac{dz2}{2} \tag{3-13}$$

$$V_{bv} = V_b \times \varepsilon \tag{3-14}$$

The fluxes entering and leaving the control volume, represented by N_{in} and N_{out}, respectively, are calculated by:

$$N_{i_{in}} = N_i(Ngrid1-1) \tag{3-15}$$

$$N_{i_{out}} = N_i(Ngrid1+1) \tag{3-16}$$

After determining each term in equation (3-9), the material balance for the interface layer is now fully specified.

3.3 Flux Equations

Now that the material balance equations for each component in the gas, bed and interface layer are specified, the flux of each component should be determined. As previously stated, different diffusion theories have been used to simulate diffusion and reaction in the gasification process. For instance, Malekshahian et al. used Fick's law to model the process (Malekshahian et al., 2014). However, in this work, different diffusion theories for the gas and the bed part have been used to model the process.

3.3.1 Case I: Fick's law – Fick's law

In this section, CO_2 and CO flux equations are obtained using Fick's law as the main theory of the diffusion and advection in both gas and the bed part. A binary mixture of CO_2 and CO is considered for this case using Fick's law. The following equations are used to determine the flux:

$$N = vc \therefore v = \frac{N}{c} \tag{3-17}$$

where N is the total flux ($N = \sum N_i$). The flux of an individual component (N_i) is calculated by:

$$N_i = vc_i + J_i \tag{3-18}$$

Replacing v by equation (3-17) and applying Fick's law of diffusion leads to:

$$N_i = \frac{N}{c} c_i - D_{ij} \frac{dc_i}{dz}$$

$$N_i = N y_i - D_{ij} \frac{dc_i}{dz}$$

Thus, for a binary mixture of CO_2 (1) and CO (2), we have:

$$N_1 = y_1(N_1 + N_2) - D_{12} \frac{dc_1}{dz}$$

$$N_2 = y_2(N_1 + N_2) - D_{21} \frac{dc_2}{dz}$$

For the present case, and in the absence of H and O in the solid, the reaction results in the following stoichiometric relation.

$$CO_2 + C \longrightarrow 2\,CO$$

$$N_{CO} = -2\,N_{CO_2} \quad or \quad N_2 = -2\,N_1$$

The flux of CO_2 can be determined as a function of CO_2 properties:

$$N_1 = y_1(N_1 - 2\,N_1) - D_{12} \frac{dc_1}{dz}$$

$$N_1 = y_1(-N_1) - D_{12} \frac{dc_1}{dz}$$

$$N_1(1 + y_1) = -D_{12} \frac{dc_1}{dz}$$

$$N_1 = -\frac{D_{12}}{1 + y_1} \frac{dc_1}{dz} \qquad (3\text{-}19)$$

Thus, the flux of CO also can be determined just as a function of CO properties.

$$N_2 = y_2(N_1 + N_2) - D_{21} \frac{dc_2}{dz}$$

$$N_2 = y_2\left(-\frac{N_2}{2} + N_2\right) - D_{21} \frac{dc_2}{dz}$$

$$N_2 = y_2\left(\frac{N_2}{2}\right) - D_{21} \frac{dc_2}{dz}$$

$$N_2\left(1 - \frac{y_2}{2}\right) = -D_{21} \frac{dc_2}{dz}$$

$$N_2 = -\frac{2\,D_{21}}{2 - y_2}\frac{dc_2}{dz} \tag{3-20}$$

3.3.2 Case II: Stefan Maxwell Model (SMM) – Dusty Gas Model (DGM)

In the case of multicomponent mixtures, Fick's law is only an approximation. Multicomponent flux diffusion theories are required to model the process accurately. In this case, the Stefan Maxwell model (SMM) is considered for the gas part and the dusty-gas model (DGM) is chosen to model the diffusion in the porous bed.

$$\frac{\partial c_i}{\partial z} = \sum_{\substack{i=1 \\ j\neq 1}}^{N} \frac{N_j c_i - N_i c_j}{c D_{ij}} \tag{3-21}$$

Equation (3-21) shows the general form of SMM equations. Due to the implicit flux equations, solving SMM equations using MATLAB is not straightforward. For instance, in the case of a three-component mixture (n=3) it leads to three equations in which only two of them are independent. Therefore, the total flux should be calculated and used as the third equation:

$$N_z = \sum_{i=1}^{N} N_{i,z} \tag{3-22}$$

In order to calculate the total flux when the pressure drop is not negligible, velocities should be calculated in each grid point, for instance, using Navier-Stokes equations. Consequently, the total flux is obtained by multiplying the velocity by the total concentration:

$$N_z = v_{s,z} c \tag{3-23}$$

In an unsteady state system, Darcy's law is used to calculate the velocity in each point using the equation below.

$$v_{s,z} = \frac{k'}{\mu}\left(-\frac{dp}{dz}\right) \tag{3-24}$$

In the previous equation, k' is the permeability. Once the total flux is available, individual fluxes can be calculated using the below set of equations:

$$-\left(\frac{y_2}{D_{12}}+\frac{y_3}{D_{13}}\right)N_1+\frac{y_1}{D_{12}}N_2+\frac{y_1}{D_{13}}N_3=c\frac{\partial y_1}{\partial z} \tag{3-25}$$

$$\frac{y_2}{D_{12}}N_1-\left(\frac{y_1}{D_{12}}+\frac{y_3}{D_{23}}\right)N_2++\frac{y_2}{D_{23}}N_3=c\frac{\partial y_2}{\partial z} \tag{3-26}$$

$$N_1+N_2+N_3=N \tag{3-27}$$

The above set of equations with three equations and three unknowns is solved to determine the fluxes. Note that, subscript 1 refers to CO_2, subscript 2 refers to CO and subscript 3 refers to H_2 or H_2O.

On the other hand, in the bed part, as the pore diameter is getting narrow, molecule-wall collision becomes more frequent and Knudsen diffusion becomes more significant. The dusty-gas model is chosen to model the diffusion and reaction in the porous bed. Based on the conventional formulation of the DGM for a three-component mixture:

$$-\left(\frac{1}{D_{1,K}}+\frac{y_2}{D_{12}}+\frac{y_3}{D_{13}}\right)N_1+\frac{y_1}{D_{12}}N_2+\frac{y_1}{D_{13}}N_3=\frac{p}{RT}\frac{\partial y_1}{\partial z}+\frac{y_1}{RT}\frac{\partial p}{\partial z}(1+\frac{B_0p}{\mu D_{1,K}}) \tag{3-28}$$

$$\frac{y_2}{D_{12}}N_1-\left(\frac{y_1}{D_{12}}+\frac{1}{D_{2,K}}+\frac{y_3}{D_{23}}\right)N_2+\frac{y_2}{D_{23}}N_3=\frac{p}{RT}\frac{\partial y_2}{\partial z}+\frac{y_2}{RT}\frac{\partial p}{\partial z}(1+\frac{B_0p}{\mu D_{2,K}}) \tag{3-29}$$

$$\frac{y_3}{D_{13}}N_1+\frac{y_3}{D_{23}}N_2-\left(\frac{y_1}{D_{13}}+\frac{y_2}{D_{23}}+\frac{1}{D_{3,K}}\right)N_3=\frac{p}{RT}\frac{\partial y_3}{\partial z}+\frac{y_3}{RT}\frac{\partial p}{\partial z}(1+\frac{B_0p}{\mu D_{3,K}}) \tag{3-30}$$

where B_0 in equations (3-28), (3-29) and (3-30) is a fitting parameter about the porous medium's permeability and in the slip-flow regime ($0.01 < Kn < 0.1$), it is calculated by the following equation:

$$B_0=\frac{\mu D_{i,k}^{eff}}{p}(\frac{p\varepsilon D^2(1+4Kn)}{32\tau\mu D_{i,K}^{eff}}-1) \tag{3-31}$$

In equation (3-31) μ is the viscosity of the mixture, $D_{i,k}^{eff}$ is the effective Knudsen diffusion coefficient, ε is the porosity, D is the pore diameter, Kn is the Knudsen number and τ is the tortuosity.

The above set of equations with three equations and three unknowns is solved simultaneously to determine the individual fluxes.

3.3.3 Case III: Stefan Maxwell Model (SMM) – Cylindrical Pore Interpolation Model (CPIM)

CPIM, with clearer assumptions and a compact set of equations, provides a potentially better treatment for the transitional flow. In the last case, the DGM is replaced by the CPIM to model the diffusion in the porous solid bed, whereas the SMM remained the same in the gas part. According to the research of Young and Todd (2005), the original equation of the CPIM is presented as below (Young & Todd, 2005):

$$\frac{dy_j}{dz} = \frac{\tau^2 R_g T}{\varepsilon p} \sum_{i=1}^{N} \left[\frac{y_j J_i}{D_{A,ij}} - \frac{y_i J_j}{D_{A,ji}}\right] \tag{3-32}$$

$$\frac{dp}{dz} = -\frac{\tau^2 A_A}{\varepsilon} \sum_{i=1}^{n} M_i^{\frac{1}{2}} J_i \tag{3-33}$$

A_A and D_A are the CPIM parameters and they can be obtained by the following equations:

$$\frac{1}{D_{A,ij}} = \frac{1}{D_{i,K}} + \frac{1}{D_{ij}} \tag{3-34}$$

$$\frac{1}{A_A} = \frac{1}{A_K} + \frac{1}{A_C} \tag{3-35}$$

where $D_{K,i}$ and D_{ij} are the Knudsen diffusivity and the molecular diffusivity, respectively. A_K and A_C in equation (3-35) are calculated using the following equations:

$$A_K = \frac{3}{4R_{pore}} \left(\frac{\pi R_g T}{2}\right)^{\frac{1}{2}} \tag{3-36}$$

$$A_C = \frac{8\mu}{cR_{Pore}^2 \sum_{i=1}^{N} X_i M_i^{\frac{1}{2}}} \tag{3-37}$$

It should be noted that, $(n-1)$ equations from equation (3-32) are independent of each other. Thus, in order to solve the problem by CPIM, one of the equations from equation (3-32) is replaced by equation (3-33).

In the case of 3 components, considering $N_i = J_i$, the flux equations can be written as below:

$$\left(-\frac{\tau^2}{\varepsilon}\left(\frac{y_2}{D_{A,12}}+\frac{y_3}{D_{A,13}}\right)\right)N_1+\left(\frac{\tau^2}{\varepsilon}\left(\frac{y_1}{D_{A,21}}\right)\right)N_2+\left(\frac{\tau^2}{\varepsilon}\left(\frac{y_1}{D_{A,31}}\right)\right)N_3 = c\frac{\partial y_1}{\partial z} \tag{3-38}$$

$$\left(\frac{\tau^2}{\varepsilon}\left(\frac{y_2}{D_{A,12}}\right)\right)N_1+\left(-\frac{\tau^2}{\varepsilon}\left(\frac{y_1}{D_{A,21}}+\frac{y_3}{D_{A,23}}\right)\right)N_2+\left(\frac{\tau^2}{\varepsilon}\left(\frac{y_2}{D_{A,32}}\right)\right)N_3 = c\frac{\partial y_2}{\partial z} \tag{3-39}$$

$$\left(-\frac{\tau^2}{\varepsilon}\,A_A M_1^{\frac{1}{2}}\right)N_1+\left(-\frac{\tau^2}{\varepsilon}\,A_A M_2^{\frac{1}{2}}\right)N_2+\left(-\frac{\tau^2}{\varepsilon}\,A_A M_3^{\frac{1}{2}}\right)N_3 = \frac{dp}{dz} \tag{3-40}$$

N_1 , N_2 and N_3 are found by solving the above set of ordinary differential equations numerically in MATLAB.

3.4 Effectiveness Factors

The effectiveness factor, which is typically described as a function of the Thiele modulus, is defined as the reaction rate considering diffusion limitations over the reaction rate at the bulk conditions. Determining the Thiele modulus which is described as the ratio of the surface reaction rate to the rate of diffusion requires information about the intrinsic rate constant. In this work, the intrinsic rate used in the modelling was obtained from experimental results from the literature (Malekshahian et al., 2014).

In this section, effectiveness factor equations are obtained in three different diffusion steps:

- Particle and mean particle effectiveness factor ($\eta_p, \overline{\eta_p}$)
- Bed effectiveness factor (η_b)
- External effectiveness factor (η_e)

By determining the effectiveness factor in each step, it is possible to obtain the bed reaction rate and the overall reaction rate from the intrinsic reaction rate.

3.4.1 Particle and Mean Particle Effectiveness Factor

The intrinsic reaction rate in the absence of intraparticle diffusion can be written as:

$$R_V = k c_{sp}^n \tag{3-41}$$

where k is the intrinsic rate constant, c_{sp} is the concentration of the particle surface and n is the reaction order. However, the presence of the pores in the porous sphere particles causes diffusion limitations. The particle effectiveness factor, which is defined as the ratio of the particle overall reaction rate $(R'_{V,p})$ to the intrinsic reaction rate of the particle (R_V), can be used to account for the diffusion limitations inside the particle. Equations (3-42) and (3-43) are used to determine the particle effectiveness factor (η_p) as well as the Thiele modulus (θ_p) for porous spheres particles (Walker et al., 1959); (Laurendeau, 1978); (Malekshahian et al., 2014):

$$\eta_p = \frac{3}{\theta_p}\left(\frac{1}{\tan\theta_p} - \frac{1}{\theta_p}\right) \tag{3-42}$$

And θ_p can be obtained by:

$$\theta_p = \frac{d}{6}\sqrt{\frac{(n+1)\, k' c_{sp}^{n-1}}{2\, D_p^{eff}}} \tag{3-43}$$

D_p^{eff} is the general effective diffusion coefficient in the particle and d is the average particle diameter. It should be noted that the use of Thiele modulus to calculate the diffusion limitations is due to the significance of Knudsen diffusion inside the particle (refer to section 4.2.1). Knudsen diffusion follows Fick's law in a fixed frame of reference, which is consistent with the assumptions underlying equation (3-42). Nevertheless, the reactant gas diffuses through the pores within the bed, causing a CO_2 concentration gradient to reach the external surface of the particles. Therefore, at a specific height in the bed, the particle surface concentration (c_{sp}) is equal to the CO_2 concentration in the bed (c_b). That expresses the dependence of the particle effectiveness factor (η_p) to the bed height (z). Thus, the mean particle effectiveness factor is defined throughout the bed as the ratio of the integrals of the reaction rate considering and neglecting the intraparticle limitations.

$$\overline{\eta_p} = \frac{\int_0^{\delta} k'\, c_{sp}^n\, \eta_p\, dz}{\int_0^{\delta} k'\, c_{sp}^n\, dz} \tag{3-44}$$

In the model presented here, the intraparticle diffusion limitations are taken into account by implementing the mean particle effectiveness factor into the intrinsic reaction rate. Therefore the overall reaction rate (the rate affected by the diffusion limitations) of the particle is given by:

$$R'_{V,p} = \overline{\eta_p}\, k c_{sp}^n \tag{3-45}$$

3.4.2 Bed effectiveness factor

In this study, it was assumed that the sample bed is a homogeneous porous flat plate with a rate constant of $\eta_p \,.\, k$ in reaction with CO_2. In order to calculate the bed effectiveness factor, the flux of CO_2 to the bed must be calculated. Based on the definition, bed effectiveness factor (η_b) is equal to the ratio of actual reaction rate considering diffusion limitations to the reaction rate if CO_2 concentration was equal to the surface concentration.

$$\eta_b = \frac{\frac{1}{\delta} \int_0^{\delta} k\, \eta_p\, c_b^n dz}{k.\overline{\eta_p}.c_{sb}^n} \tag{3-46}$$

In equation (3-46), δ is the bed height, k is the intrinsic rate constant, n is the reaction order, c_{sb} is the concentration at the bed surface, and c_b is the local concentration of CO_2 in the bed. The numerator of the equation (3-46) represents the reaction rate considering diffusion limitations in the particle and bed, whereas the denominator shows the reaction rate if the concentration of CO_2 was equal to the surface concentration in the bed. The overall reactant gas consumption in the bed can be obtained by:

$$R'_{V,b} = \overline{\eta_p}\, \eta_b\, k c_{sb}^n \tag{3-47}$$

3.4.3 External effectiveness factor

At the beginning of this chapter, the external diffusion of the reactant gas (CO_2) from the top of the crucible to the surface of the solid bed was mentioned. There is a CO_2 concentration gradient between the surface of the bed and the mouth of the crucible in the stagnant gas layer. The flux of

CO_2 is constant in this zone since there is no reaction happening. In order to determine the external effectiveness factor, the rate when the CO_2 concentration is the concentration at the bed surface (c_{sb}) should be divided by the rate if the CO_2 concentration were the concentration of the bulk flow (c_0). Hence, it can be obtained by:

$$\eta_e = \left(\frac{c_{sb}}{c_0}\right)^n \tag{3-48}$$

where c_{sb} is the concentration of CO_2 at the bed surface, c_0 is the concentration at the bulk and n is the reaction order. Eventually, the overall reaction rate can be written as:

$$R'_V = \overline{\eta_p}\,\eta_b \eta_e k\, c_0^n \tag{3-49}$$

3.5 Numerical solution method

The numerical solution for the material balance in the bed surface was discussed in section 3.2.3. In this section, the numerical solution of the other parts of the system will be discussed. The impact of mass transfer in the system was evaluated by solving equations (3-6) to (3-49) simultaneously and calculating the effectiveness factors. The CO_2 concentration profile should be known to determine the effectiveness factors in each diffusion step. In this work, a numerical s (3-50) method has been adopted using MATLAB ODE 15s to solve the set of ordinary differential equations. This integration method (ODE 15s) is usually used for stiff sets of differential equations and it features a variable step size (De Visscher 2019). The MATLAB implementation of the current problem consists of two files: Firstly, **the main file** (`main.m`), where the variables and the constants are defined as well as the numerical integration function and output of the results. Secondly, **the function file (**`f.m`**)**, where the differential equations are defined**.** The concentration gradients were resolved numerically using the finite difference method. In this method, *Ngrid1* and *Ngrid2* grid points were used to divide the length of the gas and the bed part to *Ngrid1-1* increments of *dz1* and *Ngrid2-1* increments of *dz*2, respectively. According to the central finite difference method, the first and second-order derivatives of the concentration on grid point "*n*" can be written as:

$$\frac{\partial c_n}{\partial z} \approx \frac{-c_{n-1} + c_{n+1}}{2\Delta z} \tag{3-50}$$

$$\frac{\partial^2 c_n}{\partial z^2} \approx \frac{c_{n-1} - 2c_n + c_{n+1}}{(\Delta z)^2} \tag{3-51}$$

where the concentrations $(c_1, c_2, c_3, \dots, c_n)$ are defined on the grid points $(z_1, z_2, z_3, \dots, z_n)$ and $\Delta z = (z_2 - z_1) = (z_3 - z_2) = \cdots$. Due to instability problems, the correct use of these grid points is important in modeling the multicomponent diffusion. Calculating the flux between each two consecutive grid points is one way to avoid the instability of the algorithm.

3.6 Physical properties

The physical properties of petcoke and activated carbon particles and the sample bed used in our calculations are provided in Table (3-1). This table is for the petcoke particle size of less than 90 μm and the bed at 1273 *K*.

Table 3-1. physical properties of unreacted petcoke and act. carbon and the sample bed (Malekshahian et al.l, 2014)

	Properties	Equation	Petcoke	Act. Carbon
Particle	Average particle diameter (d)	-	45×10^{-6} m	1.3×10^{-3} m
	Density (ρ)	-	1.4×10^{6} g/m^3	0.4×10^{6} g/m^3
	Pore diameter (D)	BJH equation	2.8×10^{-8} m	2.9×10^{-9} m
	Pore volume	BJH equation	1.6×10^{-8} m^3/g	0.39×10^{-6} m^3/g
	Porosity (ε_p)	$\frac{pore\ volume}{total\ volume}$	0.06	
	Tortuosity(τ_p)	$\tau = 1 - 0.5\ln(\varepsilon)$	2.4	
Bed	Bed diameter	-	19×10^{-3} m	19×10^{-3} m
	Bulk density(ρ_b)	-	0.7×10^{6} g/m^3	0.3×10^{6} g/m^3

Pore diameter (D)	$d_b = \frac{2}{3}\left(\frac{\varepsilon}{1-\varepsilon}\right) d$	3×10^{-5} m	0.288×10^{-3} m
Porosity (ε_b)	$\varepsilon = 1 - \frac{\rho_b}{\rho}$	0.5	0.25
Tortuosity (τ_b)	$\tau = 1 - 0.5\ln(\varepsilon)$	1.3	1.6931

3.6.1 Diffusivities and Tortuosity

The binary diffusion coefficients were determined using the Fuller method. For instance, the binary diffusion coefficient of CO_2 and CO at 0.1 MPa was calculated using the equation below (Malekshahian et al., 2014); (Fuller et al., 1966):

$$D_{CO_2-CO} = 1.39 \times 10^{-5}\left(\frac{T}{273.2}\right)^{1.75} \quad (m^2/s) \tag{3-52}$$

In the case of three components in the system (water or hydrogen) the pseudo-binary diffusion coefficient of CO_2 was obtained by:

Case (1)

$$D_{CO_2,m} = \frac{1 + 1.27x_{CO_2}}{\frac{x_{CO} + 2x_{CO_2}}{D_{CO_2-CO}} + \frac{x_{H_2} + \frac{7}{26}x_{CO_2}}{D_{CO_2-H_2}}} \tag{3-53}$$

Case (2)

$$D_{CO_2,m} = \frac{1 + x_{CO_2}}{\frac{x_{CO} + \frac{59}{33}x_{CO_2}}{D_{CO_2-CO}} + \frac{x_{H_2O} + \frac{7}{33}x_{CO_2}}{D_{CO_2-H_2O}}} \tag{3-54}$$

The correction of these coefficients due to the change in the pressure was obtained using the following equation (De Visscher, 2019).

$$D_{ij,p} = D_{ij,p_{ref}} \times \frac{p_{ref}}{p} \tag{3-55}$$

Tortuosity value is a function of the porous media characteristics such as porosity, pore diameter, channel shape, etc. The bed tortuosity was calculated using the following equation (Malekshahian et al., 2014); (Delgado, 2006):

$$\tau = 1 - 0.5 \ln(\varepsilon) \tag{3-56}$$

The Knudsen diffusion coefficient in the gases was calculated using the equation below.

$$D_{i,K} = \frac{D}{3}\sqrt{\frac{8\,R\,T}{\pi\,M_i}} \tag{3-57}$$

In this equation, D is the pore diameter, R is the gas constant, T is temperature and M_i is the molecular weight expressed in kg/mol. The Knudsen diffusion prevailed in the char particle due to the narrower pores, whereas the molecular diffusion prevails in the bed because of the wider pores.

The general effective diffusivity in the porous media can be obtained by the kinetic theory model which is the inverse of the sum of the inverses of the effective binary and Knudsen diffusivities (Gibilaro, 1970).

$$\frac{1}{D^{eff}} = \frac{1}{D_{ij}^{eff}} + \frac{1}{D_{i,K}^{eff}} \tag{3-58}$$

It is important to consider that, in porous media, the effective diffusivities are determined by multiplying the molecular diffusivity by the porosity and divided by the tortuosity:

$$D_{ij}^{eff} = D_{ij,p} \times \frac{\varepsilon}{\tau} \tag{3-59}$$

$$D_{i,K}^{eff} = D_{i,K} \times \frac{\varepsilon}{\tau} \tag{3-60}$$

3.6.2 Viscosity of the mixture

The viscosity of each component in the mixture is calculated by:

$$\mu_i = \mu_c \cdot a\left(1 - \exp\left(-b\left(\frac{T}{n_c T_c}\right)^{n_1}\right)\right)\left(\frac{T}{n_c T_c}\right)^{n_2} \tag{3-61}$$

where *a, b,* n_1 and n_2 are the empirical constants and equal to 1.37369, 1.30184, 0.65455 and 0.61732 respectively. μ_c , n_c and T_c are the critical properties of the component (De Visscher,

2019). After determining the viscosity of each component, the viscosity of the mixture is calculated using Wilke (1950) equation (Poling et al., 2001); (De Visscher, 2019):

$$\mu = \sum_{i=1}^{n} \frac{y_i \mu_i}{\sum_{j=1}^{n} y_j \emptyset_{ij}} \tag{3-62}$$

where:

$$\emptyset_{ij} = \frac{\left(1 + \left(\frac{\mu_i}{\mu_j}\right)^{\frac{1}{2}} \left(\frac{M_j}{M_i}\right)^{\frac{1}{4}}\right)^2}{\left(8\left(1 + \frac{M_i}{M_j}\right)\right)^{\frac{1}{2}}} \tag{3-63}$$

y_i shows the molar fraction of component i, M_i is the molar mass of component i and n is the number of components in the mixture.

3.6.3 Bed height

The bed height for different initial masses can be calculated using equation (3-64) by assuming the bed as a spherical cap with the height of (δ) and the volume of (V_{cap}):

$$V_{cap} = \frac{m_0}{\rho_b} = \frac{\pi . \delta^2 . (3 \times r_c - \delta)}{3} \tag{3-64}$$

Therefore, the bed height (δ) can be found for any given initial mass of the sample (m_0) by solving the equation (3-64) for (δ), where ρ_b is the density of the bulk and r_c is the radius of the crucible.

3.7 Key equations

The key equations used in the MATLAB implementation of the presented model are summarized in Table 3-2.

Table 3-2. Key equations in the model

Equation Number	Equation	Description
(3-6)	$r = \sqrt{2\, r_c(L_C - z) - (L_C - z)^2}$	Radius of crucible (r) as a function of its depth (z) in bed
(3-7)	$\frac{\partial c_i}{\partial t} = -\frac{dN_i}{dz}$	material balance in the gas part
(3-8)	$\frac{\partial c_i}{\partial t} = -\frac{1}{\varepsilon r_{avg}^2}\left(2N_{CO_2}(-z + L_C - r_c) + r^2\frac{dN_i}{dz}\right) + \frac{v_i.\overline{\eta_p}.k.c_{CO_2}^n}{\varepsilon}$	material balance in the bed part
(3-9)	$\frac{\partial c_i}{\partial t} = \frac{N_{i_{in}}A_{in} - N_{i_{out}}A_{out} + \left(v_i.\overline{\eta_p}.k.c_{sb}^n\right)V_b}{V_g + V_{bv}}$	Material balance in the bed surface
(3-19)	$N_1 = -\frac{D_{12}}{1 + y_1}\frac{dc_1}{dz}$	Flux equations for CO_2 and CO using **Fick's law**
(3-20)	$N_2 = -\frac{2\, D_{21}}{2 - y_2}\frac{dc_2}{dz}$	
(3-25)	$-\left(\frac{y_2}{D_{12}} + \frac{y_3}{D_{13}}\right)N_1 + \frac{y_1}{D_{12}}N_2 + \frac{y_1}{D_{13}}N_3 = c\frac{\partial y_1}{\partial z}$	**Stefan maxwell** model equations for the presented model
(3-26)	$\frac{y_2}{D_{12}}N_1 - \left(\frac{y_1}{D_{12}} + \frac{y_3}{D_{23}}\right)N_2 + + \frac{y_2}{D_{23}}N_3 = c\frac{\partial y_2}{\partial z}$	
(3-27)	$N_1 + N_2 + N_3 = N$	
(3-28)	$-\left(\frac{1}{D_{1,K}} + \frac{y_2}{D_{12}} + \frac{y_3}{D_{13}}\right)N_1 + \frac{y_1}{D_{12}}N_2 + \frac{y_1}{D_{13}}N_3 = \frac{p}{RT}\frac{\partial y_1}{\partial z} + \frac{y_1}{RT}\frac{\partial p}{\partial z}(1 + \frac{B_0 p}{\mu D_{1,K}})$	**Dusty-gas model** equations for the presented model
(3-29)	$\frac{y_2}{D_{12}}N_1 - \left(\frac{y_1}{D_{12}} + \frac{1}{D_{2,K}} + \frac{y_3}{D_{23}}\right)N_2 + \frac{y_2}{D_{23}}N_3 = \frac{p}{RT}\frac{\partial y_2}{\partial z} + \frac{y_2}{RT}\frac{\partial p}{\partial z}(1 + \frac{B_0 p}{\mu D_{2,K}})$	
(3-30)	$\frac{y_3}{D_{13}}N_1 + \frac{y_3}{D_{23}}N_2 - \left(\frac{y_1}{D_{13}} + \frac{y_2}{D_{23}} + \frac{1}{D_{3,K}}\right)N_3 = \frac{p}{RT}\frac{\partial y_3}{\partial z} + \frac{y_3}{RT}\frac{\partial p}{\partial z}(1 + \frac{B_0 p}{\mu D_{3,K}})$	
(3-31)	$B_0 = \frac{\mu D_{i,k}^{eff}}{p}(\frac{p\varepsilon D^2(1 + 4Kn)}{32\tau\mu D_{i,K}^{eff}} - 1)$	Fitting parameter in dusty-gas model

(3-38)	$\left(-\frac{\tau^2}{\varepsilon}(\frac{y_2}{D_{A,12}}+\frac{y_3}{D_{A,13}})\right)N_1+\left(\frac{\tau^2}{\varepsilon}(\frac{y_1}{D_{A,21}})\right)N_2+\left(\frac{\tau^2}{\varepsilon}(\frac{y_1}{D_{A,31}})\right)N_3 = c\frac{\partial y_1}{\partial z}$	**CPIM** equations for the presented model
(3-39)	$\left(\frac{\tau^2}{\varepsilon}(\frac{y_2}{D_{A,12}})\right)N_1+\left(-\frac{\tau^2}{\varepsilon}(\frac{y_1}{D_{A,21}}+\frac{y_3}{D_{A,23}})\right)N_2+\left(\frac{\tau^2}{\varepsilon}(\frac{y_2}{D_{A,32}})\right)N_3 = c\frac{\partial y_2}{\partial z}$	
(3-40)	$\left(-\frac{\tau^2}{\varepsilon}A_A M_1^{\frac{1}{2}}\right)N_1+\left(-\frac{\tau^2}{\varepsilon}A_A M_2^{\frac{1}{2}}\right)N_2+\left(-\frac{\tau^2}{\varepsilon}A_A M_3^{\frac{1}{2}}\right)N_3 = \frac{dp}{dz}$	
(3-42)	$\eta_p = \frac{3}{\theta_p}\left(\frac{1}{\tan\theta_p}-\frac{1}{\theta_p}\right)$	Particle effectiveness factor
(3-43)	$\theta_p = \frac{d}{6}\sqrt{\frac{(n+1)\,k' c_{sp}^{n-1}}{2\,D_p^{eff}}}$	Thiele Modulus
(3-44)	$\overline{\eta_p} = \frac{\int_0^\delta k'\,c_{sp}^n\,\eta_p\,dz}{\int_0^\delta k'\,c_{sp}^n\,dz}$	Mean particle effectiveness factor
(3-45)	$R'_{V,p} = \overline{\eta_p}\,k c_{sp}^n$	Particle overall reaction rate
(3-46)	$\eta_b = \frac{\frac{1}{\delta}\int_0^\delta k\,\eta_p\,c_b^n dz}{k.\overline{\eta_p}.c_{sb}^n}$	Bed effectiveness factor
(3-47)	$R'_{V,b} = \overline{\eta_p}\,\eta_b\,k c_{sb}^n$	Bed overall reaction rate
(3-48)	$\eta_e = \left(\frac{c_{sb}}{c_0}\right)^n$	External effectiveness factor
(3-49)	$R'_V = \overline{\eta_p}\eta_b\eta_e k\,c_0^n$	Overall reaction rate
(3-50)	$\frac{\partial c_n}{\partial z} \approx \frac{-c_{n-1}+c_{n+1}}{2\Delta z}$	Numerical first and second order derivatives
(3-51)	$\frac{\partial^2 c_n}{\partial z^2} \approx \frac{c_{n-1}-2c_n+c_{n+1}}{(\Delta z)^2}$	

3.8 Chapter summary and conclusions

This chapter described the mathematical model for the CO_2 gasification of petroleum coke and activated carbon in a TGA. Assumptions, material balances, flux equations and effectiveness factors were also discussed. Eventually, the numerical model and the physical properties were summarized at the end of this chapter.

CHAPTER FOUR: RESULTS AND DISCUSSION

The simulation results for modeling the CO_2 gasification of petroleum coke and activated carbon in a thermogravimetric analyzer (TGA) are presented in this chapter. These results were obtained by solving a set of ordinary differential equations simultaneously using MATLAB. In this chapter, the mole fraction profile of CO_2 within the crucible is compared among the various cases. The influence of intraparticle, inter-particle and external diffusion on the overall rate of the reaction is also discussed. Eventually, after studying the effect of initial mass on the modeling, the model is validated with the experimental work of Malekshahian et al. (2014).

4.1 CO_2 mole fraction profile

The concentration profile of CO_2 in the bed is required to evaluate the diffusion limitations on the overall reaction rate by calculating the effectiveness factors. Figures (4-1) to (4-8) show the CO_2 mole fraction profile within the crucible as a function of its depth. Petcoke and activated carbon have a significant difference in their reactivity, and they are used in this study to show the diffusion limitations. As a reference, the results were compared to the model of Malekshahian et al. (2014). They used four different initial masses of the sample (25 mg, 50 mg, 100 mg and 150 mg) in their modeling with the temperature of 1223 K and atmospheric pressure. In this section, however, the initial mass of 150 mg was used due to the highest mass transfer limitations expected at this mass compared to the others. It is worth mentioning that the primary goal of this section is to compare the CO_2 mole fraction profile in different case studies and to evaluate the diffusion limitations for the two samples. Therefore, various cases are summarized below[7]:

- **FICK'S CASE-A**[8]: Using **Fick's law** for a binary mixture as the main theory of diffusion and advection for both gas and the bed part for **petcoke**.
- **FICK'S CASE-B**: Using **Fick's law** for a binary mixture as the main theory of diffusion and advection for both gas and the bed part for **activated carbon**.

[7] For convenience, unique names are chosen for different case studies.
[8] The first term represents the diffusion theory used in the modeling; A and B stand for petcoke and activated carbon, respectively; and 1 and 2 show the case "1" or "2" for the multicomponent flux theories.

- **DGM CASE-A1**: Modelling the multicomponent diffusion for the gas and the bed part using the **Stefan Maxwell model** (SMM) and the **dusty-gas model** (DGM), respectively, considering **case (1)** for **petcoke** (hydrogen production).
- **DGM CASE-B1**: Modelling the multicomponent diffusion for the gas and the bed part using the **SMM** and the **DGM,** respectively, considering **case (1)** for **activated carbon** (not releasing the oxygen).
- **DGM CASE-A2**: Modelling the multicomponent diffusion for the gas and the bed part using the **SMM** and the **DGM**, respectively, considering **case (2)** for **petcoke** (water production).
- **DGM CASE-B2**: Modelling the multicomponent diffusion for the gas and the bed part using the **SMM** and the **DGM**, respectively, considering **case (2)** for **activated carbon** (releasing the oxygen).
- **CPIM CASE-A1**: Using **SMM** for the gas part and **cylindrical pore interpolation model** (CPIM) for the bed part to model the multicomponent diffusion, considering the **case (1)** for **petcoke** (hydrogen production).
- **CPIM CASE-B1**: Using **SMM** for the gas part and **CPIM** for the bed part to model the multicomponent diffusion, considering the **case (1)** for **activated carbon** (not releasing the oxygen).
- **CPIM CASE-A2**: Using **SMM** for the gas part and **CPIM** for the bed part to model the multicomponent diffusion, considering the **case (2)** for **petcoke** (water production).
- **CPIM CASE-B2**: Using **SMM** for the gas part and **CPIM** for the bed part to model the multicomponent diffusion, considering the **case (2)** for **activated carbon** (releasing the oxygen).

4.1.1 Case I: Fick's law - Fick's law

In this case, Fick's law, as the simplest diffusion theory, was used to model the diffusion and advection in the gas and the bed part for a binary mixture of CO_2 and CO. The simulation results in comparison with the literature are shown below.

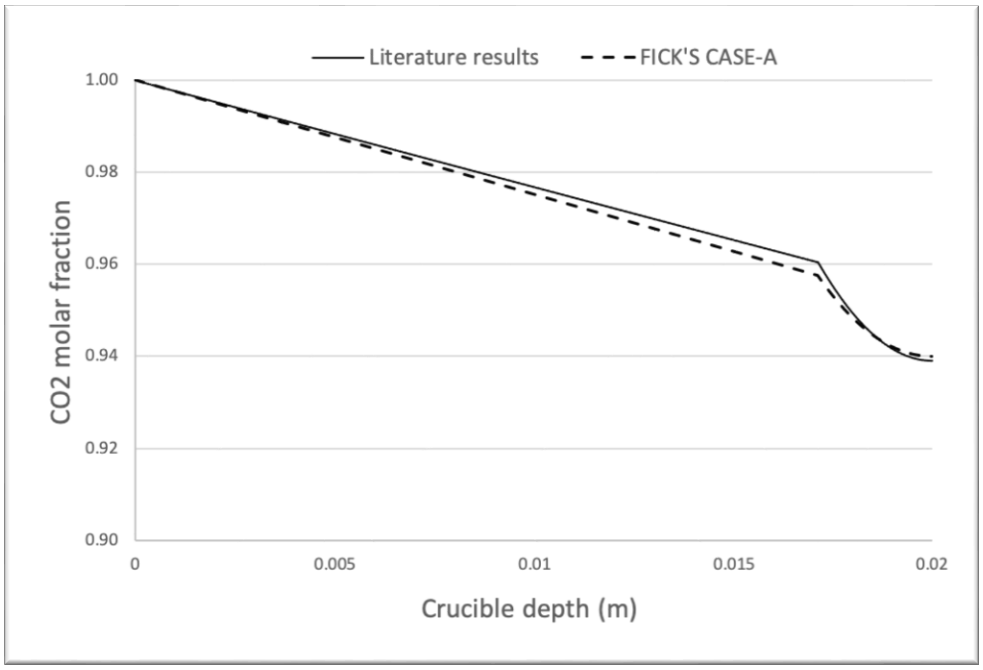

Figure 4-1. CO_2 mole fraction profile for petcoke as a function of the crucible depth, using Fick's law compared to the results of Malekshahian et al. (2014)

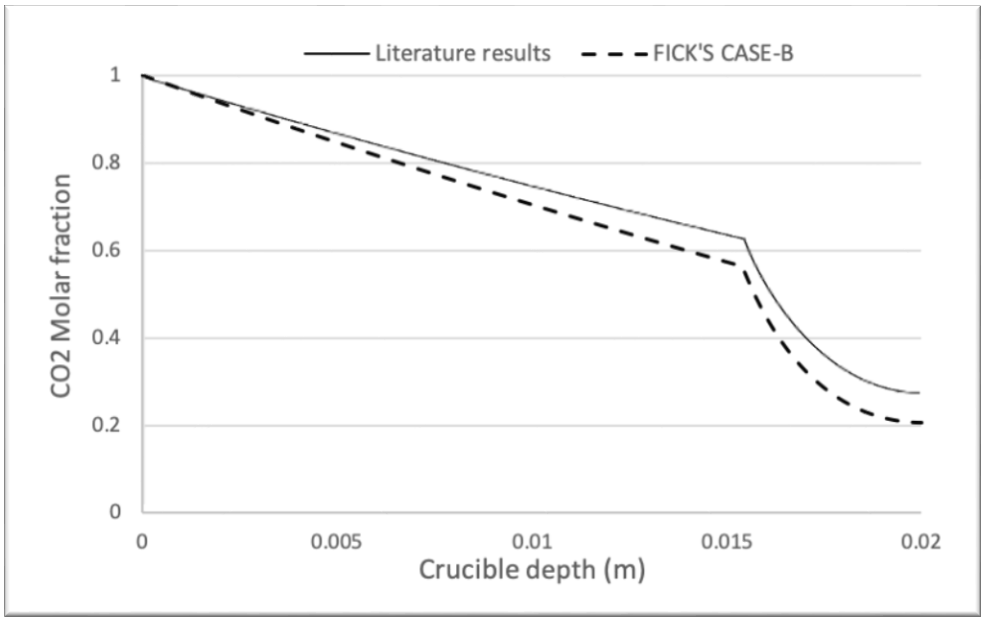

Figure 4-2. CO_2 mole fraction profile for activated carbon as a function of the crucible depth, using Fick's law compared to the results of Malekshahian et al. (2014)

Figures (4-1) and (4-2) show the CO_2 mole fraction profile within the crucible for petcoke and activated carbon in comparison with the work of Malekshahian et al. (2014) both using Fick's law. As can be seen, the mole fraction of CO_2 slightly decreases through the gas part. Then, there is a sudden drop in the concentration by reaching the bed surface in the solid part. This dramatic

decrease is due to the reaction happening in the bed and inter-particle and intraparticle diffusion limitations.

Both models predict almost the same behaviour for the mole fraction profile of CO_2. However, the presented model here tends to show a lower profile than Malekshahian's model. It can be due to the different numerical methods used in the modeling or the difference in the operating conditions despite efforts to use the same conditions in the simulation as the literature. For instance, the heat transfer was considered in the literature model, whereas it is not included in the model developed here. It should be noted, for activated carbon, which is the more reactive sample, the difference between the two models is even more pronounced. This shows that the diffusion limitation has more effect on the more reactive component and should be considered in the kinetic studies.

4.1.2 Case II: Stefan Maxwell model (SMM) – dusty gas model (DGM)

As mentioned in the previous chapter, neglecting hydrogen and oxygen in petcoke and activated carbon may affect the results. Unlike the previous section, a multicomponent diffusion flux theory is considered here to model the CO_2 gasification of the chosen samples in TGA in two different cases.

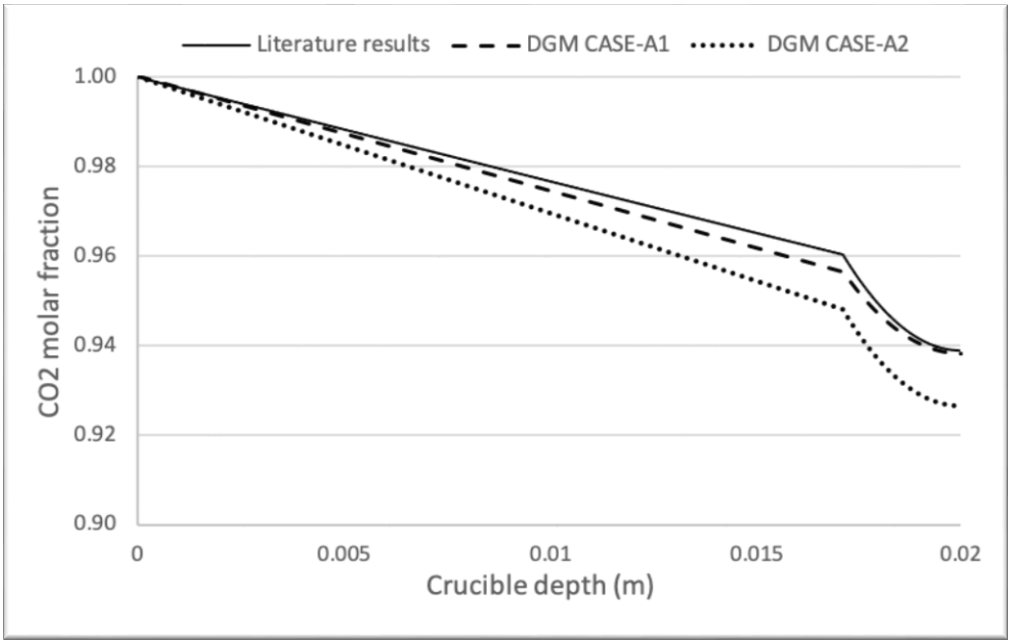

Figure 4-3. CO_2 mole fraction profile for petcoke as a function of the crucible depth, using SMM-DGM compared to the results of Malekshahian et al. (2014)

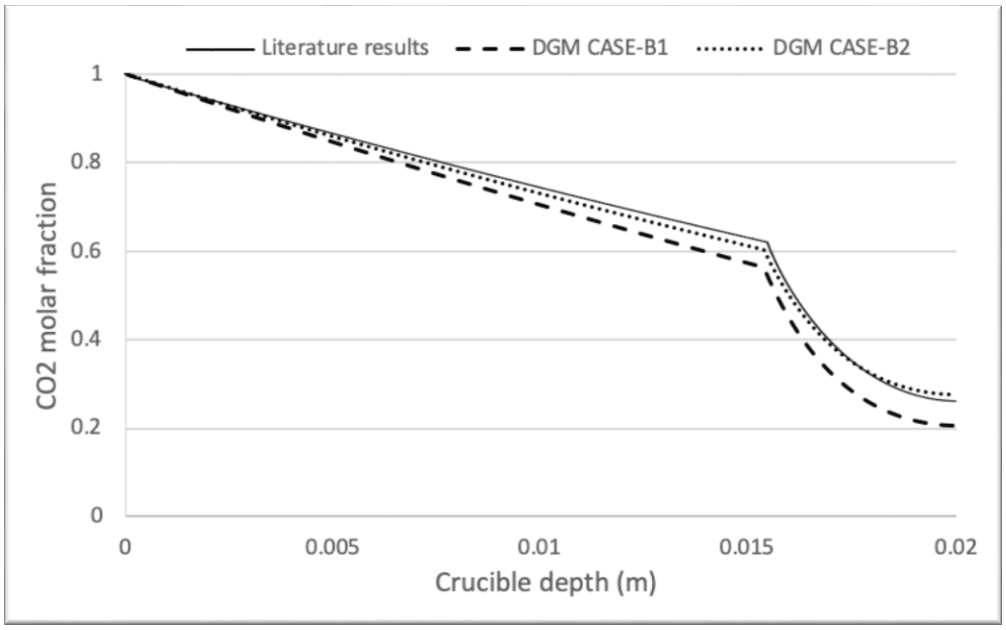

Figure 4-4. CO_2 mole fraction profile for activated carbon as a function of the crucible depth, using SMM-DGM compared to the results of Malekshahian et al. (2014)

Figures (4-3) and (4-4) compare the mole fraction profile of CO_2 for petcoke and activated carbon, considering a multicomponent mixture using the Stefan-Maxwell equations to model the diffusion in the gas part and the dusty-gas model in the bed part, to the results of Malekshahian et al. (2014). Looking more closely at the figures, considering a multicomponent mixture reveals a level of uncertainty in the simulation results.

For petcoke, case (1) which considers H_2 as the third component, leads to concentration profiles very similar to binary diffusion. This is because H_2 has a much higher diffusivity than CO or CO_2. So, its concentration remains low and the impact on the diffusion of CO and CO_2 is minimal. On the other side, the production of water which is case (2) for this sample, has more influence on the gradient of CO_2 and shows a lower profile than the other two. Case (2), for activated carbon, estimates a higher mole fraction profile than case (1). This is due to the release of oxygen in the activated carbon which diffuses against the flux of CO_2, causing an increase of CO_2 gradient.

However, the more realistic scenario would be something between case (1) and (2) for each sample. For instance, in the CO_2 gasification of petcoke, the release of hydrogen gas may neither be the real case nor the production of the water. Therefore, the more realistic case would be the combination of these two cases.

4.1.3 Case III: Stefan Maxwell model (SMM) – cylindrical pore interpolation model (CPIM)

CPIM is one of the most recent multicomponent diffusion flux theories developed by Young and Todd, (2005). In this section, the dusty-gas model from the previous section is replaced by the CPIM model to test its applicability to the presented model here. The results are demonstrated below:

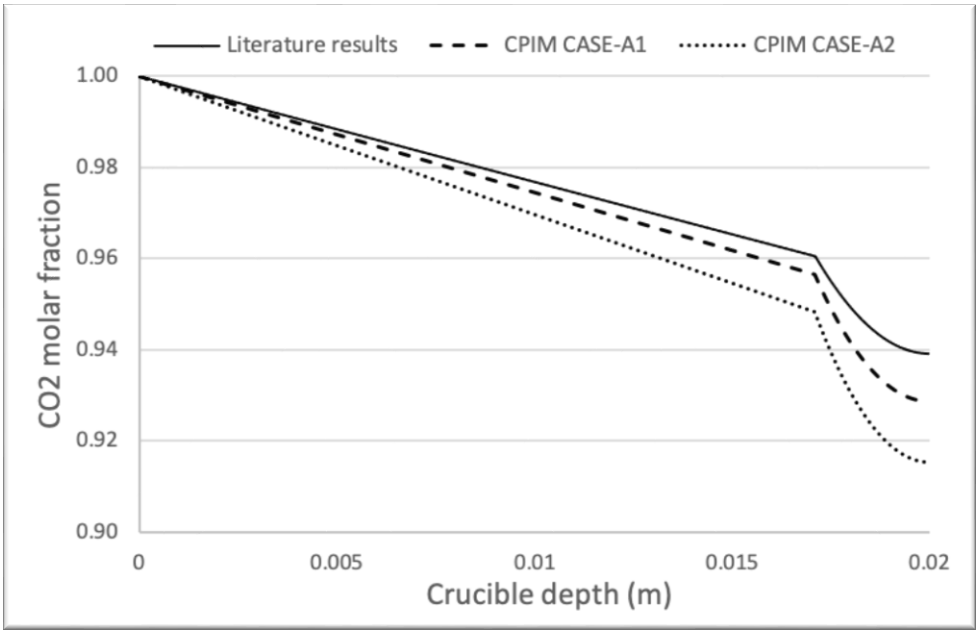

Figure 4-5. CO_2 mole fraction profile for petcoke as a function of the crucible depth, using SMM-CPIM compared to the results of Malekshahian et al. (2014)

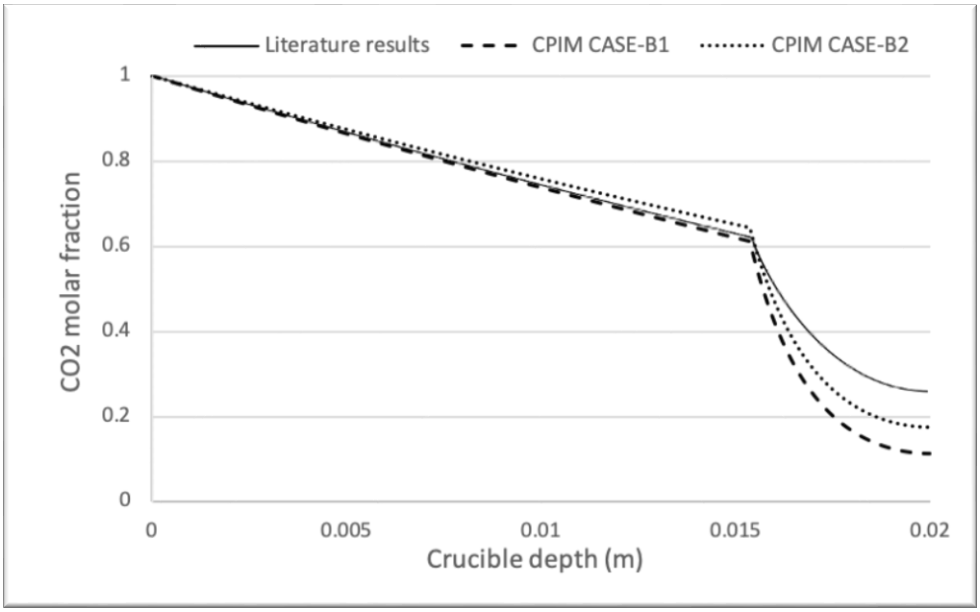

Figure 4-6. CO_2 mole fraction profile for activated carbon as a function of the crucible depth, using SMM-CPIM compared to the results of Malekshahian et al. (2014)

Before discussing the results, it is worth noting that, CPIM provides a potentially better treatment for the transitional flow ($0.1<Kn<10$). Transitional flow is the condition where molecular diffusion and Knudsen diffusion are of the same order of magnitude. In other words, the number of molecule-molecule collisions is of the same order of magnitude as molecule-wall collisions. This does not mean it necessarily outperforms the DGM or other multicomponent flux theories. In fact, each diffusion flux theory works well in a particular situation.

According to Figure (4-5), for petcoke, the diffusion limitation predicted by the model is higher than the literature prediction and slightly higher than the dusty-gas model results (section 4.1.2). Similar to the previous section, the predicted mole fraction profile for case (2) is lower than case (1). For activated carbon, again, the difference between case (1) and case (2) is more pronounced, and the diffusion limitation is greater in the case of the CPIM than in the case of the dusty-gas model.

4.1.4 Comparison of different diffusion theories

In this section, the CO_2 mole fraction profile of different cases for each sample are compared. Studying all of the cases with different diffusion theories (multicomponent or binary) in one figure can give valuable information.

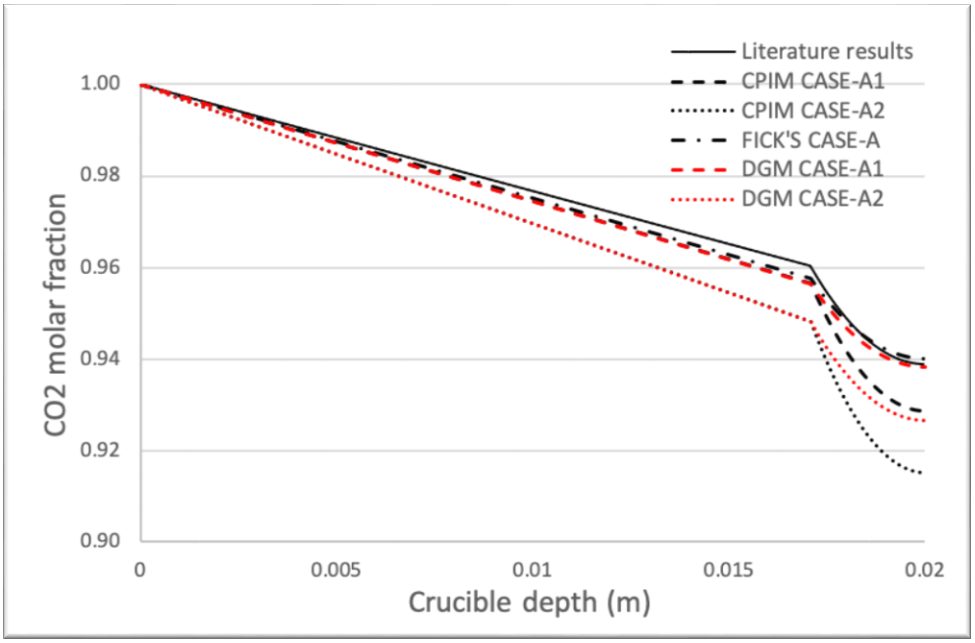

Figure 4-7. CO_2 mole fraction profile for petcoke as a function of the crucible depth,

comparing all diffusion models to the results of Malekshahian et al. (2014)

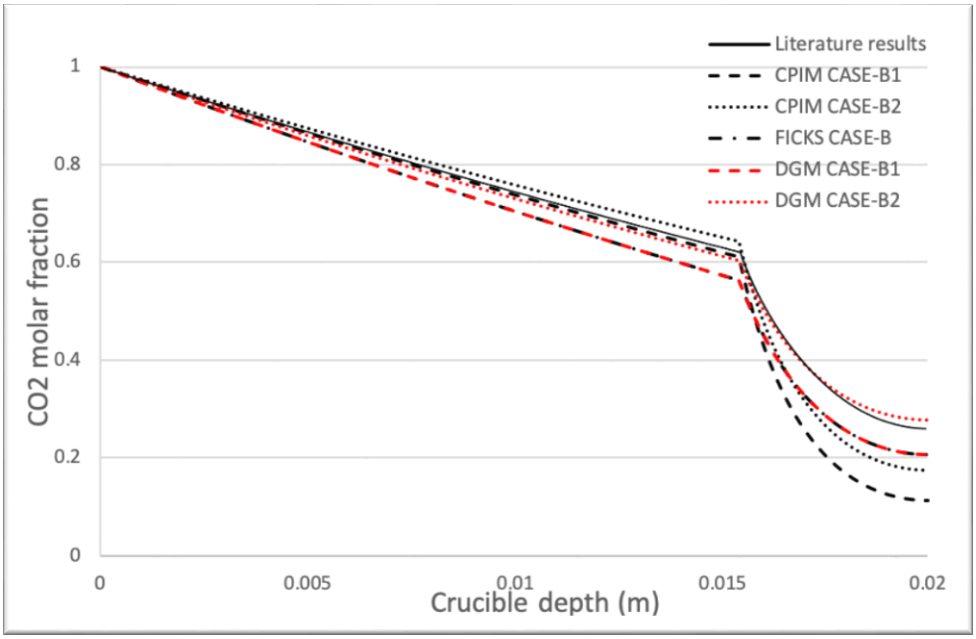

Figure 4-8. CO_2 mole fraction profile for activated carbon as a function of the crucible depth, comparing all diffusion models to the results of Malekshahian et al. (2014)

As previously explained, each diffusion theory works best in a particular condition. For example, the dusty-gas model predicts the diffusion behaviour of a porous media in slip-flow regime or CPIM provides a potentially better treatment for transitional flow (Evans et al., 1961); (Evans et al., 1962); (Young & Todd, 2005). Therefore, the purpose of this study is to find an appropriate diffusion theory that describes the diffusion limitations of gasification in TGA in the best agreement with the experimental results.

From Figures (4-7) and (4-8), it is observed that Fick's law and the dusty-gas model lead to similar results, whereas the CPIM model leads to more pronounced concentration gradients in both petcoke and activated carbon. Because the regime is slip-flow, where the DGM model is expected to be more accurate. It follows that the CPIM model likely overestimates diffusion limitation.

Comparing figures (4-7) and (4-8), once again, proves that the diffusion limitations are more important for the more reactive component. For petcoke, the concentration of CO_2 drops to 0.915 and for activated carbon it decreases to 0.13. Almost all the diffusion theories, for both samples, predict more diffusion limitations than literature in the porous bed except for DGM case (2) for activated carbon. This indicates that Fick's law (assuming binary diffusion), which is the most

common approach in gasification studies, underestimates the actual diffusion limitation. The CPIM also estimates more diffusion limitations in both samples compared to the other theories.
In order to support the calculations and to evaluate our assumptions, Knudsen numbers in different diffusion steps are calculated for petcoke and activated carbon in the next section (refer to section 4.2).

4.2 Effect of different diffusion steps on the overall rate

In the model development chapter, the effectiveness factor equations for intraparticle, inter-particle and external diffusion were derived to evaluate the mass transfer limitations. Each diffusion step has its own effect on the overall reaction rate. In this part, in addition to evaluating the effect of different diffusion steps on the overall rate, Knudsen numbers are also compared to support the calculations and the assumptions. These effectiveness factors are compared for petcoke and activated carbon samples with the same initial mass of 150 mg and a particle size of less than 90 μm for petcoke. Atmospheric pressure and the temperature of 1223 K is chosen for the operating conditions.

4.2.1 Intraparticle diffusion

The porous structure of the sphere particles causes mass transfer limitations in diffusing the reactant gas through the pores into the particle. Thiele modulus and mean particle effectiveness factor evaluate these limitations by using equations (3-42), (3-43) and (3-44) in the previous chapter. By looking more closely to these equations, we realize that these numbers depend on the particle diameter, the diffusion coefficient (which is a factor of the temperature and pressure) and the concentration on the surface of the particle which at the same height is equal to the bed concentration. Since changing the operating conditions and particle diameter were not the purpose of this study, the only variable changing here is the concentration on the surface of the particle. Considering the scale of particles when compared to the size of bed the concentration gradient inside the particle is negligible. Therefore, in the presented model here, the mean particle effectiveness factor is constant for all cases for each sample at the same operating conditions and particle diameter.
As discussed in the previous chapter, using the Thiele modulus to calculate the intraparticle mass transfer limitations is appropriate because of the Knudsen regime inside the particle. In order to

prove that, Knudsen numbers are calculated in this section. This dimensionless number is the ratio of the mean free path of the molecule (λ) to the pore diameter (D). The intraparticle Knudsen number specifies weather the molecular or Knudsen diffusion are predominant inside the particle. For instance, particle pore diameter (D) for petcoke is equal to $2.8 \times 10^{-8}\ m$ and the mean free path of CO_2 molecules is $\lambda = 4.49324 \times 10^{-7}\ m$. So, the intraparticle Knudsen number is equal to 16.0473 ($Kn > 10$) which indicates pure Knudsen regime. That means where molecule-wall collisions are more frequent than molecule-molecule collisions. For activated carbon, the intraparticle Knudsen number is even higher than petcoke due to the narrower particle pores ($D = 2.9 \times 10^{-9}\ m$). Therefore, for both samples, all diffusion theories are simplified to Knudsen diffusion inside the particle and the Thiele modulus is a proper way to model the intraparticle diffusion.

For petcoke, with particle size less than 90 μm, the overall rate of the reaction is free from the intraparticle diffusion limitations and $\overline{\eta_p} = 1$, which is the same among different diffusion models. That means the particle reaction rate is equal to the particle intrinsic reaction rate, which is a result of the negligible concentration gradient inside the particle.

As an example, the Thiele modulus and particle effectiveness factor calculations for petcoke particles at the bed surface are shown below. After substituting all the parameters in equation (3-43), the particle Thiele modulus (θ_p) is equal to:

$$\theta_p = \frac{d}{6}\sqrt{\frac{(n+1)\,k' C_{sp}^{n-1}}{2\,D_p^{eff}}} = 4.4122 \times 10^{-4} \tag{3-43}$$

Therefore, the particle effectiveness factor for particles at the surface of the bed is equal to:

$$\eta_p = \frac{3}{\theta_p}\left(\frac{1}{\tan\theta_p} - \frac{1}{\theta_p}\right) = 1 \tag{3-42}$$

Since the Thiele modulus (θ_p) is a small number, η_p is equal to 1 for all the particles in the bed. Therefore, the mean particle effectiveness factor ($\overline{\eta_p}$) which is the average of η_p throughout the bed is equal to 1, showing that the intraparticle diffusion is negligible for petcoke particles less than 90 μm.

However, for the more reactive sample, activated carbon, intraparticle diffusion becomes more significant, but it still has minor effects on the overall rate of the reaction. The mean particle

effectiveness factor value for activated carbon particles is 0.9996. It is due to the larger particle diameter (d) and higher rate constant (k') in equation (3-43), which increases the Thiele modulus ($\theta_p = 0.0767$, $\eta_p = 0.9996$ for particles at the bed surface), showing more diffusion limitations inside the activated carbon particles.

In summary, for both activated carbon and petcoke, the mean particle effectiveness factors at the conditions of this model are higher than 0.99. That means intraparticle diffusion plays a minor role in the diffusion limitations of this model.

4.2.2 Inter-particle diffusion

The bed effectiveness factor, calculated in section (3.4.2) of the previous chapter, evaluates the mass transfer limitations in diffusing the reactant gas thorough the porous bed. For petcoke, the reactant gas experiences a slip-flow regime ($0.01 < Kn = 0.0150 < 0.1$) within the bed because of the slightly wider pores in the bed ($D = 3 \times 10^{-5}$). In slip-flow regime, there is no effects of the finite mean free path on the fluid, but the molecules collide the wall at an angle, causing a non-zero velocity of the gas at the wall. For activated carbon, there is a continuum flow in the bed, due to the wider pores ($D = 0.288 \times 10^{-3}$), which means molecule-molecule collisions are more frequent and molecular diffusion is predominant.

Figure (4-9) shows the bed effectiveness values for different cases in comparison with the results of Malekshahian et al. (Malekshahian et al., 2014).

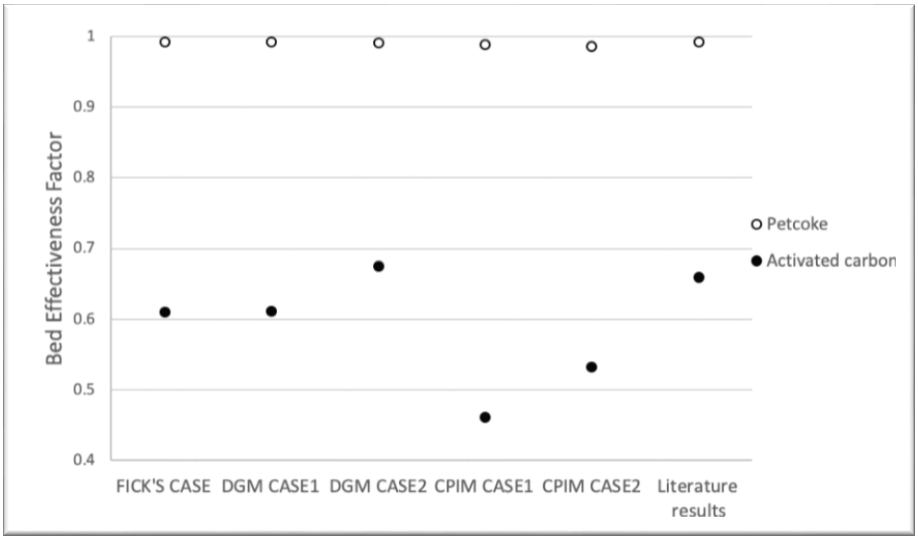

Figure 4-9. Comparison of the bed effectiveness factors for different cases with the literature results (Malekshahian et al., 2014)

The bed effectiveness factor shows the ratio of the actual reaction rate, considering diffusion limitations in the bed, to the reaction rate at the bed surface. The numbers for the less reactive sample, petcoke, range around 0.99 which shows less diffusion limitations in the bed. For activated carbon, inter-particle diffusion is much more significant, and it ranges between 0.5 and 0.7. Again, for the more reactive sample, diffusion limitations play a more important role and should be considered in the kinetic studies. In addition to the higher reactivity of activated carbon, the lower porosity and higher tortuosity of the activated carbon in the bed causes additional diffusion limitations.

For petcoke, almost all the diffusion theories predict a bed effectiveness factor of 0.99. SMM-DGM case (1) and Fick's case are the closest ones to the literature results (Malekshahian et al., 2014). On the other side, for activated carbon, the bed effectiveness factor predicted by different models varies between 0.46 and 0.67. SMM-DGM case (2) has the closest results to the literature. The numbers predicted by the model tend to show more diffusion limitations than Malekshahian's model in the case of petcoke. It may be due to the consideration of reaction products other than CO, which have to move out of the bed, and leads to more diffusion limitations in the bed. In particular, when the reaction product is water vapor (case (2)), the counter diffusion has a pronounced effect on diffusion limitation. In the case of activated carbon, the release of oxygen atoms (case (2)) causes more weight loss in the solid relative to the molecular flux. In other words, the same weight loss of the solid bed can be explained with a smaller molar flux, and hence with less diffusion limitation.

4.2.3 External diffusion

There is a stagnant gas layer between the mouth of crucible and the bed surface. The diffusion limitation in this layer is evaluated by the external effectiveness factor. Keeping in mind that, the stagnant gas layer is in continuum regime due to the pure molecular diffusion in this zone. Figure (4-10) compares the external effectiveness factor values in different cases to the model of Malekshahian et al. (2014).

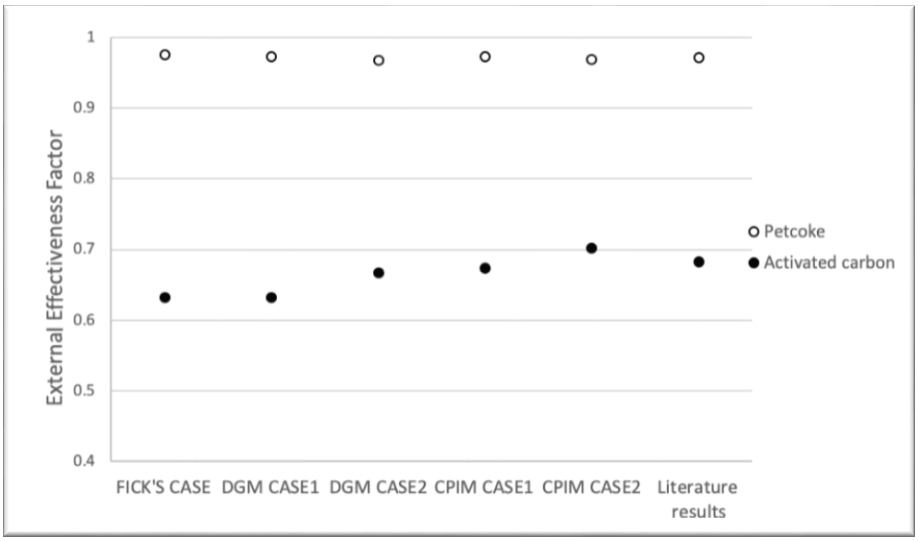

Figure 4-10. Comparison of the external effectiveness factors for different cases with the literature results (Malekshahian et al., 2014)

For petcoke, external diffusion is predominant on the overall rate of the reaction. The external effectiveness factor values range between 0.97 to 0.98, which indicates more diffusion limitations in the stagnant gas layer than the porous bed and the particle. However, for activated carbon, external and inter-particle diffusion are in the same order of magnitude, which means they have almost the same effect on the overall rate of the reaction. The external effectiveness factor is defined as the ratio of reactant gas concentration at the surface of the bed to the concentration at bulk. Since the bulk concentration is not a changing value in different case studies, the difference in this factor is due to the variation of CO_2 concentration at the bed surface. For instance, in Figure (4-10), CPIM case (2) predicts the highest concentration of CO_2 at the bed surface compared to the other theories.

Briefly, although for petcoke all the effectiveness factors are above 0.9, and have minor effects on the overall rate, the external diffusion prevails more than other diffusion steps. Almost all the diffusion theories were able to predict the effectiveness factors in a good agreement with the literature results.

4.3 Effect of initial mass on the modeling

External and inter-particle diffusion are affected by the initial mass of the sample. This effect is evaluated for different case studies in comparison with the modeling results of Malekshahian et al. (2014). In section 4.4, the model variants will be compared to the experimental data. Figures (4-

11) to (4-14) show the bed and external effectiveness factor as a function of initial mass for petcoke and activated carbon.

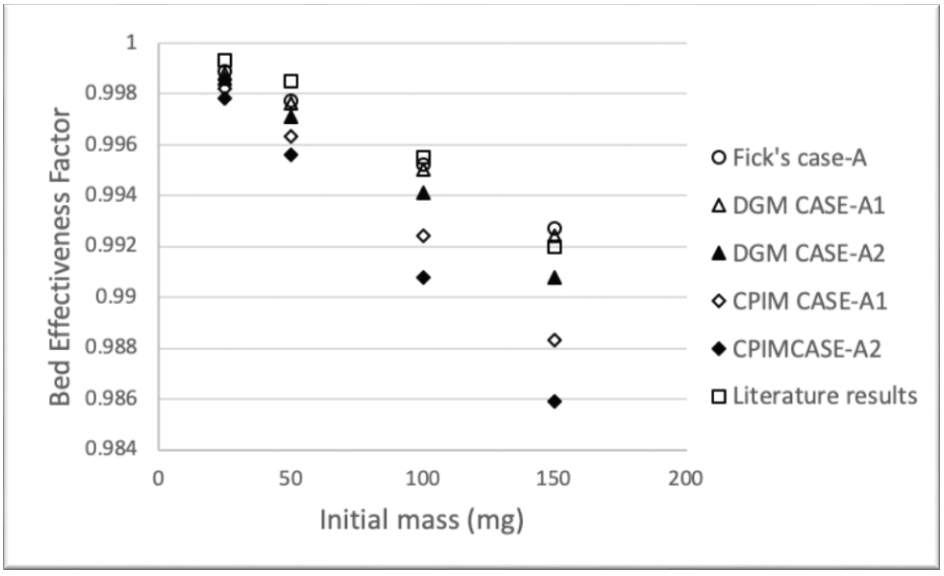

Figure 4-11. Variation of the bed effectiveness factor as a function of initial mass for different cases compared to the modeling results of Malekshahian et al. (2014) for petcoke

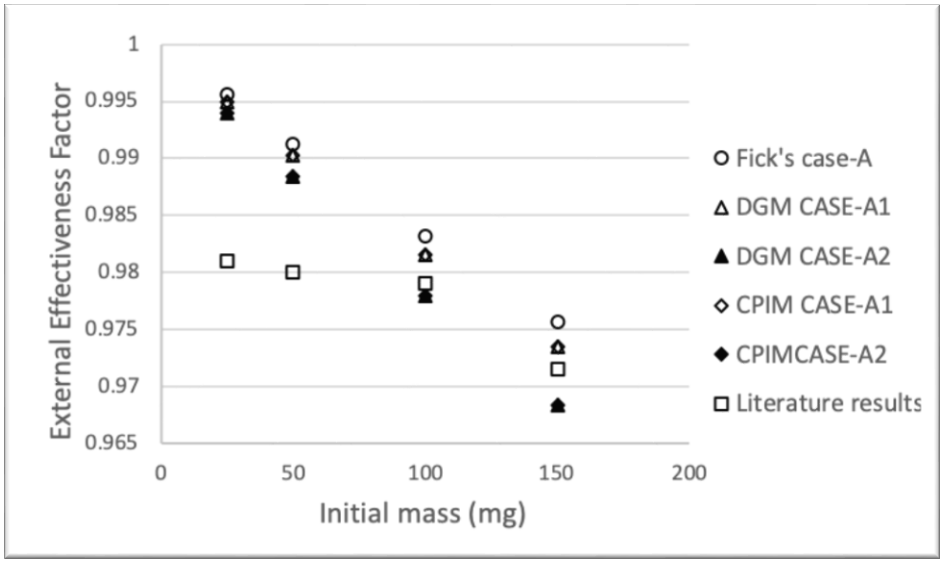

Figure 4-12. Variation of the external effectiveness factor as a function of initial mass for different cases compared to the modeling results of Malekshahian et al. (2014) for petcoke

Initial mass of the sample along with the other variables such as temperature and particle size influence the overall rate of the gasification in TGA. For petcoke, the effectiveness factors are smaller for higher initial masses in all of the cases. That means more diffusion limitations in the

bed and stagnant gas layer by increasing the initial mass of the sample. However, this decrease is clearer for the external effectiveness factor.

Both bed and external effectiveness factors are above 0.95 for all the diffusion theories and different initial masses. The bed effectiveness factor decreases from 0.998 for 25 mg to 0.986 for 150 mg. This decrease is due to the deficient supply of the reactant gas (CO_2) in the bed, as for higher initial mass of the sample, more gas is consumed, causing an increased concentration gradient (Malekshahian et al., 2014).

The external effectiveness factor, which changes more significantly, reduces from 0.995 to 0.968. As stated, the external effectiveness factor is described as the concentration of the reactant gas at the bed surface, to the concentration at bulk. So, due to the same bulk concentration for different cases and various initial masses, this factor varies with the concentration at the bed surface. Thus, the CO_2 concentration at the bed surface is higher for smaller masses.

The predictions of the different diffusion theories are closer in the case of small initial masses (25 mg and 50 mg), and they diverge as the mass increases. In the case of a greater mass (such as 150 mg), maximum diffusion limitation is expected. Therefore, this is the most challenging mass for the proposed model to evaluate the diffusion limitations.

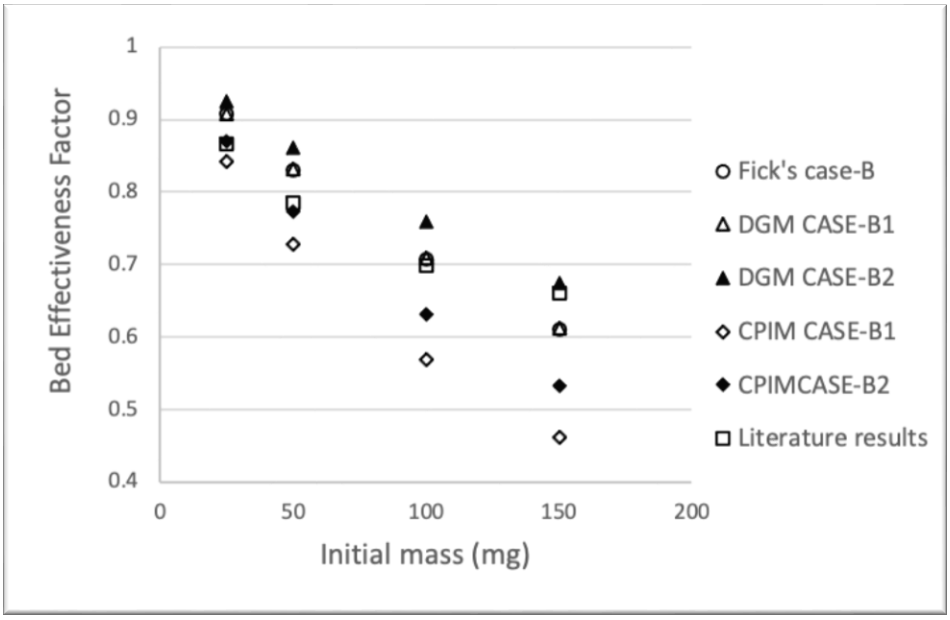

Figure 4-13. Variation of the bed effectiveness factor as a function of initial mass for different cases compared to the modeling results of Malekshahian et al. (2014) for activated carbon

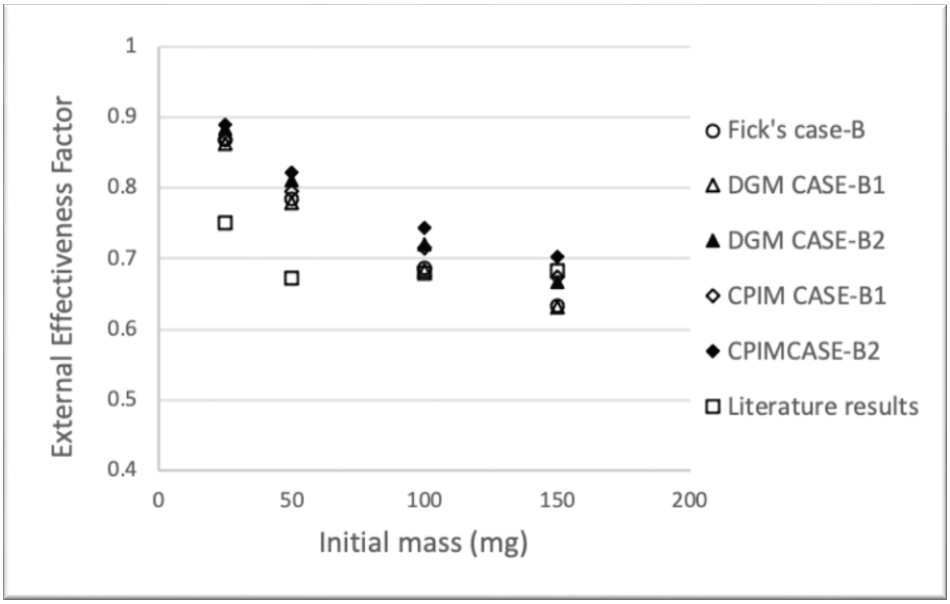

Figure 4-14. Variation of the external effectiveness factor as a function of initial mass for different cases compared to the modeling results of Malekshahian et al. (2014) for activated carbon

By increasing the initial mass of activated carbon sample, the effectiveness factors tend to decrease with a steeper slope than petcoke. Once again, this proves the impact of diffusion limitations on the more reactive component and the essence of considering it.

There is more divergence between the models for the bed effectiveness factor than for the external effectiveness factor. It is due to the use of various diffusion theories in the bed part, whereas the same theory (Stefan-Maxwell diffusion) is used in the gas phase for both the DGM cases and the CPIM cases. External effectiveness factor for activated carbon has a minimum value of 0.63 for the initial mass of 150 mg. As it is already explained, the external effectiveness factor is varied by the surface bed concentration whereas the bed effectiveness factor depends on the reactant gas concentration gradient in the bed.

Comparing the results of the presented model to the work of Malekshahian et al. (2014), their model shows less change in the bed and external effectiveness factor by varying the initial mass compared to the model presented here.

4.4 Model validation

In order to validate the proposed model, the overall reaction rates in various initial masses for activated carbon are compared to the experimental data of Malekshahian et al. (2014). They

determined the reaction rate of consumption of CO_2 for activated carbon in a flow-through crucible[9] in which the intraparticle diffusion limitation was the only mass transfer limiting step. Because the intraparticle diffusion limitation is negligible, this leads to an intrinsic rate constant. Hence, if this intrinsic rate constant is used, and the calculated external and inter-particle effectiveness factor by the model are applied, the predicted reaction rate should be the same as the reaction rate determined in the closed-bottom crucible. Figure (4-15) compares the experimental reaction rate observed in the CO_2 gasification of activated carbon in a closed-bottom crucible at 1223 K to the reaction rate determined from the model of Malekshahian et al. and the reaction rate calculated by the presented model for various initial masses.

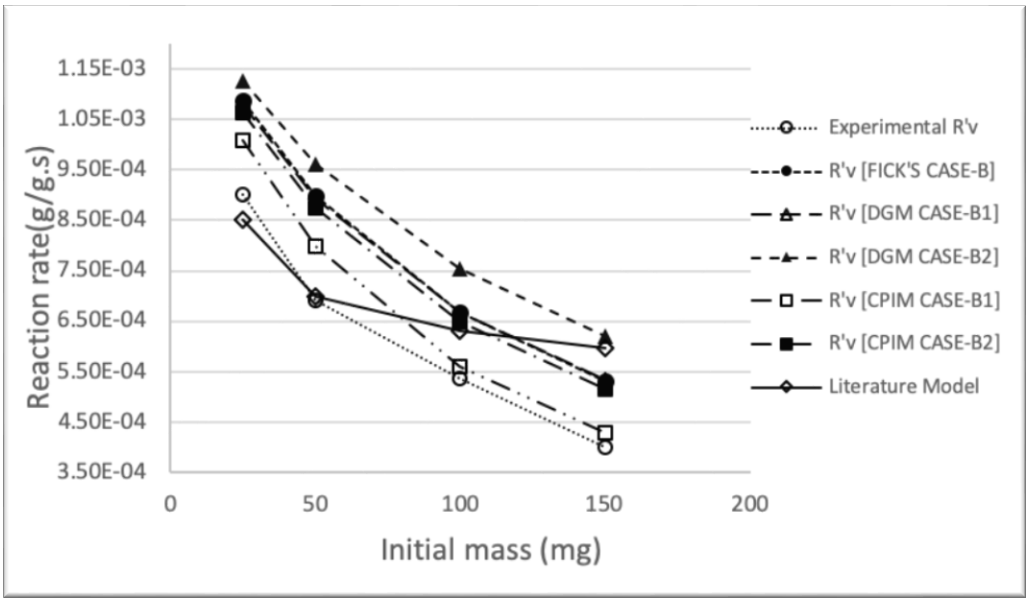

Figure 4-15. Comparison of the overall reaction rate for different cases with the model of Malekshahian et al. (2014) and their experimental results for activated carbon

Comparing the experimental results to the model of Malekshahian et al. (2014), it may be noticed that, although they found a good agreement in lower initial masses, the predictions are not very consistent in higher masses like 100 mg and 150 mg. As the authors explained, it can be due to the inhibition effect of CO which is not considered in the calculations. In a flow-through crucible, CO is swept away quickly by the gas flow, whereas it accumulates in a closed-bottom crucible. The accumulated CO can cause inhibition, lowering the reaction rate. By increasing the initial mass this effect and deviation from the experimental results becomes more significant due to the more

[9] The reactant gas flows through the solid bed in this type of crucible.

CO production. In Figure (4-15), the round-dot line with empty circles shows the trend for the experimental results and the solid line is showing the Malekshahian's model.

If it is assumed that there is no CO inhibition effect, then all the model variants presented here overestimate the reaction rate. However, they follow the experimental trend (i.e., the slope) better than the model of Malekshahian. In that case, the CPIM CASE-B1 has the best agreement with the experimental data. On the other side, if it is assumed that the inhibition effect exists, but does not have a strong dependence on the CO mole fraction, then the DGM cases are likely to provide the best agreement with the data. However, in order to test this, a gasification kinetic model with CO inhibition is needed. Fick's law and the DGM case (1) (without releasing oxygen) give very similar result.

Furthermore, the calculation of the Knudsen number in sections 4.2 indicates that the DGM is an appropriate model for this case. This number indicates whether the reactant gas flow is in the continuum regime ($Kn < 0.01$), Knudsen regime ($Kn > 10$), transitional regime ($0.1 < Kn < 10$) or in the slip-flow regime ($0.01 < Kn < 0.1$). Each diffusion theory performs better in one of these regimes. For instance, the original publication of the dusty-gas model explained how this theory outperform others in slip-flow and continuum regime (Evans eta al., 1961). This is due to the fitting parameter (B_0), in the formulation of the dusty-gas model (section (3.3)) which was determined in the slip-flow regime in the bed. Young and Todd explained how the CPIM outperforms other theories in transitional regime where Knudsen and molecular diffusion are mixed.

4.5 Chapter summary and conclusion

This chapter provided the simulation results for the CO_2 gasification of petroleum coke and activated carbon in TGA. The results in different cases were compared to the model of Malekshahian et al. (2014) as a starting point. For the more reactive sample, activated carbon, the diffusion limitations were more important than petcoke. Then, the effects of different diffusion steps and various initial masses on the modeling were evaluated by discussing the effectiveness factors. Finally, the reaction rates calculated by the model were validated with the experimental results of Malekshahian et al. (2014). The proposed model showed more consistency with the experimental results compared to Malekshahian's model. However, the intrinsic reaction rate

(intrinsic rate constant) should be corrected with a kinetic model accounting for CO inhibition to get the best match with the experimental results.

CHAPTER FIVE: CONCLUSIONS AND RECOMMENDATIONS

5.1 Concluding remarks

This thesis developed a mathematical model to compare different diffusion theories and scenarios for the CO_2 gasification of petroleum coke and activated carbon in a Thermogravimetric Analyzer (TGA). A numerical solution had been adopted to solve the set of ordinary differential equations in MATLAB. The obtained results in different cases were compared to the results of Malekshahian et al. (2014). In addition, the effect of different diffusion steps (intraparticle, inter-particle and external diffusion) and various initial masses of the sample on the overall rate of the gasification were discussed by comparing the effectiveness factors. These factors were used to evaluate the mass transfer limitations in each diffusion step.

In general, the reaction rate calculated by the model showed a good consistency with the experimental rates obtained in a closed-bottom crucible for all the selected initial masses. Using Fick's law as the main theory of diffusion and advection for a binary mixture of CO_2 and CO, as Malekshahian et al. (2014) did, does not cover all factors affecting the diffusion limitations in the gas and the bed part. Particularly because the minor components in the solid (H and O) can have a non-negligible effect on diffusion limitation. Therefore, it seems crucial to consider a multicomponent flux theory to model the diffusion and reaction.

Ultimate analysis of petcoke and activated carbon showed a considerable amount of hydrogen in petcoke and oxygen in activated carbon. Thus, different case studies were chosen to model the multicomponent diffusion and reaction using diffusion theories like the Stefan-Maxwell model (SMM), the dusty-gas model (DGM) and the cylindrical pore interpolation model (CPIM). Using the SMM in the gas part and the DGM in the bed part provided a more realistic estimation of the experimental overall reaction rate compared to Fick's law (binary case) and the CPIM.

For both samples, the reactant gas flow was in the Knudsen regime ($Kn > 10$) inside the particle. Hence, the Thiele modulus and mean particle effectiveness factor was a proper choice to model the intraparticle diffusion, since every diffusion model can be simplified to Knudsen diffusion in this regime, which follows Fick's law in a fixed frame of reference. The inter-particle Knudsen number for petcoke and activated carbon showed a slip-flow ($0.01 < Kn < 0.1$) and a continuum regime ($Kn < 0.01$) inside the porous bed, respectively. According to the original publication of

the DGM, this diffusion theory has the best performance in these two regimes (Evans et al., 1961). Therefore, Knudsen diffusion prevailed in the particle, and molecular diffusion and the slip-flow regime were predominant in the porous bed. Furthermore, the CPIM was not a proper choice either, since this theory was designed for the transitional regime where the Knudsen and molecular diffusion are mixed ($0.1 < Kn < 10$). The CPIM model showed significantly more diffusion limitation than the corresponding DGM in all cases.

By comparing the effectiveness factors for the two samples, the importance of evaluating the diffusion limitations is observed, especially for the more reactive component (activated carbon). The analysis of the mean particle, bed and external effectiveness factor values indicated the significance of external diffusion for petcoke as the main diffusion limiting step. For activated carbon, however, both inter-particle and external diffusion had almost the same impact on the overall rate of the reaction. For both samples, mean particle effectiveness factor values showed that the least diffusion limitation is expected inside the porous particle.

It was shown that incorporating minor elements (H and O) in the solid material into the model has a pronounced effect on the predicted diffusion limitations. It follows that these elements should not be neglected in the modeling of gasification.

The effect of initial mass on the modeling was investigated using the effectiveness factors for four different initial masses (25mg, 50 mg, 100mg and 150 mg). The increase of the initial mass of the sample also increased the diffusion limitations. For higher initial masses, CO_2 is consumed at the top of the bed, and this leads to the deficient supply of CO_2 at the bottom, causing more diffusion limitations in the crucible. The models tended to overpredict the apparent reaction rate of the solid. This was attributed to CO inhibition of the gasification process, which was not incorporated in the models.

5.2 Future work and recommendations

Although the developed model showed a good consistency in estimating the experimental reaction rate values for different initial masses, the intrinsic rate constant should incorporate CO inhibition to improve the match with the experimental results.

Another recommendation for future research might be evaluating the effects of other parameters such as pressure, temperature, other compositions of the sample, etc., on the CO_2 gasification of petroleum coke and activated carbon.

Lastly, modeling the diffusion in gasification reaction in transitional regime ($0.1 < Kn < 10$) can be a potential area for future research, since there is no clear formulation for the fitting parameter (B_0) of the dusty-gas model in this regime.

REFERENCES

Abashar, M. E., & Elnashaie, S. S. (1993). Mathematical modelling of diffusion-reaction, and solution algorithm for complex reaction networks in porous catalyst pellets-steam reforming of natural gas. *Mathematical and Computer Modelling*. https://doi.org/10.1016/0895-7177(93)90060-C

Ahmed, I. I., & Gupta, A. K. (2011). Kinetics of woodchips char gasification with steam and carbon dioxide. *Applied Energy*, *88*(5), 1613–1619. https://doi.org/10.1016/j.apenergy.2010.11.007

Bandyopadhyay, D., Chakraborti, N., & Ghosh, A. (1991). Heat and mass transfer limitations in gasification of carbon by carbon dioxide. *Steel Research*, *62*(4), 143–151. https://doi.org/10.1002/srin.199101264

Bhatia, S. K., & Perlmutter, D. D. (1980). A random pore model for fluid- solid reactions: I. Isothermal, kinetic control. *AIChE Journal*. https://doi.org/10.1002/aic.690260308

Bremaud, M., Fongarland, P., Anfray, J., Jallais, S., Schweich, D., & Khodakov, A. Y. (2005). Influence of syngas composition on the transient behavior of a Fischer-Tropsch continuous slurry reactor. *Catalysis Today*, *106*(1–4), 137–142. https://doi.org/10.1016/j.cattod.2005.07.126

Callaghan, C. A. (2006). Kinetics and Catalysis of the Water-Gas-Shift Reaction: A Microkinetic and Graph Theoretic Approach. *Department of Chemical Engineering*.

Chi, W. - K, & Perlmutter, D. D. (1989). The effect of pore structure on the char- steam reaction. *AIChE Journal*. https://doi.org/10.1002/aic.690351105

Coats, A. W., & Redfern, J. P. (1963). Thermogravimetric analysis. A review. *The Analyst*. https://doi.org/10.1039/AN9638800906

Coda, B., Cieplik, M. K., de Wild, P. J., & Kiel, J. H. A. (2007). Slagging behavior of wood ash under entrained-flow gasification conditions. *Energy and Fuels*, *21*(6), 3644–3652. https://doi.org/10.1021/ef700247t

Collot, A. G. (2006). Matching gasification technologies to coal properties. *International Journal*

of Coal Geology. https://doi.org/10.1016/j.coal.2005.05.003

Delgado, J. M. P. Q. (2006). A simple experimental technique to measure tortuosity in packed beds. *Canadian Journal of Chemical Engineering*. https://doi.org/10.1002/cjce.5450840603

De Visscher, A. (2019). Advanced lecture notes in heat, mass, and momentum transfer. *Senneville, QC, Canada*. ISBN-10:1492792640

Evans, R. B., Watson, G. M., & Mason, E. A. (1961). Gaseous diffusion in porous media at uniform pressure. *The Journal of Chemical Physics*. https://doi.org/10.1063/1.1732211

Evans, R. B., Watson, G. M., & Mason, E. A. (1962). Gaseous diffusion in porous media. II. Effect of pressure gradients. *The Journal of Chemical Physics*. https://doi.org/10.1063/1.1701287

Fermoso, J., Arias, B., Pevida, C., Plaza, M. G., Rubiera, F., & Pis, J. J. (2008). Kinetic models comparison for steam gasification of different nature fuel chars. *Journal of Thermal Analysis and Calorimetry*, *91*(3), 779–786. https://doi.org/10.1007/s10973-007-8623-5

Fermoso, J., Stevanov, C., Moghtaderi, B., Arias, B., Pevida, C., Plaza, M. G., Rubiera, F., & Pis, J. J. (2009). High-pressure gasification reactivity of biomass chars produced at different temperatures. *Journal of Analytical and Applied Pyrolysis*. https://doi.org/10.1016/j.jaap.2008.09.017

Fuller, E. N., Schettler, P. D., & Giddings, J. C. (1966). A new method for prediction of binary gas-phase diffusion coefficients. *Industrial and Engineering Chemistry*. https://doi.org/10.1021/ie50677a007

Gibilaro, L. G. (1970). Mass Transfer in Heterogeneous Catalysis. *The Chemical Engineering Journal*. https://doi.org/10.1016/0300-9467(70)80010-7

Gómez-Barea, A., Ollero, P., & Arjona, R. (2005). Reaction-diffusion model of TGA gasification experiments for estimating diffusional effects. *Fuel*, *84*(12–13), 1695–1704. https://doi.org/10.1016/j.fuel.2005.02.003

Graaf, G. H., Scholtens, H., Stamhuis, E. J., & Beenackers, A. A. C. M. (1990). Intra-particle diffusion limitations in low-pressure methanol synthesis. *Chemical Engineering Science*. https://doi.org/10.1016/0009-2509(90)85001-T

Haberman, B. A., & Young, J. B. (2006). Diffusion and chemical reaction in the porous structures of solid oxide fuel cells. *Journal of Fuel Cell Science and Technology*. https://doi.org/10.1115/1.2211637

Hernández, J. J., Ballesteros, R., & Aranda, G. (2013). Characterisation of tars from biomass gasification: Effect of the operating conditions. *Energy*, *50*(1), 333–342. https://doi.org/10.1016/j.energy.2012.12.005

Higman, C., & van der Burgt, M. (2008). Gasification, 2nd ed. In *Environmental Impact Assessment Review*. https://doi.org/10.1016/0195-9255(91)90020-K

Hill, J. M., Karimi, A., & Malekshahian, M. (2014). Characterization, gasification, activation, and potential uses for the millions of tonnes of petroleum coke produced in Canada each year. *Canadian Journal of Chemical Engineering*, *92*(9), 1618–1626. https://doi.org/10.1002/cjce.22020

Hoffmann, B. S., & Szklo, A. (2011). Integrated gasification combined cycle and carbon capture: A risky option to mitigate CO2 emissions of coal-fired power plants. *Applied Energy*. https://doi.org/10.1016/j.apenergy.2011.04.002

Jess, A., & Andresen, A. K. (2010). Influence of mass transfer on thermogravimetric analysis of combustion and gasification reactivity of coke. *Fuel*. https://doi.org/10.1016/j.fuel.2009.09.002

Kabe, T., Ishihara, A., Qian, E. W., Sutrisna, I. P., & Kabe, Y. (2004). Coal and coal-related compounds: Structures, reactivity and catalytic reactions. In *Studies in Surface Science and Catalysis*.

Kajitani, S., Suzuki, N., Ashizawa, M., & Hara, S. (2006). CO2 gasification rate analysis of coal char in entrained flow coal gasifier. *Fuel*. https://doi.org/10.1016/j.fuel.2005.07.024

Kaza, K. R., & Jackson, R. (1980). Diffusion and reaction of multicomponent gas mixtures in isothermal porous catalysts. *Chemical Engineering Science*. https://doi.org/10.1016/0009-2509(80)85108-6

Kaza, K. R., Villadsen, J., & Jackson, R. (1980). 3 Intraparticle diffusion effects in the methanation reaction. *Chemical Engineering Science*. https://doi.org/10.1016/0009-2509(80)80065-0

Kerkhof, P. J. A. M. (1996). A modified Maxwell-Stefan model for transport through inert membranes: The binary friction model. *Chemical Engineering Journal and the Biochemical Engineering Journal*. https://doi.org/10.1016/S0923-0467(96)03134-X

Khalil, R., Várhegyi, G., Jäschke, S., Grønli, M. G., & Hustad, J. (2009). CO2 gasification of biomass chars: A kinetic study. *Energy and Fuels*. https://doi.org/10.1021/ef800739m

Kong, W., Zhu, H., Fei, Z., & Lin, Z. (2012). A modified dusty gas model in the form of a Fick's model for the prediction of multicomponent mass transport in a solid oxide fuel cell anode. *Journal of Power Sources*. https://doi.org/10.1016/j.jpowsour.2012.01.107

Laurendeau, N. M. (1978). Heterogeneous kinetics of coal char gasification and combustion. *Progress in Energy and Combustion Science*. https://doi.org/10.1016/0360-1285(78)90008-4

Levenspiel, O. (1999). Chemical reaction engineering. In *Industrial and Engineering Chemistry Research*. https://doi.org/10.1021/ie990488g

Lim, J. Y., & Dennis, J. S. (2012). Modeling reaction and diffusion in a spherical catalyst pellet using multicomponent flux models. *Industrial and Engineering Chemistry Research*. https://doi.org/10.1021/ie302528u

Ma, L., Liao, C., Zhu, Y., Chen, H., & Ding, Y. (2011). An environment friendly energy recovery technology: Municipal solid waste gasification. *Proceedings - 3rd International Conference on Measuring Technology and Mechatronics Automation, ICMTMA 2011*, *1*, 407–409. https://doi.org/10.1109/ICMTMA.2011.103

Mahinpey, N., & Gomez, A. (2016). Review of gasification fundamentals and new findings: Reactors, feedstock, and kinetic studies. *Chemical Engineering Science*, *148*, 14–31. https://doi.org/10.1016/j.ces.2016.03.037

Malekshahian, M., De Visscher, A., & Hill, J. M. (2014). A non-equimolar mass transfer model for carbon dioxide gasification studies by thermogravimetric analysis. *Fuel Processing Technology*. https://doi.org/10.1016/j.fuproc.2014.02.009

Malekshahian, M. (2011). Effect of pressure on gasification of petroleum coke with carbon dioxide (Unpublished doctoral thesis). University of Calgary, Calgary, AB. doi:10.11575/PRISM/4645

Malekshahian, M., & Hill, J. M. (2011a). Kinetic analysis of CO2 gasification of petroleum coke at high pressures. *Energy and Fuels*, *25*(9), 4043–4048. https://doi.org/10.1021/ef2009259

Malekshahian, M., & Hill, J. M. (2011b). Kinetic analysis of CO2 gasification of petroleum coke at high pressures. *Energy and Fuels*. https://doi.org/10.1021/ef2009259

Mandapati, R. N., Daggupati, S., Mahajani, S. M., Aghalayam, P., Sapru, R. K., Sharma, R. K., & Ganesh, A. (2012). Experiments and kinetic modeling for CO2 gasification of indian coal chars in the context of underground coal gasification. *Industrial and Engineering Chemistry Research*. https://doi.org/10.1021/ie3022434

Mani, T., Mahinpey, N., & Murugan, P. (2011). Reaction kinetics and mass transfer studies of biomass char gasification with CO2. *Chemical Engineering Science*. https://doi.org/10.1016/j.ces.2010.09.033

Marsh, H., & Rodríguez-Reinoso, F. (2006). Characterization of Activated Carbon. In *Activated Carbon*. https://doi.org/10.1016/b978-008044463-5/50018-2

McKendry, P. (2002). Energy production from biomass (part 3): Gasification technologies. *Bioresource Technology*. https://doi.org/10.1016/S0960-8524(01)00120-1

Minchener, A. J. (2005). Coal gasification for advanced power generation. *Fuel*. https://doi.org/10.1016/j.fuel.2005.08.035

Molina, A., & Mondragón, F. (1998). Reactivity of coal gasification with steam and CO 2. *Fuel*. https://doi.org/10.1016/S0016-2361(98)00123-9

Ollero, P., Serrera, A., Arjona, R., & Alcantarilla, S. (2002). Diffusional effects in TGA gasification experiments for kinetic determination. *Fuel*, *81*(15), 1989–2000. https://doi.org/10.1016/S0016-2361(02)00126-6

Perry's chemical engineers' handbook. (2008). *Choice Reviews Online*. https://doi.org/10.5860/choice.45-4393

Qian, F., Kong, X., Cheng, H., Du, W., & Zhong, W. (2013). Development of a kinetic model for industrial entrained flow coal gasifiers. *Industrial and Engineering Chemistry Research*, *52*(5), 1819–1828. https://doi.org/10.1021/ie301630x

Sansaniwal, S. K., Rosen, M. A., & Tyagi, S. K. (2017). Global challenges in the sustainable

development of biomass gasification: An overview. In *Renewable and Sustainable Energy Reviews*. https://doi.org/10.1016/j.rser.2017.05.215

Solsvik, J., & Jakobsen, H. A. (2011). Modeling of multicomponent mass diffusion in porous spherical pellets: Application to steam methane reforming and methanol synthesis. *Chemical Engineering Science*. https://doi.org/10.1016/j.ces.2011.01.060

Song, J., Jeon, C. H., & Boehman, A. L. (2010). Impacts of oxygen diffusion on the combustion rate of in-bed soot particles. *Energy and Fuels*. https://doi.org/10.1021/ef900692m

Song, Q., He, B., Yao, Q., Meng, Z., & Chen, C. (2006). Influence of diffusion on thermogravimetric analysis of carbon black oxidation. *Energy and Fuels*, *20*(5), 1895–1900. https://doi.org/10.1021/ef0600659

Stanmore, B., Gilot, P., & Prado, G. (1994). The influence of mass transfer in DTG combustion tests. *Thermochimica Acta*. https://doi.org/10.1016/0040-6031(94)87030-6

Su, J. - L, & Perlmutter, D. D. (1985). Effect of pore structure on char oxidation kinetics. *AIChE Journal*. https://doi.org/10.1002/aic.690310614

Szekely, J., & Evans, J. W. (1970). A structural model for gas-solid reactions with a moving boundary. *Chemical Engineering Science*. https://doi.org/10.1016/0009-2509(70)85053-9

Totten, G., Westbrook, S., & Shah, R. (2003). Fuels and Lubricants Handbook: Technology, Properties, Performance, and Testing. In *Fuels and Lubricants Handbook: Technology, Properties, Performance, and Testing*. https://doi.org/10.1520/mnl37-eb

Tremel, A., & Spliethoff, H. (2013). Gasification kinetics during entrained flow gasification - Part II: Intrinsic char reaction rate and surface area development. *Fuel*, *107*, 653–661. https://doi.org/10.1016/j.fuel.2012.10.053

Tuas, M. A., & Masduqi, A. (2019). Removal of copper content in jewelry industry wastewater using commercial activated carbon. *Pollution Research*, *38*, S53–S58.

Tyler, R. J., & Smith, I. W. (1975). Reactivity of petroleum coke to carbon dioxide between 1030 and 1180 K. *Fuel*. https://doi.org/10.1016/0016-2361(75)90064-2

Walker, P. L., Rusinko, F., & Austin, L. G. (1959). Gas Reactions of Carbon. *Advances in Catalysis*. https://doi.org/10.1016/S0360-0564(08)60418-6

Wall, T. F., Liu, G. S., Wu, H. W., Roberts, D. G., Benfell, K. E., Gupta, S., Lucas, J. A., & Harris, D. J. (2002). The effects of pressure on coal reactions during pulverised coal combustion and gasification. In *Progress in Energy and Combustion Science*. https://doi.org/10.1016/S0360-1285(02)00007-2

Wigmans, T., Hoogland, A., Tromp, P., & Moulijn, J. A. (1983). The influence of potassium carbonate on surface area development and reactivity during gasification of activated carbon by carbon dioxide. *Carbon*. https://doi.org/10.1016/0008-6223(83)90151-3

Young, J. B., & Todd, B. (2005). Modelling of multi-component gas flows in capillaries and porous solids. *International Journal of Heat and Mass Transfer*. https://doi.org/10.1016/j.ijheatmasstransfer.2005.07.034

Zhan, X., Zhou, Z. J., & Wang, F. (2010). Catalytic effect of black liquor on the gasification reactivity of petroleum coke. *Applied Energy*, *87*(5), 1710–1715. https://doi.org/10.1016/j.apenergy.2009.10.027

Zhao, Y., Sun, S., Tian, H., Qian, J., Su, F., & Ling, F. (2009). Characteristics of rice husk gasification in an entrained flow reactor. *Bioresource Technology*, *100*(23), 6040–6044. https://doi.org/10.1016/j.biortech.2009.06.030

Zou, J. H., Zhou, Z. J., Wang, F. C., Zhang, W., Dai, Z. H., Liu, H. F., & Yu, Z. H. (2007). Modeling reaction kinetics of petroleum coke gasification with CO2. *Chemical Engineering and Processing: Process Intensification*. https://doi.org/10.1016/j.cep.2006.08.008

APPENDICES

Appendix A: Thermodynamic calculations for the water-gas shift reaction

The equilibrium constant of the water-gas shift reaction is calculated as follows (Callaghan, 2006):

$$log(K_{eq}) = -2.4198 + 0.0003855T + \frac{2180.6}{T}$$

This equation defines the thermodynamic limitations of the water-gas shift reaction over the temperature range of 600 K to 2000 K.

$$T = 1223\ K \rightarrow \boldsymbol{K_{eq} = 0.6833}$$

Appendix B: Developed MATLAB code for the CO_2 gasification of petcoke and activated carbon using **Fick's law** (binary mixture)

Main file:

```
% Fick's law - Modeling Diffusion and Reaction inside a crucible
% Numerical integration of a set of differential equations along the crucible

clc
clear all
close all
code = 2;                              %code=1: act. carbon and code= 2:petcoke

%% ==============Part1: parameters and variables calculation=================

tic
tspan = 0:1e-2:3;                      %simulation time
Lc = 0.02;                             %length of crucible(m)
N_grid1 = 51;                          %number of grid points in the gas
N_grid2 = 51;                          %number of grid points in the bed
N_grid = N_grid1 + N_grid2;            %number of grid points
N_comp  = 2;                           %number of compounds
% 1 = CO2
% 2  = CO
p_begin = 91192.5;                     %pressure(Pa) p = 0.9 atm
w0 = input('Initial mass(mg)=');       %initial mass (mg)
w0 = w0*10^-3;                         %converting to g
diam = 18e-3;                          %crucible (bed) diameter(m)
radius = diam/2;
Temp = 1223;                           %bed temperature (K)
R = 8.3144598;                         %gas constant
for j = 1:N_grid
    p(j) = p_begin;
    c_total(j) = p(j)/(R*Temp);        %total concentration in each grid
point(mol/m3)
end
% Diffusion coefficients at 0.9 atm pressure
for j = 1:N_comp
    D(j,j) = 0;
end
D(1,2) = (1.39e-5)*((Temp/273.2)^1.75); %binary diffusivity at 0.1 MPa (m2/s)
D(2,1) = D(1,2);
mu(1) = (15.4336*1.37369*(1-exp(-
1.30184*(Temp/304.13)^0.65455))*(Temp/304.13)^0.61732)*1e-6;    %CO2 viscosity
(Pa.s) - Append. E Transport Phenomena
mu(2) = (8.8697*1.37369*(1-exp(-
1.30184*(Temp/132.86)^0.65455))*(Temp/132.86)^0.61732)*1e-6;     %CO viscosity
(Pa.s) - Append. E Transport Phenomena
M(1) = 44;                             %molar mass for CO2
M(2) = 28;                             %molar mass for CO

%=========================activated carbon Data============================
if code == 1
diam_pore = 0.288e-3;                  %bed pore diameter
radius_pore = diam_pore/2;
diam_p = 1.3e-3;                       %particle diameter for Act. carbon
Rop = 0.4e6;                           %particle density(g/m3)
Ro = 0.3e6;                            %bulk density(g/m3)
K = 5.962;                             %intrinsic rate constant
Eb = 1-(Ro/Rop);                       %bed porosity
n = 0.8;                               %intrinsic reaction order
```

```
to = 1-(0.5*log(Eb));                          %bed tortuosity
ap = [-pi/3 pi*radius 0 -w0/Ro];
a = roots(ap);
delta = a(2);                                  %bed depth(alpha) for act. carbon
%============================Petcoke Data=====================================
else
diam_pore = 3e-5;                              %bed pore diameter
radius_pore = diam_pore/2;
diam_p = 45e-6;                                %particle diameter for petcoke
Rop = 1.4e6;                                   %particle density(g/m3)
Ro = 0.7e6;                                    %bulk density(g/m3)
K = 0.776;                                     %intrinsic rate constant
Eb = 1-(Ro/Rop);                               %bed porosity
n = 0.6;                                       %intrinsic reaction order
to = 1-(0.5*log(Eb));                          %bed tortuosity for petcoke
ap = [-pi/3 pi*radius 0 -w0/Ro];
a = roots(ap);
delta = a(2);                                  %bed depth(alpha) for petcoke(m)
end
%==========================================================================
dz1 = (Lc - delta)/(N_grid1 - 1);
dz2 = delta/(N_grid2 - 1);
for j = 1:N_grid1
    z(j) = (j-1)*dz1;
end
for j = 1:N_grid2
    z(N_grid1+j) = (Lc - delta) + (j-1)*dz2;
end
for j = 1:N_grid1
    r_cruc(j) = radius;
end
for j = N_grid1+1:N_grid
    del(j) = Lc - z(j);
    r_cruc(j) = (del(j)*(2*radius - del(j)))^0.5;
end
%Knudsen diffusion coefficient
for k = 1:N_comp
    D_K(k) = (8*radius_pore/3)*sqrt(R*Temp/(2*pi()*(M(k)/1000)));
end
%General effective diffusivity
for k = 1:N_comp
    D_eff(k) = 1/((1/(D_K(k)*(Eb/to)))+(1/(D(1,2)*(Eb/to))));
end
%Initial conditions(just reactant gas)-initializing our concentrations
for j = 1:N_grid
    C(j,1) = 1.0*c_total(j);
    C(j,2) = 0.0*c_total(j);
    for k = 1:N_comp
        y0((j-1)*N_comp+k) = C(j,k);
    end
end

%% ===================Part 2: Numerical Integration=======================

options = odeset('RelTol', 1e-6, 'AbsTol', 1e-8, 'InitialStep', 0.01);
[T,Y] =
ode15s(@f_BASE_CASE,tspan,y0,options,N_grid1,N_grid2,N_comp,D,Temp,dz1,dz2,Lc,
R,Eb,n,K,to,r_cruc,z,radius,diam_p,D_eff);

%% ===================Part3: Output of results============================
figure(1)
plot(T,Y)
xlabel('time(s)')
ylabel('C_{CO_2} and C_{CO}')
```

```
% T
% Y
[s1,s2] = size(T);
for j = 1:s1
    for k = 1:N_grid
        C_tot(j,k) = 0;
        for ii = 1:N_comp
            C_(j,k,ii) = Y(j,(k-1)*N_comp+ii);
            C_tot(j,k) = C_tot(j,k) + C_(j,k,ii);
        end
    end
end
figure(2)
plot(T,C_tot)
xlabel('time(s)')
ylabel('total concentration(mol/m^3)')
figure(3)
plot(z,C_tot(end,:))
xlabel('z(m)')
ylabel('total concentration(mol/m^3)')
figure(4)
for k = 1:N_grid
    p_profile(k) = C_tot(s1,k)*R*Temp;
    C_profile_CO2(k) = C_(s1,k,1);
    x_profile_CO2(k) = (C_profile_CO2(k))/C_tot(s1,k);
    C_profile_CO(k) = C_(s1,k,2);
    x_profile_CO(k) = (C_profile_CO(k))/C_tot(s1,k);
end
plot(z,p_profile) %pressure profile along the crucible
xlabel('z(m)')
ylabel('pressure(Pa)')
title('Pressure Profile')
figure(5)
z_rel = 1-(Lc-z)/Lc;
plot(z_rel,x_profile_CO2)
xlabel('(L-z)/L')
ylabel('x_{CO_{2}}')
title('CO_{2} molar fraction profile in the crucible')
figure(6)
z_rel = 1-(Lc-z)/Lc;
plot(z_rel,x_profile_CO)
xlabel('(L-z)/L')
ylabel('x_{CO}')
title('CO molar fraction profile in the crucible')

%%==================Part4: Calculating Effectiveness Factors===============

for j = 1:N_grid
% particle thiele modulus
    tetap(j) = (diam_p/6)*(sqrt(((n+1)*K*(C_tot(j,1))^(n - 1))/(2*D_eff(1))));
% particle effectiveness factor
    etap(j) = (3/tetap(j))*((1/tanh(tetap(j))) - (1/tetap(j)));
end

o = 0;
q = 0;

for i = N_grid1+1:N_grid-1
    w(i) = K*etap(i)*(C_profile_CO2(i))^n;
    w(i+1) = K*etap(i+1)*(C_profile_CO2(i+1))^n;
    g(i) = K*(C_profile_CO2(i))^n;
    g(i+1) = K*(C_profile_CO2(i+1))^n;
    o = o + ((w(i)+w(i+1))/2*dz2);
    q = q + ((g(i)+g(i+1))/2*dz2);
```

```
end

Etap_av = o/q

Etab = ((1/delta)*o)/(K*Etap_av*(C_profile_CO2(N_grid1))^n)

Etae = (C_profile_CO2(N_grid1)/c_total(1))^n

Rv = Eb/Ro*M(1)*Etap_av*Etab*Etae*K*c_total(1)^n

toc
```

Function file:

```
function dydt =
f_BASE_CASE(t,y,N_grid1,N_grid2,N_comp,D,T,dz1,dz2,Lc,R,Eb,n,K,to,r_cruc,z,rad
ius,diam_p,D_eff)

N_grid = N_grid1 + N_grid2;
N_eq = N_grid*N_comp;
dydt = zeros(N_eq,1);          %defining dydt for each node and each component

%% Just to show the time...

t_out = random('uniform',0,1);
if t_out < 0.001
   t
end

%% Calculation of C_i, C_total, and p_total

for j = 1:N_grid
    c_total(j) = 0;
    for k = 1:N_comp
        C(j,k) = y((j-1)*N_comp+k);
        c_total(j) = c_total(j) + C(j,k);
    end
    p_total(j) = c_total(j)*R*T;
end

c_total(N_grid+1) = 0;

for k = 1:N_comp         %applying zero flux boundary conditions
    C(N_grid+1,k) = C(N_grid-1,k);
    c_total(N_grid+1) = c_total(N_grid+1) + C(N_grid+1,k);
end

for j = 1:N_grid1-1
    for k = 1:N_comp
        dcdz(j,k) =  (C(j+1,k) - C(j,k))/dz1;
    end
end

for j = N_grid1+1:N_grid
    for k = 1:N_comp
        dcdz(j,k) =  (C(j+1,k) - C(j,k))/dz2;
    end
end
```

```
for j = 1:N_grid
    dcdz_tot(j) = dcdz(j,1) + dcdz(j,2);
end

%% Calculation of Molar Fraction and Molar Fraction variation in z

for j = 1:N_grid
    for k = 1:N_comp
        x(j,k) = C(j,k)/c_total(j);
    end
end

for k = 1:N_comp
    x(N_grid+1,k) = x(N_grid-1,k);
end

for j = 1:N_grid1-1
    for ii = 1:N_comp
        dxdz(j,ii) = (x(j+1,ii) - x(j,ii))/(dz1);
    end
end

for j = N_grid1+1:N_grid
    for ii = 1:N_comp
        dxdz(j,ii) = (x(j+1,ii) - x(j,ii))/(dz2);
    end
end

%% Calculation of Diffusivities

for j = 1:N_grid1
    D_local(j,1,2)= D(1,2)*100000/p_total(j);
end

for j = N_grid1+1:N_grid
    D_local(j,1,2)= ((Eb/to)*D(1,2))*100000/p_total(j);
end

%% Calculation of Flux

for j = 1:N_grid1-1
    N_all(j,1) = (-D_local(j,1,2))/(1 + x(j,1))*dcdz(j,1);
    N_all(j,2) = -2*D_local(j,1,2)/(2 - x(j,2))*dcdz(j,2);
end

for j = N_grid1+1:N_grid
    N_all(j,1) = (-D_local(j,1,2))/(1 + x(j,1))*dcdz(j,1);
    N_all(j,2) = -2*D_local(j,1,2)/(2 - x(j,2))*dcdz(j,2);
end

%% Stoichiometric Relation

stoich(1) = -1;
stoich(2) = 2;

%% Calculation of mean eta p

for j = 1:N_grid
% particle thiele modulus
    tetap(j) = (diam_p/6)*(sqrt(((n+1)*K*(C(j,1))^(n - 1))/(2*D_eff(1))));
% particle effectiveness factor
```

```
    etap(j) = (3/tetap(j))*((1/tanh(tetap(j))) - (1/tetap(j)));
end

o = 0;
q = 0;

for i = N_grid1+1:N_grid
    w(i) = K*etap(i)*(C(i,1))^n;
    g(i) = K*(C(i,1))^n;
    o = o + (w(i)*dz2);
    q = q + (g(i)*dz2);
end

Etap_av = o/q;

for j = 1:N_grid-1
    r_avg(j) = (r_cruc(j) + r_cruc(j+1))/2;
end

%% Material Balances

for ii = 1:N_comp
    dcdt(1,ii) = 0;
end

for j = 1:N_grid1-2 % gas part
    for ii = 1:N_comp
        dNdz(j+1,ii) = (N_all(j+1,ii) - N_all(j,ii))/dz1;
        dcdt(j+1,ii) = -dNdz(j+1,ii);
    end
end

for j = N_grid1+1:N_grid-1 % bed part
    for ii = 1:N_comp
        dNdz(j+1,ii) = (N_all(j+1,ii) - N_all(j,ii))/(dz2);
        dcdt(j+1,ii) = (-1/(Eb*r_avg(j)^2)).*(2*N_all(j,ii).*(-z(j+1) + Lc -
radius) + r_cruc(j+1)^2.*dNdz(j+1,ii))+(stoich(ii)*Etap_av*K*(C(j,1))^n)/Eb;
%reaction in the bed
    end
end

% M.B. for interface layer
rc_sq_in = (r_cruc(N_grid1-1)^2 + r_cruc(N_grid1)^2)/2;
rc_sq_out = (r_cruc(N_grid1+1)^2 + r_cruc(N_grid1+2)^2)/2;
vol_gas = (dz1/2)*((r_cruc(N_grid1-1)^2 + 3*r_cruc(N_grid1)^2)/4);
vol_bed = (dz2/2)*((3*r_cruc(N_grid1+1)^2 + r_cruc(N_grid1+2)^2)/4);
vol_bed_void = vol_bed*Eb;

for ii = 1:N_comp
    in_(ii) = N_all(N_grid1-1,ii)*rc_sq_in;
    out_(ii) = N_all(N_grid1+1,ii)*rc_sq_out;
    dcdt(N_grid1,ii) = ((in_(ii) - out_(ii)) +
(stoich(ii)*Etap_av*K*(C(N_grid1,1))^n)*vol_bed)/(vol_gas+vol_bed_void);
    dcdt(N_grid1+1,ii) = ((in_(ii) - out_(ii)) +
(stoich(ii)*Etap_av*K*(C(N_grid1+1,1))^n)*vol_bed)/(vol_gas+vol_bed_void);
end

%% Putting all vectors dcdt in just one vector

for j = 1:N_grid
    for k = 1:N_comp
        dydt((j-1)*N_comp+k) = dcdt(j,k);
```

```
    end
end

end
```

Appendix C: Developed MATLAB code for the CO_2 gasification of petcoke and activated carbon using **Stefan-Maxwell Model** in the gas part and the **Dusty-Gas Model** in the bed part (multicomponent mixture)

Main file:

```
% SMM-DGM - Modeling multicomponent diffusion and reaction inside a crucible
% Numerical integration of a set of differential equations along the crucible

clc
clear all
close all
code = 1;                           %code=1 for act. carbon and code=2 petcoke
product = 1;                        %product=1 for H2 or no O2 released and
product=2 for H2O or O2 released
%================Part1: parameters and variables calculation===============
tic
tspan = 0:1e-3:3;                           %simulation time
Lc = 0.02;                                  %length of crucible(m)
N_grid1 = 51;                               %number of grid points in the gas
N_grid2 = 51;                               %number of grid points in the bed
N_grid = N_grid1 + N_grid2;                 %number of grid points
N_comp  = 2;                                %number of compounds
% 1 = CO2
% 2 = CO
% 3 = H2 (1st CASE - product=1) or H2O (2nd CASE - product=2)
p_begin = 91192.5;                          %pressure(Pa)
w0 = input('Initial mass(mg)=');            %initial mass (mg)
w0 = w0*10^-3;                              %converting to g
diam = 18e-3;                               %crucible (bed) diameter(m)
radius = diam/2;
Temp = 1223;                                %bed temperature (K)
R = 8.3144598;                              %gas constant
for j = 1:N_grid
    p(j) = p_begin;
    c_total(j) = p(j)/(R*Temp);             %total concentration in each grid
point(mol/m3)
end
% Diffusion coefficients at 0.9 atm pressure
for j = 1:N_comp
    D(j,j) = 0;
end
D(1,2) = (1.39e-5)*((Temp/273.2)^1.75); %binary diffusivity at 0.1 MPa (m2/s)
D(2,1) = D(1,2);
mu(1) = (15.4336*1.37369*(1-exp(-
1.30184*(Temp/304.13)^0.65455))*(Temp/304.13)^0.61732)*1e-6;    %CO2 viscosity
(Pa.s) - Append. E Transport Phenomena
```

```
mu(2) = (8.8697*1.37369*(1-exp(-
1.30184*(Temp/132.86)^0.65455))*(Temp/132.86)^0.61732)*1e-6;     %CO viscosity
(Pa.s) - Append. E Transport Phenomena
M(1) = 44;                                  %molar mass for CO2
M(2) = 28;                                  %molar mass for CO
if code == 1;
%=========================activated carbon Data============================
   diam_pore = 0.288e-3;                    %bed pore diameter
   radius_pore = diam_pore/2;
   diam_p = 1.3e-3;                         %particle diameter for Act. carbon
   Rop = 0.4e6;                             %particle density(g/m3)
   Ro = 0.3e6;                              %bulk density(g/m3)
   K = 5.962;                               %intrinsic rate constant
   Eb = 1-(Ro/Rop);                         %bed porosity
   n = 0.8;                                 %intrinsic reaction order
   to = 1-(0.5*log(Eb));                    %bed tortuosity
   ap = [-pi/3 pi*radius 0 -w0/Ro];
   a = roots(ap);
   delta = a(2);                            %bed depth(alpha) for act. carbon
%==========================================================================
%==================data NOT considering oxygen in AC=======================
      if product == 1;
         ratio(1) = -1;
         ratio(2) = 2;
%====================data considering oxygen in AC=========================
      else
         ratio(1) = -46/73;
         ratio(2) = 119/73;
      end
%==========================================================================

   if (N_comp ~= 2)
       disp('Activated Carbon is simulated just with 2 components. Please,
change N_comp to 2.')
       return
   end
else
%============================Petcoke Data==================================
   diam_pore = 3e-5;                        %bed pore diameter
   radius_pore = diam_pore/2;
   diam_p = 45e-6;                          %particle diameter for petcoke
   Rop = 1.4e6;                             %%particle density(g/m3)
   Ro = 0.7e6;                              %bulk density(g/m3)
   K = 0.776;                               %intrinsic rate constant
   Eb = 1-(Ro/Rop);                         %bed porosity
   n = 0.6;                                 %intrinsic reaction order
   to = 1-(0.5*log(Eb));                    %bed tortuosity for petcoke
   ap = [-pi/3 pi*radius 0 -w0/Ro];
   a = roots(ap);
   delta = a(2);                            %bed depth(alpha) for petcoke(m)
%==========================================================================
   if N_comp ==2;
      ratio(1) = -1;
      ratio(2) = 2;
   else
%==============================data for H2=================================
      if product == 1;
         D(1,3) = (6.5e-5)*((Temp/298.15)^1.7675);
         D(3,1) = D(1,3);
         D(2,3) = (7.811e-5)*((Temp/298.15)^1.7414);
         D(3,2) = D(2,3);
         M(3) = 2;                                  %molar mass for H2
```

```
         mu(3) = (1.6959*1.37369*(1-exp(-
1.30184*(Temp/33.19)^0.65455))*(Temp/33.19)^0.61732)*1e-6;      %H2 viscosity
(Pa.s) - Append. E Transport Phenomena
         ratio(1) = -1;
         ratio(2) = 2;
         ratio(3) = 7/26;
%================================data for H2O================================
      else
         D(1,3) = (2.351e-5)*((Temp/298.15)^1.6608);
         D(3,1) = D(1,3);
         D(2,3) = (2.995e-5)*((Temp/298.15)^1.6347);
         D(3,2) = D(2,3);
         M(3) = 18;                                    %molar mass for H2O
         mu(3) = (23.5373*1.37369*(1-exp(-
1.30184*(Temp/647.1)^0.65455))*(Temp/647.1)^0.61732)*1e-6;      %H2O viscosity
(Pa.s) - Append. E Transport Phenomena
         ratio(1) = -33/26;
         ratio(2) = 59/26;
         ratio(3) = 7/26;
      end
   end
end
%=============================================================================
dz1 = (Lc - delta)/(N_grid1 - 1);       %node thickness in the gas part
dz2 = delta/(N_grid2 - 1);              %node thickness in the porous solid
for j = 1:N_grid1
    z(j) = (j-1)*dz1;
end
for j = 1:N_grid2
    z(N_grid1+j) = (Lc - delta) + (j-1)*dz2;
end
for j = 1:N_grid1
    r_cruc(j) = radius;                %Constant radius in the gas
part(assumption)
end
for j = N_grid1+1:N_grid
    del(j) = Lc - z(j);
    r_cruc(j) = (del(j)*(2*radius - del(j)))^0.5;
end

sigma_sq_co2 = sqrt((M(1)/1000)*R*Temp)/(3.14159^1.5*mu(1)*6.02214e23);
%check the eq. for sigma_sq

%Knudsen diffusion coefficient
for ii = 1:N_comp
    D_K(ii) = (8*radius_pore/3)*sqrt(R*Temp/(2*3.14159*(M(ii)/1000)));
end

%calculating viscosity of the mixture
for i = 1:N_comp
    for j = 1:N_comp
        phi(i,j) =
(1+sqrt(mu(i)/mu(j)*sqrt(M(j)/M(i))))^2/sqrt(8*(1+M(i)/M(j)));
    end
end
%initial conditions(just reactant gas)-initializing our concentrations
for j = 1:N_grid
    C(j,1) = 1.0*c_total(j);
    C(j,2) = 0.0*c_total(j);
    C(j,3) = 0.0*c_total(j);
    for k = 1:N_comp
        y0((j-1)*N_comp+k) = C(j,k);
    end
end
```

```
%====================part 2: Numerical Integration=======================

options = odeset('RelTol', 1e-6, 'AbsTol', 1e-8, 'InitialStep', 0.01);
[T,Y] =
ode15s(@f_SMM_DGM_3comp,tspan,y0,options,N_grid1,N_grid2,N_comp,D,Temp,dz1,dz2
,mu,phi,Lc,R,radius_pore,D_K,sigma_sq_co2,Eb,n,K,to,r_cruc,z,radius,diam_p,rat
io,product);

%====================part3: Output of results============================
figure(1)
plot(T,Y)
xlabel('time(s)')
ylabel('y')
% T
% Y
[s1,s2] = size(T);
for j = 1:s1
    for k = 1:N_grid
        C_tot(j,k) = 0;
        for ii = 1:N_comp
            C_(j,k,ii) = Y(j,(k-1)*N_comp+ii);
            C_tot(j,k) = C_tot(j,k) + C_(j,k,ii);
        end
    end
end
figure(2)
plot(T,C_tot)
xlabel('time(s)')
ylabel('total concentration(mol/m^3)')
figure(3)
plot(z,C_tot(end,:))
xlabel('z(m)')
ylabel('total concentration(mol/m^3)')
figure(4)
for k = 1:N_grid
    p_profile(k) = C_tot(s1,k)*R*Temp;
    C_profile_CO2(k) = C_(s1,k,1);
    x_profile_CO2(k) = (C_profile_CO2(k))/C_tot(s1,k);
    C_profile_CO(k) = C_(s1,k,2);
    x_profile_CO(k) = (C_profile_CO(k))/C_tot(s1,k);
    if N_comp == 2
    else
        if product == 1
           C_profile_H2(k) = C_(s1,k,3);
           x_profile_H2(k) = (C_profile_H2(k))/C_tot(s1,k);
        else
           C_profile_H2O(k) = C_(s1,k,3);
           x_profile_H2O(k) = (C_profile_H2O(k))/C_tot(s1,k);
        end
    end
end
plot(z,p_profile) %pressure profile along the crucible
xlabel('z(m)')
ylabel('pressure (Pa)')
title('Pressure Profile')
figure(5)
z_rel = 1-(Lc-z)/Lc;
plot(z_rel,x_profile_CO2)
xlabel('(L-z)/L')
ylabel('x_{CO_2}')
title('CO2 molar fraction profile in the crucible')
figure(6)
z_rel = 1-(Lc-z)/Lc;
plot(z_rel,x_profile_CO)
```

```
xlabel('(L-z)/L')
ylabel('x_{CCO}')
title('CO molar fraction profile in the crucible')
if N_comp == 2
else
    if product == 1
       figure(7)
       z_rel = 1-(Lc-z)/Lc;
       plot(z_rel,x_profile_H2)
       xlabel('(L-z)/L')
       ylabel('x_{H2}')
       title('H2 molar fraction profile in the crucible')
    else
       figure(7)
       z_rel = 1-(Lc-z)/Lc;
       plot(z_rel,x_profile_H2O)
       xlabel('(L-z)/L')
       ylabel('x_{H2O}')
       title('H2O molar fraction profile in the crucible')
    end
end

%% Calculation of mean eta p

% CO2 pseudo binary diff coefficient
for j = 1:N_grid1-1
    for ii = 1:N_comp
        for jj = 1:N_comp
            D_local(j,ii,jj)= D(ii,jj)*100000/p_profile(j);
%diffusivity in the gas part
        end
    end
end
for j = N_grid1+1:N_grid
    for ii = 1:N_comp
        for jj = 1:N_comp
            D_local(j,ii,jj) = ((Eb/to)*D(ii,jj))*100000/p_profile(j);
%diffusivity in the solid part
        end
    end
end

x_av(:,1) = x_profile_CO2;
x_av(:,2) = x_profile_CO;
if N_comp == 2
else
    if product == 1
       x_av(:,3) = x_profile_H2;
    else
       x_av(:,3) = x_profile_H2O;
    end
end

if N_comp == 2
Dm = D_local(:,1,2);
else
   for j = 1:N_grid
       if product == 1
          Dm(j) =
(1+1.27*x_av(j,1))/(x_av(j,2)+2*x_av(j,1)/D_local(j,1,2)+x_av(j,3)+0.27*x_av(j
,1)/D_local(j,1,3));
       else
```

```
          Dm(j) =
(1+x_av(j,1))/(x_av(j,2)+(59/33)*x_av(j,1)/D_local(j,1,2)+x_av(j,3)+(7/33)*x_a
v(j,1)/D_local(j,1,3));
        end
    end
end
%general effective diffusivity
for  j = 1:N_grid
     D_eff(j) = 1/((1/(D_K(1)*(Eb/to)))+(1/(Dm(j)*(Eb/to))));
end

C_profile_CO2 = C_profile_CO2';

for j = 1:N_grid
% particle thiele modulus
    tetap(j) = (diam_p/6)*(sqrt(((n+1)*K*(C_profile_CO2(j))^(n -
1))/(2*D_eff(1))));
% particle effectiveness factor
    etap(j) = (3/tetap(j))*((1/tanh(tetap(j))) - (1/tetap(j)));
end
o = 0;
q = 0;
for i = N_grid1+1:N_grid-1
    w(i) = K*etap(i)*(C_profile_CO2(i))^n;
    w(i+1) = K*etap(i+1)*(C_profile_CO2(i+1))^n;
    g(i) = K*(C_profile_CO2(i))^n;
    g(i+1) = K*(C_profile_CO2(i+1))^n;
    o = o + ((w(i)+w(i+1))/2*dz2);
    q = q + ((g(i)+g(i+1))/2*dz2);
end

Etap_av = o/q

Etab = ((1/delta)*o)/(K*Etap_av*(C_profile_CO2(N_grid1))^n)

Etae = (C_profile_CO2(N_grid1)/c_total(1))^n

Rv = Eb/Ro*M(1)*Etap_av*Etab*Etae*K*c_total(1)^n

Toc
```

Function file:

```
  function dydt =
f_SMM_DGM_3comp(t,y,N_grid1,N_grid2,N_comp,D,Temp,dz1,dz2,mu,phi,Lc,R,radius_p
ore,D_K,sigma_sq_co2,Eb,n,K,to,r_cruc,z,radius,diam_p,ratio,product)

N_grid = N_grid1 + N_grid2;
N_eq = N_grid*N_comp;
dydt = zeros(N_eq,1);          %defining dydt for each node and each component

%% Just to show the time...
t_out = random('uniform',0,1);
if t_out < 0.001
   t
end
```

```
%% Calculation of C_i, C_total, and p_total
for j = 1:N_grid
    c_total(j) = 0;
    for k = 1:N_comp
        C(j,k) = y((j-1)*N_comp+k);
        c_total(j) = c_total(j) + C(j,k);
    end
    p_total(j) = c_total(j)*R*Temp;
end
c_total(N_grid+1) = 0;
for k = 1:N_comp        %applying zero flux boundary conditions
    C(N_grid+1,k) = C(N_grid-1,k);
    c_total(N_grid+1) = c_total(N_grid+1) + C(N_grid+1,k);
end
p_total(N_grid+1) = c_total(N_grid+1)*R*Temp;
for j = 1:N_grid1-1
    for k = 1:N_comp
        dcdz(j,k) =  (C(j+1,k) - C(j,k))/dz1;
        dpdz(j) = (p_total(j+1)-p_total(j))/dz1;
        p_total_av(j) = (p_total(j)+ p_total(j+1))/2;
    end
end
for j = N_grid1+1:N_grid
    for k = 1:N_comp
        dcdz(j,k) =  (C(j+1,k) - C(j,k))/dz2;
        dpdz(j) = (p_total(j+1)-p_total(j))/dz2;
        p_total_av(j) = (p_total(j)+p_total(j+1))/2;
    end
end
for j = 1:N_grid
%     dcdz_tot(j) = (c_total(j+1) - c_total(j))/dz;
    dcdz_tot(j) = dcdz(j,1) + dcdz(j,2);
end

%% Calculation of x_i - molar fraction
for j = 1:N_grid
    for k = 1:N_comp
        x(j,k) = C(j,k)/c_total(j);
    end
end
for k = 1:N_comp
    x(N_grid+1,k) = x(N_grid-1,k);
end

%% Calculation of mixture viscosities and diffusivities
for j = 1:N_grid
    mu_mix(j) = 0;
    for ii = 1:N_comp
        num_ = x(j,ii)*mu(ii);
        denom_ = 0;
        for jj = 1:N_comp
            denom_ = denom_ + x(j,jj)*phi(ii,jj);
        end
        mu_mix(j) = mu_mix(j) + num_/denom_;
    end
end
for j = 1:N_grid-1
    mu_mix_av(j) = (mu_mix(j) + mu_mix(j+1))/2;
end
k_Darcy = (radius_pore^2)/8;       %for the gas part should be radius of the
crucible!
for j = 1:N_grid1-1
    for ii = 1:N_comp
        for jj = 1:N_comp
```

```
            D_local(j,ii,jj)= D(ii,jj)*100000/p_total(j);
%diffusivity in the gas part
        end
    end
end
for j = N_grid1+1:N_grid
    for ii = 1:N_comp
        for jj = 1:N_comp
            D_local(j,ii,jj) = ((Eb/to)*D(ii,jj))*100000/p_total(j);
%diffusivity in the solid part
        end
    end
end
for j = 1:N_grid1-1
    v_nonslip(j) = (0.3e-3)^2*(-dpdz(j))/(8*mu_mix_av(j));
    %ignore Knudsen effects
    vz(j) = v_nonslip(j);
    c_total_av(j) = (c_total(j) + c_total(j+1))/2;
    N_total(j) = c_total_av(j)*vz(j);
    for ii = 1:N_comp
        x_av(j,ii) = (x(j,ii) + x(j+1,ii))/2;
        dxdz(j,ii) = (x(j+1,ii) - x(j,ii))/dz1;
    end
end

%% Calculation of fluxes
for j = 1:N_grid1-1       % Bulk gas
    for ii = 1:N_comp-1
        for jj = 1:N_comp
            if ii==jj
                A_matrixg(ii,jj) = 0;
                for kk = 1:N_comp
                    if kk==ii
                    else A_matrixg(ii,jj) = A_matrixg(ii,jj) -
x_av(j,kk)/D_local(j,ii,kk);
                    end
                end
            else
                A_matrixg(ii,jj) = x_av(j,ii)/D_local(j,ii,jj);
            end
        end
    end
    for jj = 1:N_comp
        A_matrixg(N_comp,jj) = 1;
    end
    for ii = 1:N_comp-1
        B_matrixg(ii,1) = c_total_av(j)*dxdz(j,ii);
    end
    B_matrixg(N_comp,1) = N_total(j);
    A_invg = inv(A_matrixg);
    N_matrixg = A_invg*B_matrixg;
    for ii = 1:N_comp
        N_all(j,ii) = N_matrixg(ii,1);
    end
end

% porous solid flux
for j = N_grid1+1:N_grid
    for ii = 1:N_comp
        x_av(j,ii) = (x(j,ii) + x(j+1,ii))/2;
        dxdz(j,ii) = (x(j+1,ii) - x(j,ii))/dz2;
    end
end
for j = N_grid1+1:N_grid
```

```
    for ii = 1:N_comp
        for jj = 1:N_comp
            if ii==jj
                A_matrixs(ii,jj) = 0;
                for kk = 1:N_comp
                    if kk==ii
                        A_matrixs(ii,jj) = A_matrixs(ii,jj) - 1/D_K(kk);
                    else
                        A_matrixs(ii,jj) = A_matrixs(ii,jj) -
x_av(j,kk)/D_local(j,ii,kk);
                    end
                end
            else
                A_matrixs(ii,jj) = x_av(j,ii)/D_local(j,ii,jj);
            end
        end
    end
    lambda(j) = 1.38065e-23*Temp/(3.14159*sigma_sq_co2*p_total_av(j));
    Kn(j) = lambda(j)/(2*radius_pore);
    B0(j) =
(mu(1)*D_K(1)/p_total_av(j))*(p_total_av(j)*k_Darcy*(1+4*Kn(j))/(mu(1)*D_K(1))
-1);
    for ii = 1:N_comp
        B_matrixs(ii,1) = (p_total_av(j)/(R*Temp))*dxdz(j,ii) +
(x_av(j,ii)/(R*Temp))*dpdz(j)*(1 + B0(j)*p_total_av(j)/(mu_mix(j)*D_K(ii)));
    end
    A_invs = inv(A_matrixs);
    N_matrixs = A_invs*B_matrixs;
    for ii = 1:N_comp
        N_all(j,ii) = N_matrixs(ii,1);
    end
end
for ii = 1:N_comp
    N_all(N_grid,ii) = -N_all(N_grid-1,ii);
end

for ii = 1:N_comp
    dcdt(1,ii) = 0;
end

% CO2 pseudo binary diff coefficient
if N_comp == 2
Dm = D_local(:,1,2);
else
   for j = 1:N_grid
       if product == 1
          Dm(j) =
(1+1.27*x_av(j,1))/(x_av(j,2)+2*x_av(j,1)/D_local(j,1,2)+x_av(j,3)+0.27*x_av(j
,1)/D_local(j,1,3));
       else
          Dm(j) =
(1+x_av(j,1))/(x_av(j,2)+(59/33)*x_av(j,1)/D_local(j,1,2)+x_av(j,3)+(7/33)*x_a
v(j,1)/D_local(j,1,3));
       end
   end
end
%general effective diffusivity
for  j = 1:N_grid
     D_eff(j) = 1/((1/(D_K(1)*(Eb/to)))+(1/(Dm(j)*(Eb/to))));
end

%% Calculation of mean eta p
for j = 1:N_grid
% particle thiele modulus
```

```
    tetap(j) = (diam_p/6)*(sqrt(((n+1)*K*(C(j,1))^(n - 1))/(2*D_eff(1))));
% particle effectiveness factor
    etap(j) = (3/tetap(j))*((1/tanh(tetap(j))) - (1/tetap(j)));
end
o = 0;
q = 0;
for i = N_grid1+1:N_grid
    w(i) = K*etap(i)*(C(i,1))^n;
    g(i) = K*(C(i,1))^n;
    o = o + (w(i)*dz2);
    q = q + (g(i)*dz2);
end
Etap_av = o/q;
for j = 1:N_grid-1
    r_avg(j) = (r_cruc(j) + r_cruc(j+1))/2;
end

%% Material Balances
for j = 1:N_grid1-2           %M.B. in the gas part
    for ii = 1:N_comp
        dNdz(j+1,ii) = (N_all(j+1,ii) - N_all(j,ii))/dz1;
        dcdt(j+1,ii) = -dNdz(j+1,ii);
    end
end
for j = N_grid1+1:N_grid-1    %M.B. in the porous solid part
    for ii = 1:N_comp
        dNdz(j+1,ii) = (N_all(j+1,ii) - N_all(j,ii))/(dz2);
        dcdt(j+1,ii) = (-1/(Eb*r_avg(j)^2))*(2*N_all(j,ii)*(-z(j+1) + Lc -
radius) + r_cruc(j+1)^2*dNdz(j+1,ii)) + (ratio(ii)*Etap_av*K*(C(j,1))^n)/Eb;
%reaction in the bed
    end
end

%% M.B. in the interface layer

rc_sq_in = (r_cruc(N_grid1-1)^2 + r_cruc(N_grid1)^2)/2;
rc_sq_out = (r_cruc(N_grid1+1)^2 + r_cruc(N_grid1+2)^2)/2;
vol_gas = (dz1/2)*((r_cruc(N_grid1-1)^2 + 3*r_cruc(N_grid1)^2)/4);
vol_bed = (dz2/2)*((3*r_cruc(N_grid1+1)^2 + r_cruc(N_grid1+2)^2)/4);
vol_bed_void = vol_bed*Eb;

for ii = 1:N_comp
    in_(ii) = N_all(N_grid1-1,ii)*rc_sq_in;
    out_(ii) = N_all(N_grid1+1,ii)*rc_sq_out;
    dcdt(N_grid1,ii) = (in_(ii) - out_(ii) +
((ratio(ii)*Etap_av*K*C(N_grid1,1)^n))*vol_bed)/(vol_gas + vol_bed_void);
    dcdt(N_grid1+1,ii) = (in_(ii) - out_(ii) +
((ratio(ii)*Etap_av*K*C(N_grid1,1)^n))*vol_bed)/(vol_gas + vol_bed_void);
end

%% Putting all vectors dcdt in just one vector

for j = 1:N_grid
    for k = 1:N_comp
        dydt((j-1)*N_comp+k) = dcdt(j,k);
    end
end
end
```

Appendix D: Developed MATLAB code for the CO_2 gasification of petcoke and activated carbon using **Stefan-Maxwell Model** in the gas part and the **Cylindrical Pore Interpolation Model** in the bed part (multicomponent mixture).

Main file:

```
% SMM-CPIM - Modeling multicomponent diffusion and reaction inside a crucible
% Numerical integration of a set of differential equations along the crucible

clc
clear all
close all
code = 2;                              %code=1 for act. carbon and code=2 petcoke
product = 1;                           %product=1 for H2 or no O2 released and
product=2 for H2O or O2 released
%%=================Part1: parameters and variables calculation==============
tic
tspan = 0:1e-3:3;                          %simulation time
Lc= 0.02;                                  %length of crucible(m)
N_grid1 = 51;                              %number of grid points in the gas
N_grid2 = 51;                              %number of grid points in the bed
N_grid = N_grid1 + N_grid2;                %number of grid points
N_comp  = 2;                               %number of compounds
% 1 = CO2
% 2  = CO
% 3 = H2 (1st CASE - product=1) or H2O (2nd CASE - product=2)
p_begin = 91192.5;                         %pressure(Pa)
w0 = input('Initial mass(mg)=');           %initial mass (mg)
w0 = w0*10^-3;                             %converting to g
diam = 18e-3;                              %crucible (bed) diameter(m)
radius = diam/2;
Temp = 1223;                               %bed temperature (K)
R = 8.3144598;                             %gas constant
for j = 1:N_grid
    p(j) = p_begin;
    c_total(j) = p(j)/(R*Temp);            %total concentration in each grid
point(mol/m3)
end
% Diffusion coefficients at 0.9 atm pressure
for j = 1:N_comp
    D(j,j) = 0;
end
D(1,2) = (1.39e-5)*((Temp/273.2)^1.75); %binary diffusivity at o.1 MPa (m2/s)
D(2,1) = D(1,2);
mu(1) = (15.4336*1.37369*(1-exp(-
1.30184*(Temp/304.13)^0.65455))*(Temp/304.13)^0.61732)*1e-6;    %CO2 viscosity
(Pa.s) - Append. E Transport Phenomena
mu(2) = (8.8697*1.37369*(1-exp(-
1.30184*(Temp/132.86)^0.65455))*(Temp/132.86)^0.61732)*1e-6;     %CO viscosity
(Pa.s) - Append. E Transport Phenomena
M(1) = 44;                                 %molar mass for CO2
M(2) = 28;                                 %molar mass for CO
if code == 1;
%=========================activated carbon Data============================
   diam_pore = 0.288e-3;                       %bed pore diameter
   radius_pore = diam_pore/2;
   diam_p = 1.3e-3;                            %particle diameter for Act. carbon
   Rop = 0.4e6;                                %particle density(g/m3)
   Ro = 0.3e6;                                 %bulk density(g/m3)
   K = 5.962;                                  %intrinsic rate constant(T=1223 for
Act. carbon)
```

```
   Eb = 1-(Ro/Rop);                          %bed porosity
   n = 0.8;                                  %intrinsic reaction order(for Act.
carbon)
   to = 1-(0.5*log(Eb));                     %bed tortousity
   ap = [-pi/3 pi*radius 0 -w0/Ro];
   a = roots(ap);
   delta = a(2);                             %bed depth(alpha) for act. carbon
%============================================================================
%==================data NOT considering oxygen in AC=======================
      if product == 1;
         ratio(1) = -1;
         ratio(2) = 2;
%====================data considering oxygen in AC=========================
      else
         ratio(1) = -46/73;
         ratio(2) = 119/73;
      end
%============================================================================

   if (N_comp ~= 2)
       disp('Activated Carbon is simulated just with 2 components. Please,
change N_comp to 2.')
       return
   end
else
%============================Petcoke Data====================================
   diam_pore = 3e-5;                         %bed pore diameter
   radius_pore = diam_pore/2;
   diam_p = 45e-6;                           %particle diameter for petcoke
   Rop = 1.4e6;                              %%particle density(g/m3)
   Ro = 0.7e6;                               %bulk density(g/m3)
   K = 0.776;                                %intrinsic rate constant
   Eb = 1-(Ro/Rop);                          %bed porosity
   n = 0.6;                                  %intrinsic reaction order
   to = 1-(0.5*log(Eb));                     %bed tortuosity for petcoke
   ap = [-pi/3 pi*radius 0 -w0/Ro];
   a = roots(ap);
   delta = a(2);                             %bed depth(alpha) for petcoke(m)
%============================================================================
   if N_comp ==2;
      ratio(1) = -1;
      ratio(2) = 2;
   else
%==============================data for H2===================================
      if product == 1;
         D(1,3) = (6.5e-5)*((Temp/298.15)^1.7675);
         D(3,1) = D(1,3);
         D(2,3) = (7.811e-5)*((Temp/298.15)^1.7414);
         D(3,2) = D(2,3);
         M(3) = 2;                                 %molar mass for H2
         mu(3) = (1.6959*1.37369*(1-exp(-
1.30184*(Temp/33.19)^0.65455))*(Temp/33.19)^0.61732)*1e-6;      %H2 viscosity
(Pa.s) - Append. E Transport Phenomena
         ratio(1) = -1;
         ratio(2) = 2;
         ratio(3) = 7/26;
%==============================data for H2O==================================
      else
         D(1,3) = (2.351e-5)*((Temp/298.15)^1.6608);
         D(3,1) = D(1,3);
         D(2,3) = (2.995e-5)*((Temp/298.15)^1.6347);
         D(3,2) = D(2,3);
         M(3) = 18;                                %molar mass for H2O
```

```
        mu(3) = (23.5373*1.37369*(1-exp(-
1.30184*(Temp/647.1)^0.65455))*(Temp/647.1)^0.61732)*1e-6;      %H2O viscosity
(Pa.s) - Append. E Transport Phenomena
        ratio(1) = -33/26;
        ratio(2) = 59/26;
        ratio(3) = 7/26;
      end
   end
end
%=========================================================================
dz1 = (Lc - delta)/(N_grid1 - 1);       %node thickness in the gas part
dz2 = delta/(N_grid2 - 1);              %node thickness in the porous solid
for j = 1:N_grid1
    z(j) = (j-1)*dz1;
end
for j = 1:N_grid2
    z(N_grid1+j) = (Lc - delta) + (j-1)*dz2;
end
for j = 1:N_grid1
    r_cruc(j) = radius;                %Constant radius in the gas
part(assumption)
end
for j = N_grid1+1:N_grid
    del(j) = Lc - z(j);
    r_cruc(j) = (del(j)*(2*radius - del(j)))^0.5;
end

%Knudsen diffusion coefficient
for ii = 1:N_comp
    D_K(ii) = (8*radius_pore/3)*sqrt(R*Temp/(2*3.14159*(M(ii)/1000)));
end

for i = 1:N_comp
    for j = 1:N_comp
        phi(i,j) =
(1+sqrt(mu(i)/mu(j)*sqrt(M(j)/M(i))))^2/sqrt(8*(1+M(i)/M(j)));
    end
end

%initial conditions(just reactant gas)-initializing our concentrations
for j = 1:N_grid
    C(j,1) = 1.0*c_total(j);
    C(j,2) = 0.0*c_total(j);
    C(j,3) = 0.0*c_total(j);
    for k = 1:N_comp
        y0((j-1)*N_comp+k) = C(j,k);
    end
end

%%CPIM parameters
for i = 1:N_comp
  for j = 1:N_comp
       if i ~= j
          DA(i,j) = (1/((Eb/to)*D_K(i)) + 1/D(i,j))^-1;    %interpolated
Diffusivity
       else
          DA(i,j) = (Eb/to)*D_K(i);
       end
   end
end
% DA(1,2) = (1/D_K(1) + 1/D(1,2))^-1;    %interpolated Diffusivities
% DA(2,1) = (1/D_K(2) + 1/D(1,2))^-1;
```

```
%%=======================Part2: Numerical Solution=========================

options = odeset('RelTol', 1e-6, 'AbsTol', 1e-8, 'InitialStep', 0.01);
[T,Y] =
ode15s(@SMMCPIMf_3comp,tspan,y0,options,N_grid1,N_grid2,N_comp,D,p,Temp,dz1,dz
2,z,mu,M,Lc,delta,R,radius_pore,D_K,Eb,Ro,n,K,to,DA,phi,r_cruc,w0,diam_p,radiu
s,ratio,product);

%%=======================Part3: Output of results==========================
figure(1)
plot(T,Y)
xlabel('time(s)')
ylabel('y')
% T
% Y
[s1,s2] = size(T);
for j = 1:s1
    for k = 1:N_grid
        C_tot(j,k) = 0;
        for ii = 1:N_comp
            C_(j,k,ii) = Y(j,(k-1)*N_comp+ii);
            C_tot(j,k) = C_tot(j,k) + C_(j,k,ii);
        end
    end
end
figure(2)
plot(T,C_tot)
xlabel('time(s)')
ylabel('total concentration(mol/m^3)')
figure(3)
plot(z,C_tot(end,:))
xlabel('z(m)')
ylabel('total concentration(mol/m^3)')
figure(4)
for k = 1:N_grid
    p_profile(k) = C_tot(s1,k)*R*Temp;
    C_profile_CO2(k) = C_(s1,k,1);
    x_profile_CO2(k) = (C_profile_CO2(k))/C_tot(s1,k);
    C_profile_CO(k) = C_(s1,k,2);
    x_profile_CO(k) = (C_profile_CO(k))/C_tot(s1,k);
    if N_comp == 2
    else
        if product == 1
           C_profile_H2(k) = C_(s1,k,3);
           x_profile_H2(k) = (C_profile_H2(k))/C_tot(s1,k);
        else
           C_profile_H2O(k) = C_(s1,k,3);
           x_profile_H2O(k) = (C_profile_H2O(k))/C_tot(s1,k);
        end
    end
end
plot(z,p_profile) %pressure profile along the crucible
xlabel('z(m)')
ylabel('pressure (Pa)')
title('Pressure Profile')
figure(5)
z_rel = 1-(Lc-z)/Lc;
plot(z_rel,x_profile_CO2)
xlabel('(L-z)/L')
ylabel('x_{CO_2}')
title('CO2 molar fraction profile in the crucible')
figure(6)
z_rel = 1-(Lc-z)/Lc;
```

```
plot(z_rel,x_profile_CO)
xlabel('(L-z)/L')
ylabel('x_{CCO}')
title('CO molar fraction profile in the crucible')
if N_comp == 2
else
    if product == 1
       figure(7)
       z_rel = 1-(Lc-z)/Lc;
       plot(z_rel,x_profile_H2)
       xlabel('(L-z)/L')
       ylabel('x_{H2}')
       title('H2 molar fraction profile in the crucible')
    else
       figure(7)
       z_rel = 1-(Lc-z)/Lc;
       plot(z_rel,x_profile_H2O)
       xlabel('(L-z)/L')
       ylabel('x_{H2O}')
       title('H2O molar fraction profile in the crucible')
    end
end

%% Calculation of mean eta p

% CO2 pseudo binary diff coefficient
for j = 1:N_grid1-1
    for ii = 1:N_comp
        for jj = 1:N_comp
            D_local(j,ii,jj)= D(ii,jj)*100000/p_profile(j);
%diffusivity in the gas part
        end
    end
end
for j = N_grid1+1:N_grid
    for ii = 1:N_comp
        for jj = 1:N_comp
            D_local(j,ii,jj) = ((Eb/to)*D(ii,jj))*100000/p_profile(j);
%diffusivity in the solid part
        end
    end
end

x_av(:,1) = x_profile_CO2;
x_av(:,2) = x_profile_CO;
if N_comp == 2
else
    if product == 1
       x_av(:,3) = x_profile_H2;
    else
       x_av(:,3) = x_profile_H2O;
    end
end

if N_comp == 2
Dm = D_local(:,1,2);
else
   for j = 1:N_grid
       if product == 1
          Dm(j) =
(1+1.27*x_av(j,1))/(x_av(j,2)+2*x_av(j,1)/D_local(j,1,2)+x_av(j,3)+0.27*x_av(j
,1)/D_local(j,1,3));
       else
```

```
          Dm(j) =
(1+x_av(j,1))/(x_av(j,2)+(59/33)*x_av(j,1)/D_local(j,1,2)+x_av(j,3)+(7/33)*x_a
v(j,1)/D_local(j,1,3));
        end
    end
end
%general effective diffusivity
for  j = 1:N_grid
     D_eff(j) = 1/((1/(D_K(1)*(Eb/to)))+(1/(Dm(j)*(Eb/to))));
end

C_profile_CO2 = C_profile_CO2';

for j = 1:N_grid
% particle thiele modulus
    tetap(j) = (diam_p/6)*(sqrt(((n+1)*K*(C_profile_CO2(j))^(n -
1))/(2*D_eff(1))));
% particle effectiveness factor
    etap(j) = (3/tetap(j))*((1/tanh(tetap(j))) - (1/tetap(j)));
end
o = 0;
q = 0;
for i = N_grid1+1:N_grid-1
    w(i) = K*etap(i)*(C_profile_CO2(i))^n;
    w(i+1) = K*etap(i+1)*(C_profile_CO2(i+1))^n;
    g(i) = K*(C_profile_CO2(i))^n;
    g(i+1) = K*(C_profile_CO2(i+1))^n;
    o = o + ((w(i)+w(i+1))/2*dz2);
    q = q + ((g(i)+g(i+1))/2*dz2);
end

Etap_av = o/q

Etab = ((1/delta)*o)/(K*Etap_av*(C_profile_CO2(N_grid1))^n)

Etae = (C_profile_CO2(N_grid1)/c_total(1))^n

Rv = Eb/Ro*M(1)*Etap_av*Etab*Etae*K*c_total(1)^n

toc
```

Function file:

```
function dydt =
SMMCPIMf_3comp(t,y,N_grid1,N_grid2,N_comp,D,p,Temp,dz1,dz2,z,mu,M,Lc,delta,R,r
adius_pore,D_K,Eb,Ro,n,K,to,DA,phi,r_cruc,w0,diam_p,radius,ratio,product)

N_grid = N_grid1 + N_grid2;
N_eq = N_grid*N_comp;
dydt = zeros(N_eq,1);          %defining dydt for each node and each component

% Just to show time

t_out = random('uniform',0,1);
if t_out < 0.001
  t
end
%% Calculation of C_i, C_total, and p_total
```

```
for j = 1:N_grid
    c_total(j) = 0;
    for k = 1:N_comp
        C(j,k) = y((j-1)*N_comp+k);
        c_total(j) = c_total(j) + C(j,k);
    end
    p_total(j) = c_total(j)*R*Temp;
end

c_total(N_grid+1) = 0;
for k = 1:N_comp                        %applying zero flux boundary conditions
    C(N_grid+1,k) = C(N_grid-1,k);
    c_total(N_grid+1) = c_total(N_grid+1) + C(N_grid+1,k);
end

p_total(N_grid+1) = c_total(N_grid+1)*R*Temp;

for j = 1:N_grid1-1
    for k = 1:N_comp
        dcdz(j,k) =  (C(j+1,k) - C(j,k))/dz1;
        dpdz(j) = (p_total(j+1)-p_total(j))/dz1;
        p_total_av(j) = (p_total(j)+ p_total(j+1))/2;
    end
end

for j = N_grid1+1:N_grid
    for k = 1:N_comp
        dcdz(j,k) =  (C(j+1,k) - C(j,k))/dz2;
        dpdz(j) = (p_total(j+1)-p_total(j))/dz2;
        p_total_av(j) = (p_total(j)+p_total(j+1))/2;
    end
end

for j = 1:N_grid
%     dcdz_tot(j) = (c_total(j+1) - c_total(j))/dz;
    dcdz_tot(j) = dcdz(j,1) + dcdz(j,2);
end

%% Calculation of x_i - molar fraction

for j = 1:N_grid
    for k = 1:N_comp
        x(j,k) = C(j,k)/c_total(j);
    end
end

for k = 1:N_comp
    x(N_grid+1,k) = x(N_grid-1,k);
end

%% Calculation of mixture viscosivities and diffusivities

for j = 1:N_grid
    mu_mix(j) = 0;
    for ii = 1:N_comp
        num_ = x(j,ii)*mu(ii);
        denom_ = 0;
        for jj = 1:N_comp
            denom_ = denom_ + x(j,jj)*phi(ii,jj);
        end
        mu_mix(j) = mu_mix(j) + num_/denom_;
    end
```

```
end

k_Darcy = (radius_pore^2)/8;       %for the gas part should be radius of the
crucible!

for j = 1:N_grid1-1
    for ii = 1:N_comp
        for jj = 1:N_comp
            D_local(j,ii,jj)= D(ii,jj)*100000/p_total(j);
%diffusivity in the gas part
        end
    end
end

for j = N_grid1+1:N_grid
    for ii = 1:N_comp
        for jj = 1:N_comp
            D_local(j,ii,jj)= ((Eb/to)*D(ii,jj))*100000/p_total(j);
%diffusivity in the solid part
        end
    end
end

for j = 1:N_grid1-1
       v_nonslip(j) = (0.3e-3)^2*(-dpdz(j))/(8*mu_mix(j));
       %ignore Knudsen effects
       vz(j) = v_nonslip(j);
       c_total_av(j) = (c_total(j)+c_total(j+1))/2;
       N_total(j) = c_total_av(j)*vz(j);
       for ii = 1:N_comp
            x_av(j,ii) = (x(j,ii) + x(j+1,ii))/2;
            dxdz(j,ii) = (x(j+1,ii) - x(j,ii))/dz1;
        end
end

%% Calculation of fluxes
 for j = 1:N_grid1-1       % Bulk gas
        for ii = 1:N_comp-1
            for jj = 1:N_comp
                if ii==jj
                    A_matrix(ii,jj) = 0;
                    for kk = 1:N_comp
                        if kk==ii
                        else A_matrix(ii,jj) = A_matrix(ii,jj) -
x_av(j,kk)/D_local(j,ii,kk);
                        end
                    end
                else
                    A_matrix(ii,jj) = x_av(j,ii)/D_local(j,ii,jj);
                end
            end
        end
        for jj = 1:N_comp
            A_matrix(N_comp,jj) = 1;
        end
        for ii = 1:N_comp-1
            B_matrix(ii,1) = c_total_av(j)*dxdz(j,ii);
        end
        B_matrix(N_comp,1) = N_total(j);
        A_inv = inv(A_matrix);
        N_matrix = A_inv*B_matrix;
        for ii = 1:N_comp
            N_all(j,ii) = N_matrix(ii,1);
```

```
        end
 end
% calculation of the porous bed fluxes

for j = N_grid1+1:N_grid
       for ii = 1:N_comp
           x_av(j,ii) = (x(j,ii)+x(j+1,ii))/2;
           dxdz(j,ii) = (x(j+1,ii) - x(j,ii))/dz2;
       end
end

A_K = 3/(4*radius_pore)*(pi*R*Temp/2)^(1/2);

for j = N_grid1+1:N_grid
       A_C(j) =
(8*mu_mix(j))/(c_total(j)*radius_pore^2*(x_av(j,1)*M(1)+x_av(j,2)*M(2)));
       AA(j) = (1/A_K + 1/A_C(j))^-1;
       if N_comp==2
           A_matrix = [-(to^2)/Eb*x_av(j,2)/DA(1,2)
(to^2)/Eb*x_av(j,1)/DA(2,1); -(to^2)/Eb*AA(j)*M(1)^(1/2) -
(to^2)/Eb*AA(j)*M(2)^(1/2)];
           B_matrix = [c_total(j)*dxdz(j,1); dpdz(j)];
       else
           A_matrix = [-(to^2)/Eb*(x_av(j,2)/DA(1,2) + x_av(j,3)/DA(1,3))
(to^2)/Eb*x_av(j,1)/DA(2,1) (to^2)/Eb*x_av(j,1)/DA(3,1);
(to^2)/Eb*x_av(j,2)/DA(1,2) -(to^2)/Eb*(x_av(j,1)/DA(2,1) + x_av(j,3)/DA(2,3))
(to^2)/Eb*x_av(j,2)/DA(3,2); -(to^2)/Eb*AA(j)*M(1)^(1/2) -
(to^2)/Eb*AA(j)*M(2)^(1/2) -(to^2)/Eb*AA(j)*M(3)^(1/2)];
           B_matrix = [c_total(j)*dxdz(j,1); c_total(j)*dxdz(j,2); dpdz(j)];
       end
       A_inv = inv(A_matrix);
       N_matrix = A_inv*B_matrix;
       for ii = 1:N_comp
           N_all(j,ii) = N_matrix(ii,1);
       end
end

for ii = 1:N_comp
    N_all(N_grid,ii) = -N_all(N_grid-1,ii);
end

for ii = 1:N_comp
    dcdt(1,ii) = 0;
end

% CO2 pseudo binary diff coefficient
if N_comp == 2
Dm = D_local(:,1,2);
else
   for j = 1:N_grid
       if product == 1
          Dm(j) =
(1+1.27*x_av(j,1))/(x_av(j,2)+2*x_av(j,1)/D_local(j,1,2)+x_av(j,3)+0.27*x_av(j
,1)/D_local(j,1,3));
       else
          Dm(j) =
(1+x_av(j,1))/(x_av(j,2)+(59/33)*x_av(j,1)/D_local(j,1,2)+x_av(j,3)+(7/33)*x_a
v(j,1)/D_local(j,1,3));
       end
   end
end
%general effective diffusivity
for  j = 1:N_grid
```

```
     D_eff(j) = 1/((1/(D_K(1)*(Eb/to)))+(1/(Dm(j)*(Eb/to))));
end

%% Calculation of mean eta p
for j = 1:N_grid
% particle thiele modulus
    tetap(j) = (diam_p/6)*(sqrt(((n+1)*K*(C(j,1))^(n - 1))/(2*D_eff(1))));
% particle effectiveness factor
    etap(j) = (3/tetap(j))*((1/tanh(tetap(j))) - (1/tetap(j)));
end
o = 0;
q = 0;
for i = N_grid1+1:N_grid
    w(i) = K*etap(i)*(C(i,1))^n;
    g(i) = K*(C(i,1))^n;
    o = o + (w(i)*dz2);
    q = q + (g(i)*dz2);
end
Etap_av = o/q;
for j = 1:N_grid-1
    r_avg(j) = (r_cruc(j) + r_cruc(j+1))/2;
end

%% Material Balances

for j = 1:N_grid1-2          %M.B. in the gas part
    for ii = 1:N_comp
        dNdz(j+1,ii) = (N_all(j+1,ii) - N_all(j,ii))/dz1;
        dcdt(j+1,ii) = -dNdz(j+1,ii);
    end
end

for j = N_grid1+1:N_grid-1    %M.B. in the porous solid part
    for ii = 1:N_comp
        dNdz(j+1,ii) = (N_all(j+1,ii) - N_all(j,ii))/(dz2);
        dcdt(j+1,ii) = (-1/(Eb*r_avg(j)^2))*(2*N_all(j,ii)*(-z(j+1) + Lc -
radius) + r_cruc(j+1)^2*dNdz(j+1,ii)) + (ratio(ii)*Etap_av*K*(C(j,1))^n)/Eb;
%reaction in the bed
    end
end

%% M.B. in the interface layer

rc_sq_in = (r_cruc(N_grid1-1)^2 + r_cruc(N_grid1)^2)/2;
rc_sq_out = (r_cruc(N_grid1+1)^2 + r_cruc(N_grid1+2)^2)/2;
vol_gas = (dz1/2)*((r_cruc(N_grid1-1)^2 + 3*r_cruc(N_grid1)^2)/4);
vol_bed = (dz2/2)*((3*r_cruc(N_grid1+1)^2 + r_cruc(N_grid1+2)^2)/4);
vol_bed_void = vol_bed*Eb;

for ii = 1:N_comp
    in_(ii) = N_all(N_grid1-1,ii)*rc_sq_in;
    out_(ii) = N_all(N_grid1+1,ii)*rc_sq_out;
    dcdt(N_grid1,ii) = (in_(ii) - out_(ii) +
((ratio(ii)*Etap_av*K*C(N_grid1,1)^n))*vol_bed)/(vol_gas + vol_bed_void);
    dcdt(N_grid1+1,ii) = (in_(ii) - out_(ii) +
((ratio(ii)*Etap_av*K*C(N_grid1,1)^n))*vol_bed)/(vol_gas + vol_bed_void);
end

%% Putting all vectors dcdt in just one vector

for j = 1:N_grid
    for k = 1:N_comp
        dydt((j-1)*N_comp+k) = dcdt(j,k);
```

```
    end
end
end
```